CONFORMATIONAL STUDIES OF THE BETA AMYLOID PROTEIN AND *IN VITRO* MODELS FOR THE EFFECT OF APOLIPOPROTEIN E ON FIBRIL FORMATION IN ALZHEIMER'S DISEASE

by

Krista Carole Evans
B.S. Chemistry, Ithaca College
(1991)

Submitted to the Department of
Chemistry in Partial Fulfillment of the
Requirements for the Degree of

DOCTOR OF PHILOSOPHY

at the

Massachusetts Institute of Technology

June 1996

Signature of Author_____
Department of Chemistry
May 8, 1996

Certified by_____
Peter T. Lansbury, Jr.
Associate Professor of Chemistry
Thesis Supervisor

Accepted by___
Dietmar Seyferth
Chairman, Department Committee on Graduate Students

This doctoral thesis has been examined by a Committee of the Department of Chemistry as follows:

Professor JoAnne Stubbe ___ Chairperson

Professor Peter T. Lansbury, Jr. Thesis Supervisor

Professor Jonathan King

CONFORMATIONAL STUDIES OF THE BETA AMYLOID PROTEIN AND *IN VITRO* MODELS FOR THE EFFECT OF APOLIPOPROTEIN E ON FIBRIL FORMATION IN ALZHEIMER'S DISEASE

by

Krista Carole Evans

Submitted to the Department of Chemistry
on May 8, 1996 in Partial Fulfillment of the
Requirements for the Degree of Doctor of Philosophy

ABSTRACT

The presence of amyloid plaques is one of the hallmarks of Alzheimer's disease (AD) brains. The plaque is an ordered, fibrous protein aggregate of which the major component is the β protein, a 39-43 amino acid peptide. The β protein is a normal product of the constitutive proteolytic processing of the β amyloid precursor protein, and has been detected in the blood and CSF of healthy individuals. Exposure to extrinsic factors such as metals or exogenous proteins has been proposed to be a risk factor for AD.

Rodents encode for a β protein that differs from the human variant by only three residues (R5G, Y10F, H13R) but do not form amyloid plaques. β1-28, which has a conformation similar to β1-40 as measured by circular dichroism (CD), and β1-28 rodent analogs were examined by CD and the effect of metals on their conformations was examined. Unlike the human analog which undergoes large conformational changes in the presence of zinc, the rodent analog shows little change. The H13R mutation in the rodent sequence appears to be responsible for the decreased interaction of the peptide with zinc.

The β protein also forms fibrillar aggregates *in vitro* according to a nucleation-dependent mechanism. The apolipoprotein E genotype has recently been recognized as a susceptibility factor for AD. The *APOE4* allele correlates with an earlier onset of AD and with increased amyloid deposition in the brain. Apolipoprotein E (apoE) proteins may effect the rate of *in vivo* amyloidogenesis. ApoE3 inhibits amyloid nucleation at an apoE3:β protein molar ratio of 1:1000. ApoE4, which cannot form a disulfide dimer, is an equipotent or less potent inhibitor. The apoE3 dimer is a significantly more potent inhibitor than apoE4. The 22 kD receptor-binding region of recombinant apoE isoforms had an inhibitory activity comparable to the native protein. The inhibitory activity of apoE was further narrowed to a 19 kD variant. Finally, a Cys57 22 kD apoE3 mutant was a significantly less efficient inhibitor of amyloid fibril formation.

Thesis Supervisor: Dr. Peter T. Lansbury, Jr.

Title: Associate Professor of Chemistry

Table of Contents

List of Figures

Acknowledgements

I have found that this section, which is undoubtedly the most critical part of any thesis, is also the most difficult one to write. Where do I begin? Five years ago I came to MIT not knowing what I wanted to do with my life, or even if I really wanted to be here. One of the best decisions that I made during that time was joining Peter Lansbury's group.

I think that in addition to being an extraordinary scientist, Peter is also an incredible mentor. Peter's contagious enthusiasm has always made science exciting. Peter's greatest attribute, however, is his sincere concern for the well-being of his students. Because of this, Peter has earned the loyalty and respect from all of his students, past and present.

I also owe many thanks to every other member of the Lansbury lab. I would never have been successful without their help and support. Paul Weinreb has been my baymate since the beginning, or at least since we were given our own bench. Paul is not only a great scientist, but also a great teacher, mainly because he is so patient. Unfortunately, this trait often made him the target of constant prodding and practical jokes (i.e. gluing his pad of paper to his desk). He always managed to ignore us anyway.

Paul and I are also the last class to know all of the original Lansbury members (Julia Hendrix Miwa, Kurt Halverson, Shimi Cohen-Anisfeld and Annemarie Coffman-Lellouch), and take trips to Martha's Vineyard. I'll never forget sitting around the campfire drinking Southern Comfort through Twizllers listening to Irving Sucholeiki tell us about "Freaks" as only Irv could do, or the time that the skunks attacked the campsite. I'll also never forget the bikeride from Hell. Could it have rained any harder?

I would also like to thank both Joe Jarrett and Jon Come for their helpful suggestions and conversations, and Jon for his ability to make me laugh. Jon always made the lab an enjoyable place to work, even though he made fun of my cat calendar and all of my friends named Heather. Beth Berger was also a great mentor and helped me on many occasions. I look forward to hearing about her exciting travels through Papau New Guinea. I hope that Ted Ashburn is successful in his medical career. I wouldn't be surprised if someday he actually made it onto the space shuttle. To Dave Kocisko, I hope the fishing is great wherever the Army takes you.

Jim Harper, Anna Poon, and Raul Zambrano were great additions to the Lansbury lab. Jim always has great suggestions for interesting experiments, and has the ability to fix just about anything. Most importantly, he initiated poker night. I wish him all the best with his new baby. Anna was the first to introduce molecular biology to our lab. Anna added so much to

our group on both a scientific and personal level. I will never be able to listen to "Magic 106" without thinking of Raul. I am sure that Raul will be an incredible doctor. Cheon-Gyu Cho is a great chemist and has become an integral part of the lab. Santosh Nandan was unique in every way, and I hope everything is going well for him in India with his new wife. Kelly Conway, Magdalena Anguiano, Chris May, and Weiguo Zhen are the newest additions to our group and are responsible for carrying on the group traditions after the move to Harvard Medical School. I know that they will continue to do exciting work.

I would never have made it to this point without my chemistry buddy, Heather Nielsen Sugrue. We have shared so much over the years that I don't know where to begin. We managed to make chemistry fun. Remember doing shots before the chemistry banquet, the killer hangover in P-chem lab, taking candy breaks, tormenting Prof. Anderson, running through the chemistry building after jumping in the fountain during senior week, and so much more? I can't believe how much time has passed since sophomore year at Ithaca. Heather will always be a truly special friend, no matter how many miles are between us.

My deepest thanks go to my family who have always had endless faith in me. My parents, Dale and Svend Rasmussen, are the most loving and generous people that I have ever known. No sacrifice was ever too large for them when it came to either myself or my brother, Bob. My family always gave me the freedom to make my own decisions, while letting me know that they were there for me if I needed them. I know that I would never have achieved so much without them.

My husband, Jeff, is undoubtedly the best thing that ever happened to me. I can't begin to imagine what my life would be like without him. From the first time that I met Jeff at Ithaca almost seven years ago, I knew that he was very special. Jeff is a wonderful and caring person who only sees the best in people. Because of his undying optimism and support, I have accomplished so much more than I ever imagined. I look forward to spending the rest of my life with you, Jeff, which I know will be filled with a lot of excitement, success, and love.

Abbreviations

AD	Alzheimer's disease
AFM	Atomic Force Microscopy
ApoE	Apolipoprotein E
APP	β Amyloid Precursor Protein
Boc	*t*-butoxycarbonyl
BOP	benzotriazol-1-yl-oxy-*tris*-(dimethylamino)phosphonium hexafluorophosphate
CD	Circular Dichroism
CSF	Cerebrospinal fluid
DIEA	diisopropylethylamine
DMF	dimethylformamide
DMS	dimethylsulfide
DMSO	dimethylsulfoxide
EDT	ethane dithiol
EM	Electron Microscopy
FAD	Familial Alzheimer's disease
Fmoc	fluorenylmethoxycarbonyl
FTIR	Fourier-Transform Infrared Spectroscopy
HCHWA-D	Hereditary Cerebral Hemorrhage with Amyloidosis-Dutch Type
HFIP	hexafluoroisopropanol
HPLC	High Performance Liquid Chromatography
IPTG	isopropyl-β-D-thiogalactopyranoside
LDL	Low Density Lipoprotein
LDMS	Laser Desorption Mass Spectrometry
MS	Mass Spectrometry
NMR	Nuclear Magnetic Resonance
PAM	phenylacetamidomethyl
PDMS	Plasma Desorption Mass Spectrometry
PCR	Polymerase Chain Reaction
PMSF	phenylmethylsulfonyl fluoride
PMC	pentamethylchroman-6-sulfonyl
PyBOP	bromo-*tris*-pyrrolidino-phosphonium hexafluorophosphate
RPHPLC	Reverse Phase High Performance Liquid Chromatography
SDS-PAGE	sodium dodecyl sulfate polyacrylamide gel electrophoresis
TFE	trifluoroethanol

Chapter 1

The Role of the β Amyloid Protein in Alzheimer's Disease

Alzheimer's disease (AD) is a devastating neurodegenerative disorder that was first described by the German physician Alois Alzheimer in 1907.[1] The pathological characteristics are extracellular amyloid deposits and intracellular neurofibrillary tangles (NFTs) that are found among dying neurons in the brains of AD victims.[2] AD robs its victims of their most human qualities: reasoning, memory, abstraction, and judgment. Paranoid or delusional symptoms can often be a problem as well.[3] A quote from a translation of Alzheimer's 1907 case report illustrates the destructiveness of the disease: "The first noticeable symptom of illness...was suspiciousness of her husband. ...believing that people were out to murder her, [she] started to scream loudly. ...At times she is totally delirious,...and seems to have auditory hallucinations."[4]

Clinical symptoms typically begin with subtle short-term memory problems but continue to deteriorate as the disease progresses, until the victim can no longer function independently.[5] Memory, language, and orientation worsen until almost all cognitive function is lost. Death finally

occurs from secondary causes such as pneumonia. The time span between the first symptoms of memory loss to death is ten years on average. However, patients may live anywhere from two to twenty years in an increasingly dependent state.[6] This disease exacts a huge emotional, physical, and economic toll on the families of the victims and on society.

Although the disease was initially recognized by Alzheimer in a 55 year old woman, AD is now acknowledged to be the predominant cause of dementia in people over the age of 65. This contrasts with the traditional view of AD which only considered progressive dementia in people younger than 65 to be AD. Dementia in people over 65 was labeled simply as "senile dementia" and was considered to be a normal part of aging. It was not proposed until 1976 that AD should be redefined to include both presenile (less than 65 years of age) and senile (over 65 years of age) dementia.[6] It was first suggested at this time that AD could pose a major public-health threat in the future.

Currently, an estimated 4 million people in the U.S. suffer from AD.[7] This large number is due both to increases in the population and to changes in how AD is defined. AD affects predominantly older people, with more than 95% of the patients over 65 years of age. The risk of developing AD rises with increasing age: 1% of the population between the ages 65-74, 7% of ages 75-84, and 25% of ages 85 and older have severe dementia.[6]

The cost of caring for an AD patient at home approaches $50,000 a year per patient.[6] Families often are not able to provide care for relatives in the middle or late stages of AD because they require around the clock care. Overall, the burden that AD currently places on society is extremely high. In 1994, the annual cost for nursing home care for AD alone was estimated to be

$20 billion and the costs for home care was around $80 billion, bringing the total annual cost of AD to approximately $100 billion dollars.[6]

Unfortunately, all projections predict substantial growth in the population at greatest risk of needing 24-hour institutional care, such as AD patients.[8] The extension of life-spans due to medical technology will also cause an increase in the prevalence of chronic conditions, such as AD, and is seen by some as the failure of success. The number of people with AD is expected to climb to 15 million in less than fifty years, placing a huge burden on the health-care industry and added pressure on scientists to elucidate the pathogenic mechanism of AD.

Clinical Research

The lack of a well defined disease mechanism has made it extremely difficult to not only find a therapeutic drug, but to even diagnose the disease in the first place. The first clinical symptoms of memory loss occur well after the initial biological insult which is responsible for initiating the cascade of cellular processes that signal the onset of the disease. Because doctors are unable to diagnose the disease at its starting point, finding a way to prevent the onset of AD will remain a challenge for some time.

There are several other diseases of dementia where the clinical symptoms are very similar to AD such as Pick's disease, Lewy body disease, Creutzfeldt-Jakob disease, and sometimes Parkinson's disease.[4] These AD look-alike diseases complicate matters and make a clinical diagnosis very subjective. A definitive diagnosis of AD can only be made at autopsy. Additionally, accurate diagnosis is difficult in the elderly. Other causes of dementia such as multi-infarct dementia (caused from atherosclerosis), overmedication, and depression become common and confound the

diagnosis of AD.[5] There is also debate over whether AD is a single disease or a group of disorders manifesting similar symptoms and pathological changes.[9]

There are presently several approaches used in the clinical diagnosis of AD, and direct comparison of research findings across countries is complicated by the lack of uniform diagnostic criteria. For example, doctors in the U.S. are much more likely to diagnose dementia as AD than their European counterparts, possibly due to the recent overwhelming national awareness of AD in the U.S.[4]

In addition, much more emphasis has been given in the U.S. to the establishment of valid criteria for the clinical diagnosis of AD. Guidelines for the diagnosis of possible, probable, and definite AD have been published as the NINCDS/ADRDA criteria and have been validated both clinically and pathologically.[10] However, a uniform international criteria for the diagnosis of AD needs to be implemented in order to compare and contrast studies across borders and address the question of whether or not AD is a heterogeneous disease.

AD Pathology

Extensive neuronal death is observed in AD. A 15% loss of total brain weight is often a result of AD due to the considerable atrophy of the cerebral cortex.[11] Two of the hallmarks of AD are the presence of extracellular neuritic plaques and intracellular neurofibrillary tangles (NFTs). Neuritic plaques are required, by definition, for the diagnosis of definite AD.[12] The plaques are heterogeneous deposits of proteins that were initially termed "amyloid" by the German pathologist Rudolf Virchow in 1853 who erroneously believed them to be composed of a starch-like substance.[13] Five years later Friedrich

and Kekule demonstrated that these deposits were made of protein.[9] The extreme insolubility of the plaques prevented further determination of their chemical nature until 1971 when Glenner and Wong first extracted the β protein from vascular plaques using 6N guanidine HCl and a partial N-terminal sequence was produced.

Senile plaques are a complex, slowly evolving structure, and the time required to generate fully formed, mature plaques may be years or even decades. They are observed in the brain tissue of AD victims after silver staining. The plaques exist as dark, spherical masses with a diameter of 50-100 μm. The major component of the amyloid plaques was determined in 1984 to be the β amyloid protein, a 39-43 amino acid peptide.[14] It was later confirmed that the sequence of the protein found in the senile plaques was identical to the protein found in the vascular plaques.[15]

The β protein is derived by proteolysis from the much larger β amyloid precursor protein (APP). While the biological function of this protein is still unknown, it was discovered in 1992 that the β protein is a normal product of the constitutive proteolytic processing of APP in healthy individuals.[16] In addition to the central core of amyloid, which accounts for more than 60% of the total protein, the plaques also contain dystrophic neurites, altered glial cells and a number of other proteins such as NAC (the Non-β-Amyloid Component of AD), ubiquitin, apolipoprotein E (apoE), apolipoprotein J (or "Clusterin"), interleukin-1, and α_1-antichymotrypsin.[17]

Along with the senile plaques, AD brain tissue is characterized by variable numbers of NFTs which are dense, highly insoluble bundles of abnormal fibers in the cytoplasm of neurons. Ultrastructurally, NFTs appear as paired helical filaments (PHFs). Each filament is unbranched and 10 nm in width. Two filaments are then twisted about each other to produce the PHF.[18]

The major component of the PHFs is not the β amyloid protein, but rather a hyperphosphorylated form of the microtubule-associated protein tau.[17] Tau normally binds and stabilizes microtubules and promotes their assembly by polymerizing tubulin. Microtubules are necessary for neurite extension and maintenance, and for transport along axons and dendrites. NFTs occur in several chronic diseases of the human brain.

For the most part, the distinction between normal brain aging and AD is quantitative rather than qualitative. Most people who live into their late seventies or eighties will have a few senile plaques and NFTs in their hippocampus at the time of death. However, the brains of patients with progressive dementia of the AD type usually show a marked increase in both plaques and tangles than their age-matched controls.[17]

Amyloid Fibril

Three properties used to classify a substance as amyloid are birefringent staining with Congo Red (Figure 1.1), fibrillar morphology as seen by electron microscopy (EM), and an X-ray diffraction pattern consistent with a cross-β fibril. Glenner proposed that the X-ray diffraction pattern of fibrils isolated from the plaques of AD victims were very similar to the cross-β fibril structure observed by Pauling[19] in his studies of silk and polyalanine.[14]

Figure 1.1 Structure of Congo Red.

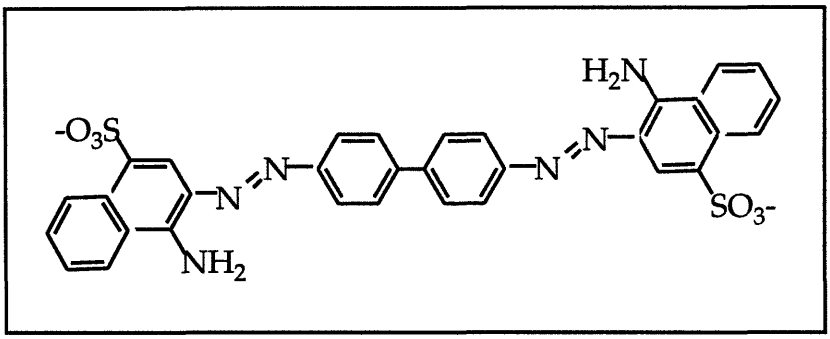

In the cross-β fibril model, the protein chains are extended and anti-parallel to the adjacent chains, forming an anti-parallel β-sheet (Figure 1.2). The β-sheets then stack on top of each other in the fibril. The fibril growth is in the direction of the hydrogen bonding, which is perpendicular to the sheet stacking. Studies by Kurt Halverson and Peter Lansbury showed that the model peptide comprising residues 34-42 of the β protein (β34-42) formed fibrils that had a similar structure to the full-length protein, as seen by X-ray diffraction, yet differed slightly in morphology, as seen by EM.[20]

Since the amyloid fibrils are non-crystalline, structural studies in the past have been limited to low resolution techniques such as EM and X-ray diffraction. Recently, two methods, Fourier-transform infrared spectroscopy (FTIR) and solid-state nuclear magnetic resonance spectroscopy (SSNMR), have been modified and utilized by Peter Lansbury and coworkers in order to create a new method for amyloid structure determination.[21-23] The method is based on the spectral deconvolution by selective incorporation of ^{13}C into the peptide backbone, and has been used to study the structure of β34-42 by measuring distances of up to 6Å between twenty pairs of ^{13}C-labeled carbon atoms in the peptide.

Figure 1.2 Pauling's model for the cross-β fibril.[24]

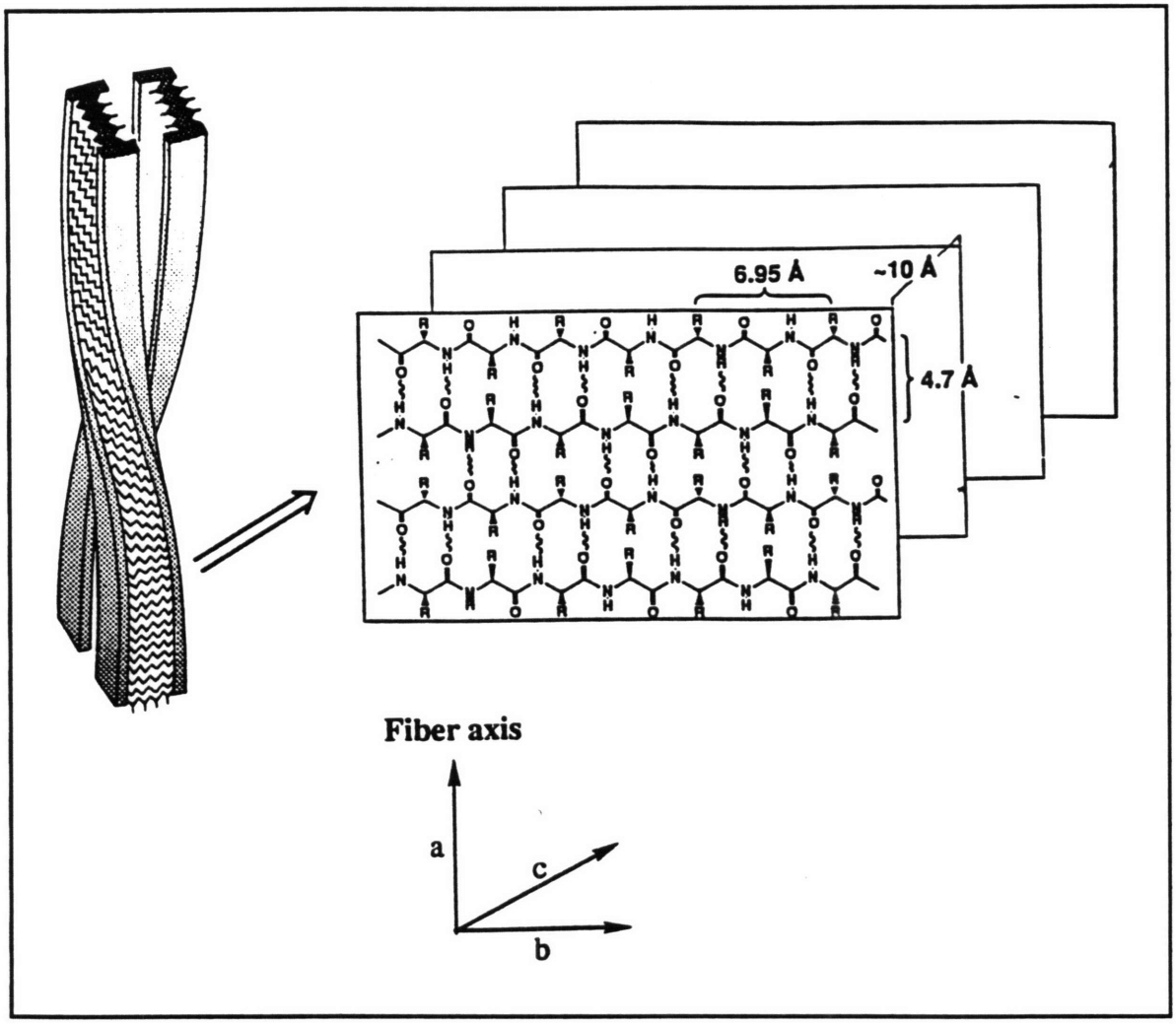

The Causative Role of β Amyloid in AD

Since the original isolation of the β protein from amyloid plaques in 1984, there has been a heated debate over whether the NFTs, the amyloid plaques, or neither is the cause of AD. Some scientists do not believe that amyloid deposition precedes the pathology of AD, but instead argue that senile plaques are produced by the neurites in the plaque periphery as they

degenerate. However, while there is no concrete evidence of the causative role of amyloid in AD, a great deal of research seems to indicate that the amyloid plaques are important in the pathogenesis of AD. Based on the large body of neuropathological, biochemical, molecular biological, and genetic data, the "amyloid-cascade hypothesis" has been made.[25] This hypothesis assumes that AD is a disorder of APP processing which may have a number of different causes and that results in the increased production of the β protein. The aggregation of soluble β protein into amyloid fibrils then sets off a chain of events that results in the formation of senile plaques which are toxic to the surrounding neurons and induce the formation of NFTs, ultimately leading to cell death.

Major support for this hypothesis came from the realization in 1988 that the earliest detectable AD-type structural change in the brains of Down's syndrome (DS) patients, who have three copies of the APP gene and invariably develop AD, is the appearance of diffuse protein deposits.[25] Diffuse plaques consist of an amorphous, largely non-fibrillar form of the β protein that is hypothesized by some to be an immature form of senile plaques. Additionally, studies of DS patients indicate that NFT's develop after senile plaques have formed.[17]

The considerable number of genetic causes for AD, which are discussed further below, are associated with a common neuropathological and clinical phenotype. The phenotype is characterized by abundant amyloid plaques in the brain. Most experts agree that amyloid is the cause of at least some forms of AD and that the formation of NFT's follow the formation of the plaques.[3]

In vitro studies also support the amyloid hypothesis. Aggregation of the soluble β protein into amyloid fibrils is required in order for the β protein to be toxic to a neuronal cell culture.[26] How the fibrillar β protein is toxic to

cells in not well understood. However, the accumulation of aggregated β protein has been associated with a local inflammatory response resulting from the release of interleukin-1β (IL-1β) and other cytokines which then stimulate the production of α1-antichymotrypsin.[25] This inflammation could possibly be responsible for augmenting the cytotoxicity of the β protein and the acceleration of APP processing into the β protein.

One observation that is often sited to disprove the amyloid-cascade hypothesis is that the total number of amyloid deposits correlates weakly with the presence and degree of dementia. However, a modest correlation does exist, but a better correlate to the degree of dementia in AD is the extent of neuritic degeneration and the degree of loss of synapses.[25]

Metabolism of APP

During 1987 and 1988, a number of groups cloned and identified three major forms of APP (695, 751, and 770).[27-32] The larger 751 and 770 forms, which are generated by alternate splicing, contain a 56 amino acid domain in the extracellular region that is homologous to the Kunitz family of serine protease inhibitors (KPI) (Figure 1.3). Additionally, the 770 form also contains a 19 amino acid insert. APP is produced in a wide variety of cell types and the relative levels of the APP isoforms vary according to cell type. APP-695 is particularly abundant in the brain and there is evidence that APP-751 is produced in large amounts in brain regions involved in senile plaque formation.[33]

Figure 1.3 Biogenesis of the β protein as derived from proteolysis of APP.

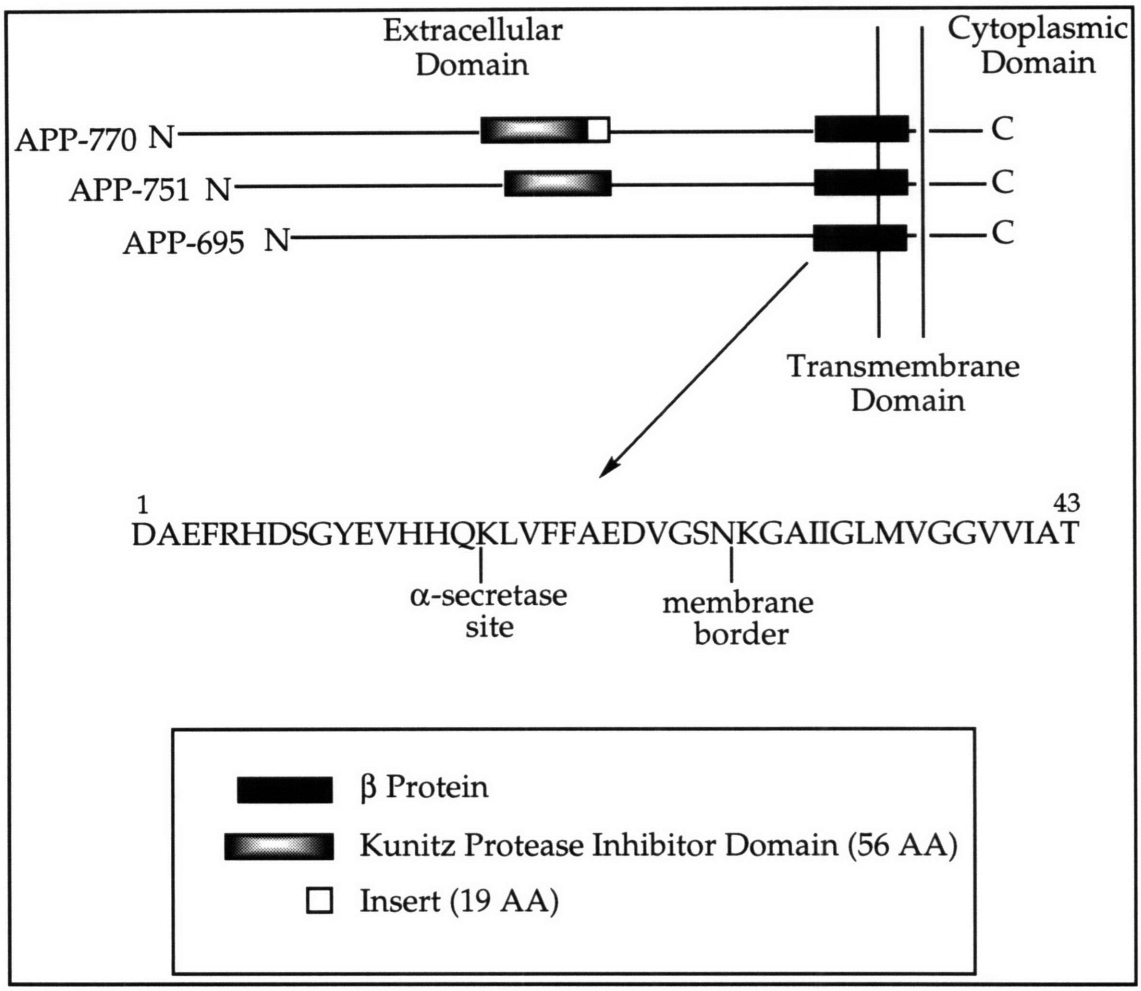

After its synthesis on ribosomes, APP is translocated into the lumen of the endoplasmic reticulum and transported through the Golgi apparatus; some molecules go to the cell-surface. During this process, it undergoes N'- and O'-linked glycosylation, sulfation, and phosphorylation.[34] APP is normally processed in constitutive secretory and putative endosomal-lysosomal pathways. Direct trafficking of βAPP from the trans-Golgi network to the endosomal-lysosomal system has been suggested, but has not been proven.

During its intracellular trafficking, APP may undergo one of two alternate cleavages prior to secretion. The first cleavage of APP is within the β protein sequence (between Lys16 and Leu17) by a protease that has been termed "α-secretase" to produce a large secreted derivative and a small membrane-associated fragment, neither of which contain the entire β protein sequence nor is amyloidogenic.[35] The second "β-secretase" cleavage is at the amino terminus of the β protein. Subsequent cleavage by "γ-secretase" results in the production of the full-length, amyloidogenic protein. It is believed that most APP molecules are cleaved by α-secretase and that only a small subset of APP is processed by β- and γ-secretases to release the β protein.[25] These secretases have not yet been identified.

The constitutive secretion of the β protein raises the question of how the putative transmembrane domain of APP is cleaved by γ-secretase. Additionally, as is evident from the isolation of the β protein from plaques present in the brains of AD victims, there is heterogeneity in the γ-secretase site resulting in C-terminally truncated β proteins ranging from 39 to 43 amino acids in length. There are mutations in APP just outside the β protein sequence that result in both an altered total amount of β protein as well as altered ratios of the C-terminally truncated β proteins (discussed below).[17]

Cleavage by α-secretase was originally demonstrated in cell-surface APP molecules, but subsequent studies have shown this cleavage, in addition to β-secretase, to also occur during intracellular exocytosis.[36] β- and γ- secretase cleavages have also been demonstrated during endocytosis, with the resulting release of the β protein occurring.[37] These studies suggest that constitutive β protein production occurs in a weakly acidic vesicle such as the endosome or a late Golgi compartment and is followed by the rapid secretion of the β protein.

The biological function of APP has not been determined. The secreted forms that contain the KPI domain might be involved in the regulation of protease activity at the cell surface or in the extracellular environment. APP may also have a role in tissue repair in the brain as it is secreted by blood platelets and has an N-terminal amino acid sequence similar to platelet coagulation Factor $X1_a$-inhibitor which is involved in blood clotting.[38] There is evidence that APP promotes cell-cell and cell-extracellular matrix adhesion. APP also promotes survival and growth of neurons in vitro.[17]

Genetic Research

After the identification of the β amyloid protein, research on AD became much more prevalent and scientists began to study with more intensity the contribution of genetics to the development of AD. Presently, data indicates that AD is a heterogeneous disease that exists in two forms. The first is the early-onset familial Alzheimer's disease (FAD), which is hereditary, and the second is the more common late-onset AD. Late-onset AD can be either genetic, as is the case with the inheritance of the *APOE4* allele (discussed below), or "sporadic". The term sporadic is used to indicate AD subjects with no family history of AD and does not necessarily imply a nongenetic etiology.

Genetic dissection of late-onset AD is more problematic than early-onset AD primarily because the disease is very common in the elderly, especially in the 75-84 year age group. Therefore, the existence of multiple AD cases in a given family does not necessarily indicate the inheritance of a common genetic factor, and could be the result of chance or could be the result of a combination of both genetic and sporadic forms of AD.

While the vast majority of AD cases are not associated with mutations, a large number of the early-onset AD cases appear to be directly caused by genetic mutations in the APP gene (Figure 1.4). These cases represent some of the strongest evidence supporting a causative role of the β amyloid protein in the pathogenesis of at least some forms of AD. There is an extraordinarily high statistical correlation between inheriting one of these rare mutations and developing the disease. These mutations are absent in large numbers of unaffected individuals and have been considered by many to be sufficient to cause the disease. Additionally, the phenotype associated with these mutations is typical of AD both clinically and neuropathologically. It is due to these two facts that the assumption was made that all cases of AD might be the result of amyloid deposition.

Figure 1.4 APP mutations associated with early-onset AD.

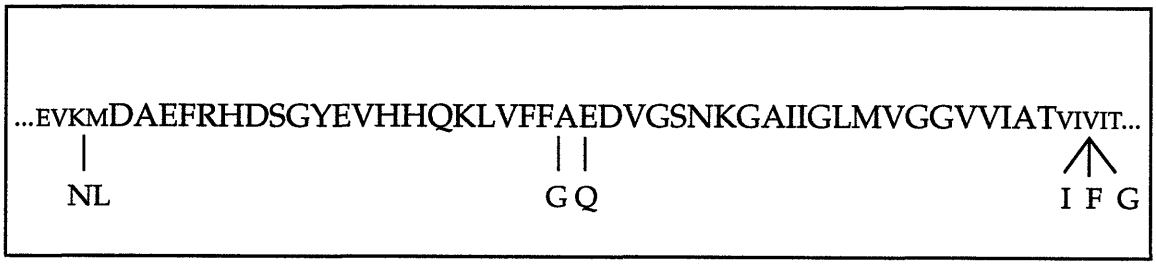

In some families AD is inherited as an autosomal dominant trait.[39] The first pathogenic APP mutation was found in a kindred with autosomal dominant hereditary hemorrhage with amyloidosis of the Dutch type (HCHWA-D). In this disease, a mutation in APP results in a Glu to Gln substitution at position 22 of the β protein.[40] Victims experience strokes after the age of 25 with death occurring by the age of 60. In this disease there is

cerebral amyloid angiopathy, but few AD-type amyloid plaques or NFTs are found on autopsy. The identification of the HCHWA-D mutation was the first demonstration that a APP mutation could result in amyloid deposition and neurologic disease.[5]

Another pathogenic APP mutation was identified in a Dutch family with both cerebral hemorrhage disease and dementia.[41] The disease in this family is a variant of both HCHWA-D disease and AD. There is a mutation in this disease at codon 692 in APP that results in an Ala to Gly mutation at position 21 of the β protein. An exhaustive screening of early-onset FAD victims has proven these mutations to be very rare because they have never been seen in controls and they are clearly pathogenic mutations.[5]

Autosomal dominant APP mutations found in a Swedish familial Alzheimer's disease (FAD) pedigree, in which Val is replaced by either Ile, Phe, or Gly at position 717 in APP770, cause a marked increase in the production of a β protein-bearing, carboxyl terminal, APP derivative. The mutations, which were studied in human neuroblastoma cells (M17) transfected with constructs expressing the wild-type or mutant APP, resulted in five times more β protein in the mutant cells than in the cells expressing wild-type APP. The mutant cell line also released six times more Aβ into the medium.[39] A fourth double mutation (K670N and M671L in APP770) produced a normal total amount of the β protein, but a greater proportion of the variant β1-42.[42] This longer variant has previously been shown to form amyloid more rapidly than the shorter β protein variant, β1-40, *in vitro*.[43]

The clinical, neuropathologic, and genetic characteristics of AD observed in subjects with APP mutations have several features in common.[5] The first is that the age of onset is early, anywhere from 41-64 years of age, depending on the specific mutation. The second is that inheritance is

dominant with complete penetration by the early sixties. No APP mutation carrier living past the age of 67 has been reported.[5] This indicates that in every type of FAD caused by mutations in the APP gene, the genetic defects are sufficient, but not necessary, for causing AD. Lastly, the clinical and neuropathological features of AD caused by genetic mutations are indistinguishable from those of non-APP mutation AD subjects.

A large step forward in AD research was made with the creation of the first real animal model in 1995, the Athena mouse.[44] This transgenic animal has marked overexpression of an FAD-linked mutant APP gene and forms AD-like plaques.[10] However, while the mouse possesses pathology characteristic of AD (without NFTs), clinical symptoms have yet to be observed.

As further evidence indicating the importance of amyloid in AD, Down's syndrome (DS) patients are trisomic for chromosome 21 and therefore have three copies of the APP gene. DS victims show signs of amyloid formation in childhood and always develop early-onset AD.[45] The increase in the amount of the β protein produced by DS patients appears to be responsible for the onset of the disease.

A mutation on chromosome 14, which encodes a recently discovered membrane-associated protein, has been linked to a very early and severe form of FAD. Victims start showing signs of the illness in their early 40's.[46] S182 (or presenilin), the protein encoded by the isolated gene on chromosome 14, was found to have five different missense mutations that altered the predicted amino-acid sequence and occurred only in AD patients. The primary structure of the longest open reading frame currently identified predicts a 467 amino-acid protein with seven hydrophobic, putative membrane-spanning domains. The function of S182 may be as a receptor,

channel protein, or structural membrane protein. Mutations in S182 that alter its hypothetical role in the Golgi or membrane-trafficking might enhance β protein production.[47] It appears that carriers of the chromosome 14 mutation do actually have an increased β protein secretion.[48] Another mutation on a gene located on chromosome 1 has also been identified.[49,50] The product of this gene is a protein with homology to the protein mapped to chromosome 14.

Finally, it was shown in 1993 that the *APOE* gene on chromosome 19 is important in AD. Despite the difficulties in determining genetic causes for late-onset AD, the *APOE* gene has been shown to be a late-onset AD risk factor.[51] Scientists determined that people carrying the *APOE4* allele, which encodes one of the apoE isoforms, had a 15-fold increase in the risk for developing late-onset AD. Three *APOE* alleles exist that encode proteins differing from each other at positions 112 and 158: apoE3 (Cys-112, Arg-158), apoE4 (Arg-112, Cys-112), and apoE2 (Cys-112, Cys-158).

A large number of genetic studies have confirmed that the inheritance of one or two *APOE4* alleles significantly increases the likelihood of developing AD with the risk increasing with an increasing number of *APOE4* alleles.[51] Additionally, the age of onset of AD is decreased and the number of amyloid plaques is increased with increasing number of *APOE4* alleles. The exact mechanism of action of apoE has not yet been determined.

In one study of familial, late-onset AD, approximately 90% of *APOE4* homozygotes were found to have developed the disease by 76 years of age.[51] While this leads to the conclusion that *APOE4* homozygotes will almost inevitably develop AD if they live long enough, it should be noted that the possession of one or two copies of the *APOE4* allele is neither necessary nor sufficient for the development of AD.[52] Unlike carriers of APP mutations

who have a 100% chance of developing AD, *APOE4* heterozygotes and homozygotes may live long into their eighties, nineties, or possibly to over one hundred years of age without developing AD.

All of the evidence leads to the difficult question: How can all of the biochemical and cellular abnormalities be reconciled into a mechanism that will help to explain the pathogenesis of AD? In addition, while most of the FAD types are linked to genetic mutations, the majority of all AD victims are sporadic late-onset cases with no known genetic defects.

Therapeutic Options

Currently there is no proven therapy for victims of AD and research into possible therapeutic options has been thwarted by the complex nature of the disease. The pathology, which shows on a gross level the destructive nature of AD, is only the end-point of a lengthy disease process and is far removed from the initiating events of the disease. In addition, although the pathology of most AD victims is similar, the causes of AD appear to be heterogeneous. As previously mentioned, there are mutations on chromosomes 21 and 14 that are responsible for some forms of FAD. For late-onset AD, the *APOE4* allele is a risk factor, but its presence does not guarantee the onset of AD. The majority of all AD patients (50-60%) do not meet any of the above criteria indicating that other loci contributing to AD remain to be detected and mapped, or that environmental factors, such as the presence of metals, are important.[5] Even after all of the genes are located, substantial effort will be required to understand how each susceptibility factor is involved in AD pathogenesis.

The most ambitious efforts aim to identify probable causes and correct them in an early stage. There are approximately 20 companies developing

AD drugs; the majority have focused on finding a way to prevent amyloid buildup, thereby preventing the extracellular plaques from forming. Scientists hope to use the Athena mouse to test competence of new drug candidates. Characterization of the α-, β-, and γ-secretases involved in APP processing is also an important component of research aimed at the rational design of anti-AD drugs.

While several companies are screening small-molecule drugs that either facilitate clearance of β amyloid or prevent it from aggregating in the first place, others are looking for a drugs that delay disease onset by mimicking the proteins that protect neurons or that minimize the secondary damage by scavenging toxic free radicals.[7]

Once again, these drug candidates address biological mechanisms that are not well understood. Additionally, they are directed at patients in the early stages of disease which is problematic because without any reliable diagnostic test, no one is really sure who is at risk until it is too late. Other companies are looking for drugs that treat the symptoms of AD and are studying genetically engineered cell implants that will deliver nerve-growth factors to areas of the brain that have been damaged by the disease. Drugs that attempt to boost memory and cognition are also being developed.[7]

AD is a complex and seemingly heterogeneous disorder that can strike its victims in the prime of their lives. Victims of this destructive disease may deteriorate into an increasingly dependent state for as long as 20 years until death. AD is devastating not only to the victims, but also to the families who are often the prime care-givers. The social and economic implications of an

ever-growing elderly population, which is expected to represent one in four people in the U.S. within the next 40 years, are frightening.

Because of the increasing importance of AD, scientists have worked intensely in the hope of developing new therapeutics for the disease. However, this process has been thwarted by the inability of these scientists to not only explain the complicated mechanisms involved in the pathogenesis of the disease, but to also diagnose AD in its initial stages.

This thesis describes *in vitro* experiments that were designed to elucidate critical factors in the pathogenesis of AD. Initially, the conformation of the β protein and the effect of mutations on its metal-binding properties was studied (chapter 2). The effect of apolipoprotein E (apoE), a risk factor for late-onset AD, on the aggregation of the β protein was also examined (chapter 3). Finally, through the use of molecular biology, several isoforms of a domain of apoE that is critical to its interaction with β protein aggregation were expressed and studied (chapter 4).

References

(1) Alzheimer, A. *Allg Z Psychiatrie* **1907**, *64*, 146.
(2) Ezzell, C. *J. of NIH Res.* **1995**, *7*, 107.
(3) Hardy, J. *Nature Genetics* **1992**, *1*, 233.
(4) Rubin, E.H. *Advances in Neurology: Alzheimer's Disease*; **1990**, Raven Press, LTD, New York, NY.
(5) Schellenberg, G.D. *Proc. Natl. Acad. Sci. USA* **1995**, *92*, 8552-8559.
(6) Gregg, D. *A Special Report: Alzheimer's Disease*; **1994**, Harvard Medical School Health Publications Group, Boston, MA.
(7) Gross, N.; Flynn, J. *Business Week* **1995**, 108.
(8) *Caring for the Elderly: Reshaping Health Policy*, Eisdorfer, C.; Kessler, D.A.; Spector, A.N., Eds.; The John Hopkins University Press: Baltimore, MD, **1989**.
(9) Selkoe, D. *Scientific American* **1991**, *68-78*,
(10) Martin, E.M. *Neurology* **1987**, *37*, 1201.
(11) Katzman, R. *NEJM* **1986**, *314*, 146.
(12) Khachaturian, Z.S. *Arch. Neurol.* **1985**, *42*, 1097-1105.
(13) Stone, M.J. *J. Am. Soc. Hemat.* **1990**, *75*, 531-545.
(14) Glenner, G.G.; Wong, C.W. *Biochem. Biophys. Res. Commun.* **1984**, *120*, 885.
(15) Masters, C.; Simms, G.; Weinman, N.; Multhaup, G.; McDonald, B.; Beyreuther, K. *Proc. Natl. Acad. Sci. USA* **1985**, *82*, 4245.
(16) Seubert, P.; Vigo-Pelfrey, C.; Esch, F.; Lee, M.; Dovey, H.; Dovey, H.; Davis, D.; Sinha, S.; Schlossmacher, M.; Whaley, J.; Swidlehurst, C.; McCormick, R.; Wolfert, R.; Selkoe, D.; Lieberburg, I.; Schenk, D. *Nature* **1992**, *359*, 325.
(17) Ashall, F.; Goate, A.M. *TIBS* **1994**, *19*, 42-46.
(18) Goedert, M.; Sisodia, S.S.; Price, D.L. *Curr. Opin. Neurobiol.* **1991**, *1*, 441-447.
(19) Marsh, R.E.; Corey, R.B.; Pauling, L. *Acta. Cryst.* **1955**, *8*, 710-715.
(20) Halverson, K.; Fraser, P.E.; Kirschner, D.A.; Lansbury, P.T., Jr. *Biochemistry* **1990**, *29*, 2639-2644.
(21) Halverson, K.H.; Sucholeiki, I.; Ashburn, T.T.; Lansbury, P.T., Jr. *J. Am. Chem. Soc.* **1991**, *113*, 6701-6703.
(22) Ashburn, T.T.; Auger, M.; Lansbury, P.T., Jr. *J. Am. Chem. Soc.* **1992**, *114*, 790.
(23) Spencer, R.G.S.; Halverson, K.J.; Auger, M.; McDermott, A.E.; Griffin, R.G.; Lansbury, P.T., Jr. *Biochemistry* **1991**, *30*, 10382-10387.
(24) Halverson, K.J., The Molecular Determinants of Amyloid Deposition in Alzheimer's Disease, *Ph.D. Thesis, MIT*, **1992.**
(25) Selkoe, D.J. *J. NIH Res.* **1995**, *7*, 57-64.
(26) Lorenzo, A.; Yankner, B. *Proc. Natl. Acad. Sci. USA* **1994**, *91*, 12243.

(27) Kang, J.; Lemaire, H.G.; Unterbeck, A.; Salbaum, J.M.; Masters, C.L.; Grzeschik, K.H.; Multhaup, G.; Beyreuther, K.; Muller-Hill, B. *Nature* **1987**, *325*, 733-736.
(28) Goldgaber, D.; Lerman, M.I.; McBride, O.W.; Saffiotti, U.; Gajdusek, D.C. *Science* **1987**, *235*, 877-880.
(29) Tanzi, R.E.; McClatchey, A.I.; Lamperti, E.D.; Villa-Komaroff, L.; Gusella, J.F.; Neve, R.L. *Nature* **1988**, *331*, 528-530.
(30) Robakis, N.K.; Ramakrishna, N.; Wolfe, G.; Wisniewski, H.M. *Proc. Natl. Acad. Sci. USA* **1987**, *84*, 4190-4194.
(31) Ponte, P.; Gonzalez-DeWhitt, P.; Schilling, J.; Miller, J.; Hsu, D.; Greenberg, B.; Davis, K.; Wallace, W.; Lieberburg, I.; Fuller, F. *Nature* **1988**, *331*, 525-527.
(32) Tanzi, R.E.; Gusella, J.F.; Watkins, P.C.; Bruns, G.A.; St. George-Hyslop, P.; Van Keuren, M.L.; Patterson, D.; Pagan, S.; Kurnit, D.M.; Neve, R.L. *Science* **1987**, *235*, 880-884.
(33) Anderson, J.P. *EMBO J.* **1989**, *8*, 3627-3632.
(34) Weidemann, A.; Konig, G.; Bunke, D.; Fischer, P.; Salbaum, J.M.; Masters, C.L. et al. *Cell* **1989**, *57*, 115.
(35) Esch, F.S.; Keim, P.S.; Beattie, E.C.; Blacher, R.W.; Culwell, T. et al. *Science* **1990**, *248*, 1122.
(36) Sambamurti, K.; Shioi, J.; Anderson, J.P.; Pappolla, M.A.; Bobakis, N.K. *J. Neurosci. Res.* **1992**, *33*, 319.
(37) Koo, E.H.; Squazzo, S. *J. Mol. Biol.* **1994**, *269*, 17386.
(38) Smith, R.P.; Higuchi, D.A.; Broze, G.J. *Science* **1990**, *248*, 1126-1128.
(39) Cai, X.D.; Golde, T.E.; Younkin, S.G. *Science* **1993**, *259*, 514.
(40) Van Broeckhoven, C.; Haan, J.; Bakker, E.; Hardy, J.A.; Van Hul, W.; Wehnert, A.; Vegter-Van Der Vlis, M.; Roos, R.A.C. *Science* **1990**, *248*, 1120-1122.
(41) Hendriks, L.; Van Duijn, C.M.; Cras, P.; Cruts, M.; Van Hul, W.; Van Harskamp, F.; Warren, A.; McInnis, M.G.; Antonarakis, S.E.; Martin, J.J.; Hofman, A.; Van Broeckhoven, C. *Nature Genetics* **1992**, *1*, 218-221.
(42) Suzuki, N. et al. *Science* **1993**, *264*, 1336-40.
(43) Jarrett, J.T.; Berger, E.P.; Lansbury, P.T., Jr. *Biochemistry* **1993**, *32*, 4693-4697.
(44) Games, D.; Adams, D.; Alessandrini, R.; Barbour, R.; Berthelette, P.; Blackwell, C.; Carr, T.; Clemens, J.; Donaldson, T. et al. *Nature* **1995**, *373*, 523.
(45) Potter, H. *Am. J. Hum. Genet.* **1991**, *48*, 1192.
(46) Sherrington, R.; Rogaev, E.I.; Liang, Y.; Rogaeva, E.A.; Levesque, G.; Ikeda, M.; Chi, H.; Lin, C.; Li, G.; Holman, K.; Tsuda, T.; Mar, L. et al. *Nature* **1995**, *375*, 754.
(47) Selkoe, D.J. *Nature* **1995**, *375*, 734-735.
(48) Querfurth, H.W.; Wijsman, E.M.; St. George-Hyslop, P.H.; Selkoe, D.J. *Mol. Brain Res.* **1995**, *28*, 319-337.

(49) Levy-Lahad, E.; Wijsman, E.M.; Nemens, E.; Anderson, L.; Goddard, K.A.B.; Weber, J.L.; Bird, T.D.; Schellenberg, G.D. *Science* **1995**, *269*, 970-973.
(50) Rogaev, E.I.; Sherrington, R.; Rogaeva, E.A.; Levesque, G.; Ikeda, M. et al. *Nature* **1995**, *376*, 775-778.
(51) Corder, E.H.; Saunders, A.M.; Strittmatter, W.J.; Schemchel, D.E.; Gaskell, P.C.; Small, G.W.; Roses, A.D.; Haines, J.L.; Pericak-Vance, M.A. *Science* **1993**, *261*, 921.
(52) Uttermann, G. *Curr. Biol.* **1994**, *4*, 362-365.

Chapter 2

Metal-Binding Studies of the β Protein

The presence of insoluble protein deposits in the form of senile plaques surrounded by damaged tissue is an invariant feature of AD. In addition to genetic studies that implicate the β amyloid precursor protein (APP) in the pathogenesis of AD,[1,2] other studies have shown that in its insoluble fibrillar form the β protein is toxic to cultured neurons.[3,4] Families where AD cosegregates with mutations in the gene on chromosome 21 encoding APP have been identified. The presence of amyloid is also a central pathological event in other diseases such as hereditary cerebral hemorrhage with amyloidosis-Dutch type (HCHWA-D) where a mutation in the β protein sequence is responsible for the fatal deposition of amyloid.[5] Furthermore, other higher mammals that encode for the same β protein develop amyloid deposits while rodents that encode for a β protein containing three amino acid substitutions do not form amyloid plaques.

In the absence of any significant quantity of brain derived material, work with synthetically derived material has proven to be necessary and important in studying the effect that a genetic mutation might have on the processing or solubility of the precursor and the resulting fragments. A

mutation may result in a change in the proteolysis of the precursor which could either liberate an insoluble fragment of an otherwise soluble precursor, or cause an increase in the production of an amyloidogenic protein. A mutation might also induce a conformational change that results in the aggregation of that protein.

This chapter describes studies of several model peptides that examine the effect of point mutations and the presence of metals on the secondary structure of the β protein. Metal-binding studies were performed on several peptides derived from the β protein and β protein analogs using circular dichroism (CD) in order to provide information that will help to determine the mechanism of amyloid formation.

Circular Dichroism

Circular Dichroism (CD) spectroscopy is a technique commonly used to study the secondary structure of polypeptides and proteins in solution. CD has become a standard tool of many protein chemists. CD spectroscopy uses chirally polarized light comprised of left- and right-circularly polarized components. The CD signal arises from the differential absorption of these components in optically active molecules, and is reported in terms of ellipticity (θ) with a unit of degrees. The CD signal of an optically active molecule most often occurs in the same region of the spectrum that it would normally absorb in standard UV-VIS spectroscopy.

In proteins and polypeptides, amide bonds, aromatic side chains, and disulfide bonds are all optically active. However, the signals from side chains and disulfide bonds are much smaller than that from the backbone amide bond.[6] The CD spectrum of proteins is primarily a result of the amide

chromophore, the most informative functionality to study because it is very sensitive to changes in the secondary structure of the polypeptide backbone. The environment in which a protein is studied (i.e. pH, solvent, temperature) can have a large effect on the secondary structure of the protein.

The four major categories of secondary structure, α-helix, β-sheet, β-turn, and random coil, each produce a characteristic CD spectrum. In an α-helix, the carbonyls and amide groups align such that a macroscopic dipole occurs which results in a strong positive signal at 192 nm and two negative signals at 208 nm and 222 nm.[7] The spectrum for a β-pleated sheet shows a maximum near 198 nm and a minimum near 217 nm. However, these transitions may shift depending on the type of β-sheet present and its degree of twist.[7]

CD data can be analyzed by a large number of techniques. The method of Greenfield and Fasman is based on the spectra of polylysine and polyglutamate under conditions where "pure" α-helical conformations were obtained. The absorbance at 208 nm is used to calculate the amount of α-helix present.[7] In the method of Morrisett, which is based on the work of Greenfield and Fasman, the amount of α-helicity is calculated by using the 222 nm absorption.[8] It has been suggested that using the absorption at 208 nm results in a much more accurate calculation of α-helix in the presence of β-sheet content because there is little contribution from other structures at this wavelength.[9] The percent of α-helical content can be calculated by the following equations according to the methods of Greenfield and Fasman (Equation 2.1) and Morrisett (Equation 2.2):

Equation 2.1

$$\alpha\text{-helix} = \frac{([\theta]_{208} - 4{,}000)}{(33{,}000 - 4{,}000)}$$

Equation 2.2

$$\alpha\text{-helix} = \frac{([\theta]_{222} + 3{,}000)}{(36{,}000 + 3{,}000)}$$

Many computer programs have been written that will calculate all of the secondary structural components in a given protein based on its CD spectrum. One of these programs is PROSEC which calculates the component contributions based on the CD spectra derived from crystalline proteins of known secondary structures.[10] Other programs are based on the CD spectra of unnatural polypeptides.

Data obtained from CD spectra can be extremely useful in examining the secondary structure of proteins. However, there are several potential sources of inaccuracy that result from improper interpretation of the data. Fitting programs can lead to false component calculations. Programs based on the structures of proteins may be inadequate for small polypeptides. Conversely, programs based on "pure" peptide structures can be inadequate for studying protein structure because the long peptide homopolymers may not be representative of those structures found in large proteins. The signal produced by an α-helix is proportional to the chain length and there are few examples of homopolymers that depict pure β-turn structures.[11] Additionally, it has been shown that unless the CD spectral data extends down to 184 nm, only the α-helical component is accurate.[12]

Solution Structure of the β protein

The solution structure of the β protein has previously been studied by several groups using CD spectroscopy in order to provide a better understanding of the relationship between the accumulation of amyloid fibrils in AD and the mechanisms involved in the aggregation of the β protein. Barrow and Zagorski have found that the β protein adopts mixtures of β-sheet, α-helix, and random coil conformations in solution with the relative ratios being strongly influenced by the solution conditions.[9] They also found that the hydrophobic residues at the C-terminus of the β protein are important in the initial stages of folding.

Helical structure was induced more readily in β1-39 with the fluorinated alcohols trifluoroacetic acid (TFE) and hexafluoroisopropanol (HFIP) than in β1-42. This indicated that β1-42 forms a more stable β-sheet structure in solution. Results also demonstrated that the β-sheet structure was intermolecular. At pH 4 to 7, the α-helical structure of β1-28, β1-39, and β1-42 was destabilized and the formation of β-sheet structure in β1-42 was concentration-dependent.

The sensitivity of the β protein conformation to pH suggests that it may be produced from APP in acidic conditions such as those found in the lysosome, and the increased β-sheet structure in β1-42 also indicates that its production could be more pathogenic than β1-40.[9] The tendency of the β protein to form β-sheet structures and subsequently aggregate at low pH has been demonstrated.[13] These observations may be useful in elucidating the molecular mechanism of AD.

A Mutation in the β Protein Causes HCHWA-D

The presence of amyloid is also a central pathological event in diseases other than AD such as hereditary cerebral hemorrhage with amyloidosis-Dutch type (HCHWA-D) in which there is extensive deposition of amyloid in the blood vessels of the leptomeninges and cerebral cortex. This leads to increased vessel deterioration and results in cerebral hemorrhages.[5] The main component of this amyloid is a 39 amino acid variant of the β protein that is missing the carboxyl terminal amino acids. This variant has an E22Q mutation in the β protein sequence. Previously it was proposed that this modification alters the normal cleavage of the β protein at the neighboring Lys_{16} - Leu_{17} site resulting in a cleavage along an amyloidogenic pathway.[14]

Increasing evidence suggests that the three C-terminal amino acids of the β protein are critical to amyloid deposition.[15] Therefore, APP mutations that produce an increased ratio of β1-42 to β1-40 may be critical in the pathogenesis of AD. However, based on this same evidence, one would not expect the preferential deposition of the HCHWA-D analog. The existence of deposits in the blood vessels of HCHWA-D victims indicates that the mutation at position 22 in the β protein sequence is critical to its aggregation and may result in a change in its conformation.

Previous studies have compared the conformations of the HCHWA-D and wild-type β protein analogs.[16] Both peptides adopt primarily β-sheet structures at pH 7 under aqueous conditions by FTIR. At pH 12 only the Dutch-type peptide possesses a significant amount of antiparallel β-sheet structure while the wild-type peptide shows absorptions characteristic of unordered structures. Analysis by CD also suggests that the Dutch-type peptide may contain a larger amount of β-structure than the wild-type

peptide. Other studies have also shown that β-conformation and the formation and stability of fibrils were greatly enhanced by the single E22Q mutation in the HCHWA-D peptide.[17]

Mammalian Sequence Variants

Although a large number of species have a gene encoding APP, the generation and deposition of the β protein into insoluble amyloid plaques is largely restricted to aged primates and other higher mammals such as the monkey, dog and bear, in addition to aged humans.[17-19] Within the β protein region, the sequences for these mammals are identical to the human form of the β protein. Rats and mice, however, encode for an APP that contains three point mutations in the β protein region (Arg5Gly, Tyr10Phe, and His13Arg) as is seen in Figure 2.1.[20] Although the rodent form of the β protein is produced by rat neuronal culture, amyloid deposits consisting of the rodent analog have not been demonstrated in rats or mice.

Figure 2.1 Sequence variability in the primate and rodent β proteins.

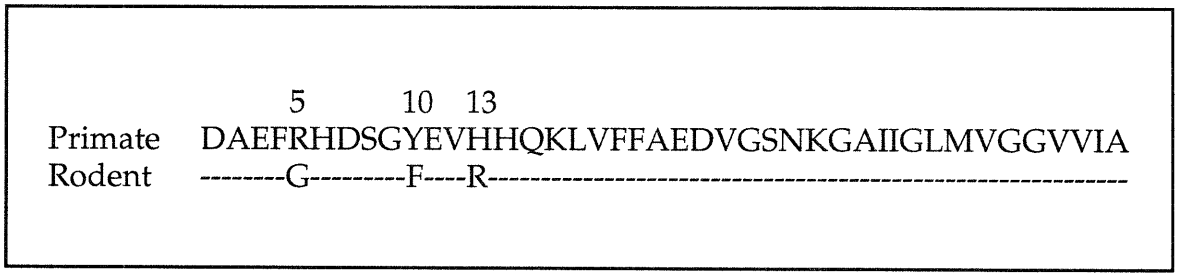

It has been suggested that the amino acid substitutions that are found in the rodent β protein might prevent the aggregation of the β protein into insoluble plaques. While the rat and mouse variants of the β protein

sequence are clearly as amyloidogenic *in vitro* as the human sequence, kinetics measurements have actually demonstrated that the rodent peptide formed a β-conformation more rapidly that the human sequence.[17] Three dimensional structural differences have been noted between rodent and human amyloid fibrils. These differences are reflected in FTIR and CD spectroscopy and demonstrate that the rodent sequence has a slightly higher content of β-turn structure.[18] However, the human β protein sequence remained in a β-sheet conformation at lower peptide concentrations than the rodent analog. It is possible, therefore, that higher peptide concentrations are required for aggregation of the rodent analog to occur *in vivo*.

While FTIR and CD studies show secondary structural differences between the human and rodent β proteins, EM has demonstrated that both types of fibrils have a similar morphology. Additionally, both show a green birefringence under polarized light after Congo red staining.[18] The lack of amyloid depositions in the brains of aged rats or mice cannot be ascribed to a lowered tendency of the rodent β protein analogs to form insoluble aggregates due to the *in vitro* studies. It may be that the rodent β protein does not form amyloid plaques *in vivo* because the point mutations alter the proteolytic processing of APP in a protective manner resulting in the production of non-amyloidogenic fragments.

Effect of Metals on the Conformation of the β Protein

Exposure to certain metals such as aluminum, zinc, and copper has been proposed to be a risk factor for the development of AD, but so far epidemiological evidence has been inconclusive.[21] Metal ions may contribute to the disease by causing a conformational change upon binding to the β

protein that accelerates its aggregation. Evidence for altered zinc metabolism, including elevated CSF levels of 80% and decreased temporal lobe levels, has been found.[22] An abnormality in the distribution of zinc may cause these high extracellular and low intracellular zinc concentrations in the AD brain.

β-sheet structures are frequently found associated with zinc-binding proteins and CD studies have shown that fibril formation is associated with the attainment of β-sheet structure.[23] A likely binding site for metals involves the pair of histidine residues at positions 13 and 14 of the β protein in conjunction with carboxylate anions from surrounding amino acids. These amino acids are known to participate in zinc-binding in several enzymes and other proteins.[24] The rat β protein variant has a His to Arg replacement at position 13 of the β protein which may result in a diminished affinity for metal ions.

Several groups have reported conflicting results regarding the affinity of the β protein towards zinc and copper. In several of these studies, a comparative analysis has been made between several β protein analogs, such as the wild-type, rodent, and Dutch forms, and the effect of zinc on their aggregation. Bush and coworkers found that the human and rat peptides differ drastically in their aggregation response to zinc, with a 100-fold lower $[Zn^{2+}]$ needed to promote aggregation of the human β protein than to promote aggregation of the rat β protein.[25] In contrast, Maggio and coworkers found no significant difference between the rat and human peptides in the $[Zn^{2+}]$ required to induce aggregation.[21]

The wild-type and Dutch β proteins showed little difference in the amount of radioactive zinc that they bound, suggesting that the Glu at position 22 in the wild-type β protein is not involved.[23] The study also found that copper, present at 20 times the concentration of zinc, was able to almost

completely displace the bound radioactivity. This result suggests that while the binding site has a greater affinity for zinc, this site may not be unique; however, some metals, such as calcium, were not able to displace the bound zinc. A study by Bush, however, found that even copper was not able to effectively displace zinc from the peptide, although it was able to stabilize dimeric forms of the β protein.[25]

The above contradictory data may be the result of the several varied experimental techniques that were used to study the problem. Interestingly, the observed binding affinity that has been widely reported is in the physiological range of zinc concentrations in various tissues.[26] The hippocampus has the highest overall zinc content of the CNS and is also an area consistently affected by pathological deposition of the β protein in AD.[27] The cerebellum, which has extremely low concentrations of zinc, also shows very few amyloid plaques in AD. The extent of zinc-binding to the β protein also depends on how much of the zinc is "free" in solution, how much zinc is bound to other proteins, and the relative affinities of these competing proteins for the available metal ions. However, it is possible that the *in vitro* metal-binding phenomenom of the β protein may have no *in vivo* relevance to AD.

Peptide Analogs

The effect of salt and HFIP on the conformation of the full length β protein was originally studied using β1-40. However, due to the high cost of β1-40, and in order to elucidate the effect of point mutations on the structure of the β amyloid protein, several model peptides were synthesized and subsequently studied by CD. Because of the extreme insolubility of the full-

length protein, and to facilitate peptide synthesis and purification, C-terminally truncated analogs were studied (Figure 2.2). Initially, the β1-17 fragment was analyzed. However, this peptide had little structure, even in the presence of HFIP. Additionally, while this peptide contains the locations for the three rodent point mutations, it does not contain any other APP mutations associated with AD.

Figure 2.2 Full-length and truncated β protein peptides.

	1	17	28	40
β1-40	DAEFRHDSGYEVHHQKLVFFAEDVGSNKGAIIGLMVGGVV			
β1-28	DAEFRHDSGYEVHHQKLVFFAEDVGSNK			
β1-17	DAEFRHDSGYEVHHQKL			

Ultimately, the peptide comprising the first 28 amino acids of the β protein sequence (β1-28) was studied. The N-terminal 28 amino acids are derived from the extracellular APP while residues 29-42 of the β protein are derived from the putative transmembrane domain. β1-28 also contains the α-secretase proteolytic site where the precursor is cleaved between residues 16 and 17 of the β protein sequence.[28] All three of the mutations found in the rodent sequence of the β protein and some of the genetic mutations are also located in the β1-28 segment of the protein.

Three truncated peptides, each containing only one of the three amino acid changes found in the rodent β-protein (β1-28 R5G, β1-28 Y10F, and β1-28 H13R), along with one truncated peptide containing two of the changes (β1-28 R5G, Y10F) were synthesized (Figure 2.3). The purpose of these peptides was

to determine whether or not the amino acids substitutions resulted in a conformation that inhibited the binding of metals to the peptides in a way that might prevent their aggregation. Additionally, a truncated peptide containing the Dutch mutation responsible for HCHWA-D (β1-28 E22Q) was synthesized.

Figure 2.3 Synthetic peptide analogs of the β protein.

```
                1     5        10  13              22        28
Human           DAEFRHDSGYEVHHQKLVFFAEDVGSNK
Rat             --------G---------F----R------------------------------
R5G             --------G-----------------------------------------------
Y10F            ------------------F-----------------------------------
R5G,Y10F        --------G---------F-----------------------------------
H13R            ------------------------R-----------------------------
E22Q            ----------------------------------------Q-------------
```

Although the C-terminus of the β protein has been shown to behave similarly to the full length protein and to produce amyloid fibrils with nearly identical EM and X-ray diffraction patterns, it has been proposed that the N-terminal portion of the protein may also be critical in determining the conformational state of the protein. While the C-terminus is comprised of mostly hydrophobic amino acid residues, the N-terminus contains a large number of hydrophilic amino acid residues. The N-terminus contains proposed metal-binding regions, where the metal cations could possibly bind to the histidine residues or carboxylate containing residues such as aspartic or glutamic acid.[22] The structural evidence obtained from pH studies also

suggests that the ionization state of key residues in the β1-28 region may affect the assembly of β-strands as influenced by His-Asp/Glu salt bridges.[13]

Analysis of the β Protein and Peptide Analogs by Circular Dichroism

The remaining portion of this chapter describes experiments that were designed to probe the effect of mutations in the β protein sequence on the metal-binding properties of the peptides. Specifically, β protein analogs were studied by CD, and differences in the conformations of the analogs in the presence of metals were examined.

Due to the inherent problems in using fitting programs, and the lack of data below 190 nm, the α-helical content of spectra described in this chapter was calculated using the methods of Greenfield and Fasman[7] and of Morrisett[8]. CD in the experiments discussed in this chapter was used primarily as a tool for quantifying changes in the α-helix content of the polypeptide structures rather than absolute values.

While conformational changes in the presence of metals as monitored by CD do not reveal specific binding interactions, this method is useful in detecting differences in conformational changes that occur in peptides differing by only one amino acid. Experiments performed in this chapter are based on the premise that if a peptide shows little conformational change in the presence of a metal, it must have a weaker interaction with that metal than a peptide that shows a large conformational change. The identification of specific metal-ligand interactions is beyond the scope of this thesis.

The peptides described above were studied in the presence of various concentrations of salt and organic solvent in order to probe the conformational properties of the peptides. The standard buffer used was 6.25

mM tris hydrochloride at pH 7.4. A phosphate buffer could not be used due to the insolubility of some of the salts. The CD spectra of most of the β protein analogs were consistent with a random-coil conformation when examined in buffer alone.

However, the peptides, excluding the β1-17 peptide, showed an increase in α-helix upon the addition of organic solvents such as TFE and HFIP. These solvents are known to *stabilize* regions of a peptide that are intrinsically α-helical rather than *induce* random helix formation. TFE and HFIP are weaker proton donors than water and therefore promote intramolecular hydrogen bonding to occur instead of intermolecular hydrogen bonding with the solvent.[9] HFIP was used for the CD studies rather than TFE because a smaller percentage of HFIP was required to stabilize helix formation.

The full-length β protein and analogs were analyzed under solvent conditions that ranged from 0% to 60% HFIP content. For several peptides, the peptides stock solution were initially dissolved in HFIP. In these cases, CD analysis of the peptides in a minimum of 12.5% HFIP was required. The CD spectra of the β1-28 peptides were taken in the presence of 16% HFIP, the minimal amount of HFIP required to observe structure.

The conformational changes in the peptides resulting from the addition of aqueous salt solutions were also analyzed. CD spectra were taken in the presence of 1 μM to 1 mM of either $CaCl_2$, $CuCl_2$, or $ZnCl_2$. The peptide and salt solutions were added to the buffer immediately prior to scanning in order to prevent aggregation of the peptides. Changes in the conformations of the peptides due to aggregation, which would decrease the amount of soluble peptide analyzed and result in a smaller CD signal, were ruled out after no insoluble material was collected by centrifugation.

The results of the conformational studies of the full-length β protein and the β protein analogs are described below. The CD spectra were interpreted using the method of Greenfield and Fasman[7] and the method of Morrisett[8]. The interpretation of results are reported as a change in the percent α-helix rather than in absolute terms due the analytical limitations of CD as discussed above.

Circular Dichroism Studies of β1-40

Prior to the synthesis of truncated peptide analogs, initial CD experiments were performed using the full-length β1-40 . Preliminary CD studies were designed to determine the effect of HFIP on secondary structure as well as determine the concentration dependence on the conformation of the peptide.

In 12.5% HFIP (the lowest amount of HFIP possible due to the necessity of making the stock peptide solution in 90% HFIP), β1-40 showed little α-helical content. However, according to the 208 nm absorption, increasing the HFIP to just 25% resulted in a 67% increase in the percent α-helix. Little change was noted from increasing the HFIP above 25%. A smaller increase in α-helix of 12% is observed as calculated by the 222 nm absorbance.

Figure 2.4 10 μM β1-40 vs. % HFIP.

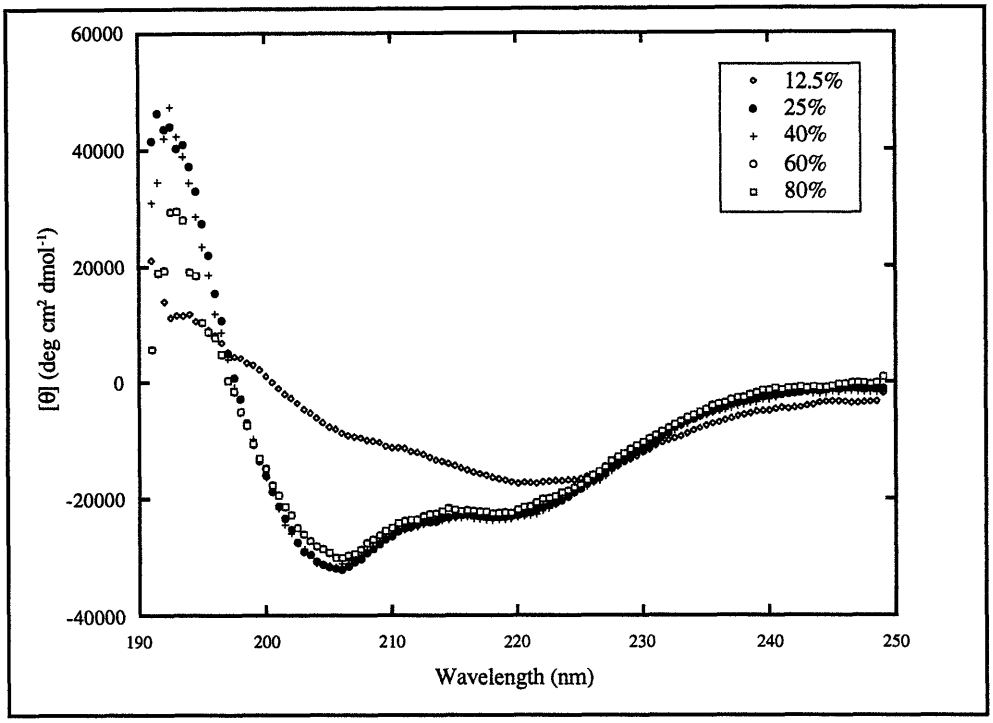

Table 2.1 Percent α-helix of 10 μM β1-40 vs. % HFIP.

	12.5%	25%	40%	60%	80%
208 nm	20	87	86	81	81
222 nm	51	63	64	59	59

Figure 2.5 shows that there is not a strong concentration dependence for β1-40 from 5 μM to 20 μM. There is only an 8% increase at 208 nm absorbance and a 3% increase at 222 nm. For all subsequent CD experiments with β1-40, the conditions were set at 10 μM β1-40 in the presence of 25% HFIP.

Figure 2.5 β1-40 (25% HFIP) vs. concentration.

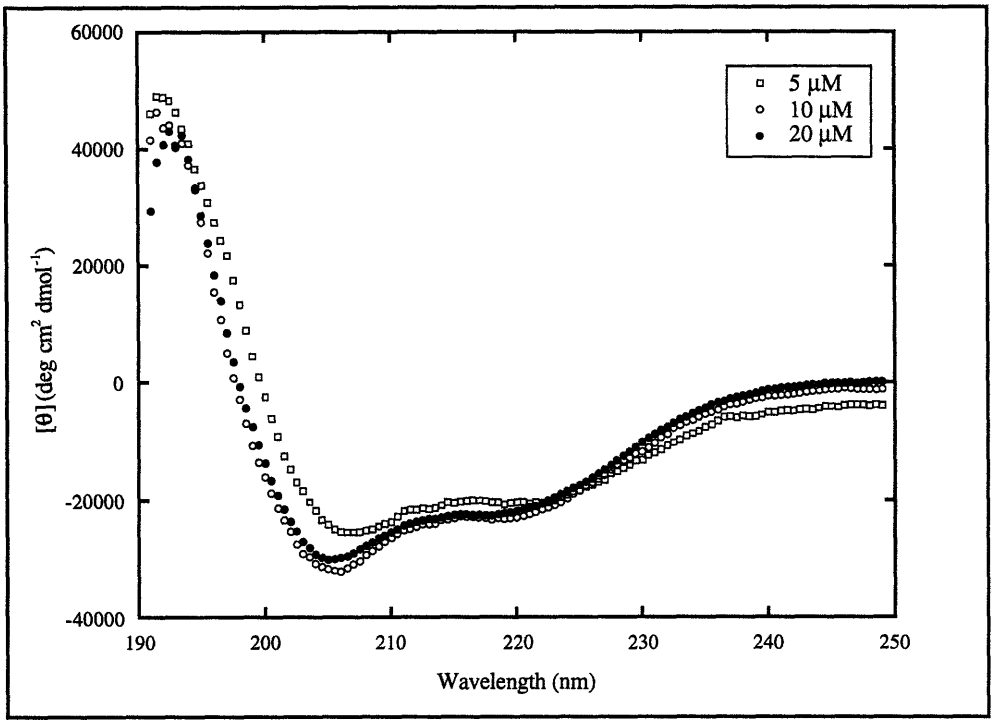

Table 2.2 Percent α-helix of β1-40 (25% HFIP) vs. concentration.

	5 μM	10 μM	20 μM
208 nm	73	87	81
222 nm	60	63	60

In order to determine the conformational changes of β1-40 that occur over time, a single 10 μM sample of β1-40 was scanned five times. Figure 2.6 shows that there is a significant decrease in the amount of α-helix present over five scans when it is manipulated at room temperature in buffer. Due to this finding, β1-40 (in a 90% HFIP stock solution) and concentrated salt stocks were added to buffer immediately prior to scanning.

Figure 2.6 β1-40 (25% HFIP) titration test.

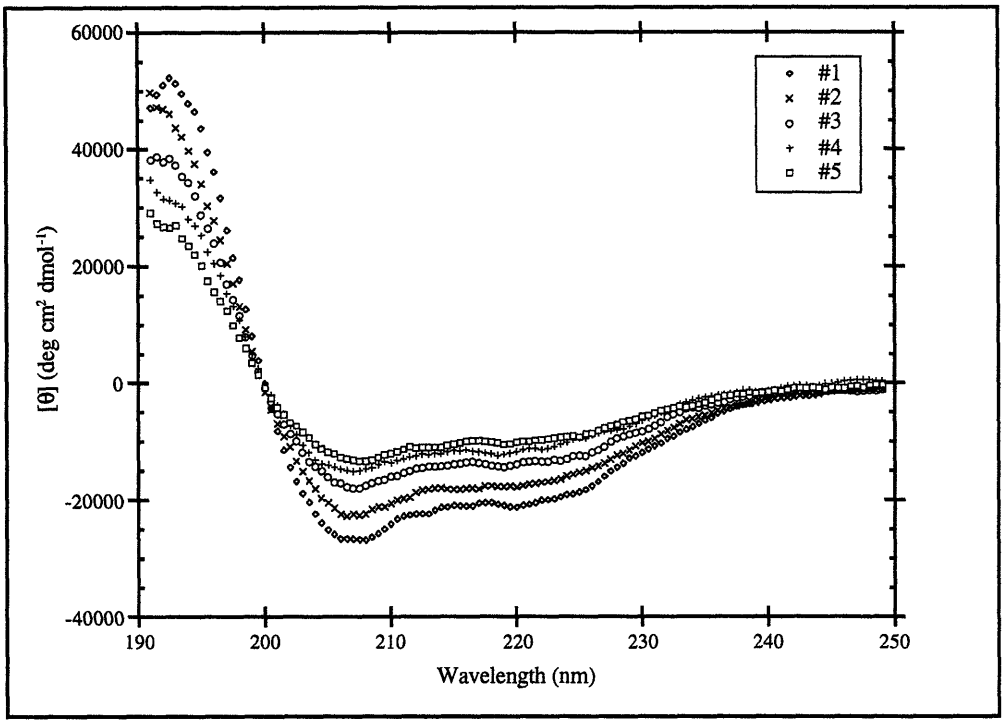

Table 2.3 Percent α-helix of a single 10 μM β1-40 sample scanned repeatedly.

	#1	#2	#3	#4	#5
208 nm	78	63	46	37	32
222 nm	59	51	42	37	32

The effect of divalent metal cations on the conformation of β1-40 was also examined. CD spectra of β1-40 were taken in the presence of 1 mM $ZnCl_2$, $CaCl_2$, and $CuCl_2$ (Figure 2.7). Very little change in secondary structure was observed upon the addition of 1 mM $CaCl_2$. However, large changes were observed in the presence of $ZnCl_2$ and $CuCl_2$. Table 2.4 shows a decrease of 87% and 47% in α-helix at the 208 nm absorbance upon the addition of

$ZnCl_2$ or $CuCl_2$, respectively. Due to these results only the effects of the $ZnCl_2$ and $CuCl_2$ salts were studied further.

Figure 2.7 10 μM β1-40 (25% HFIP) vs. salt.

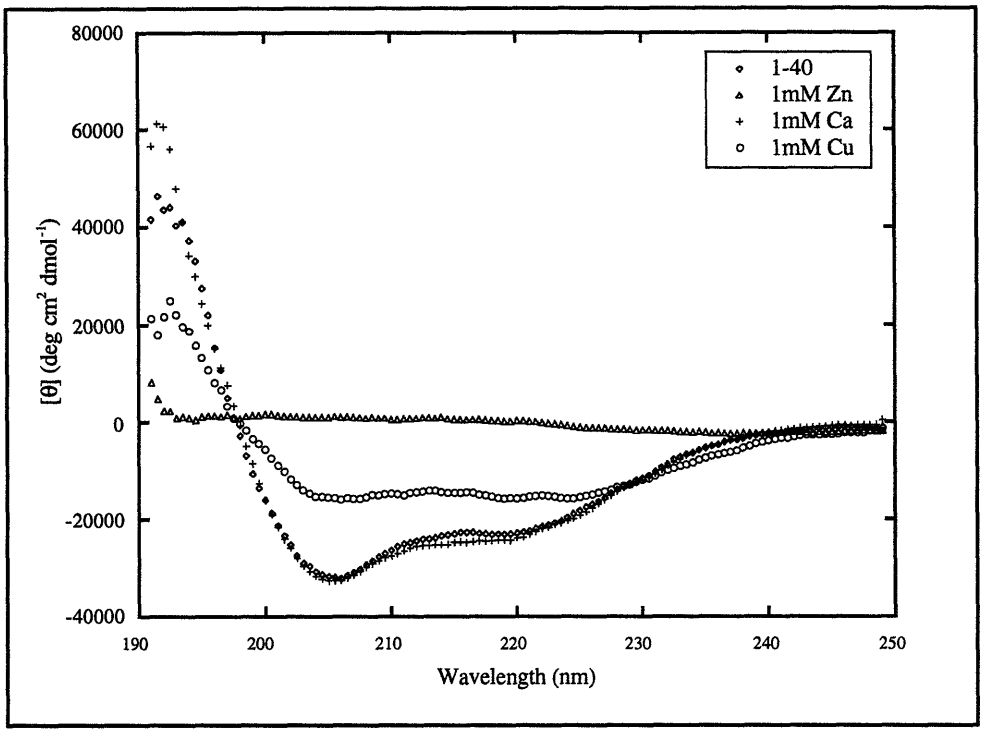

Table 2.4 Percent α-helix of 10 μM β1-40 vs. 1 mM salt.

	β1-40	$ZnCl_2$	$CaCl_2$	$CuCl_2$
208 nm	87	0	89	40
222 nm	63	8	64	46

A titration of β1-40 with $ZnCl_2$ showed that there is little change in the conformation from 100 μM to 1 mM $ZnCl_2$ (Figure 2.8) However, as is evident from Table 2.5, significant decreases in α-helical structure are observed upon the addition of small amounts of $ZnCl_2$.

Figure 2.8 10 μM β1-40 (25% HFIP) vs. $ZnCl_2$.

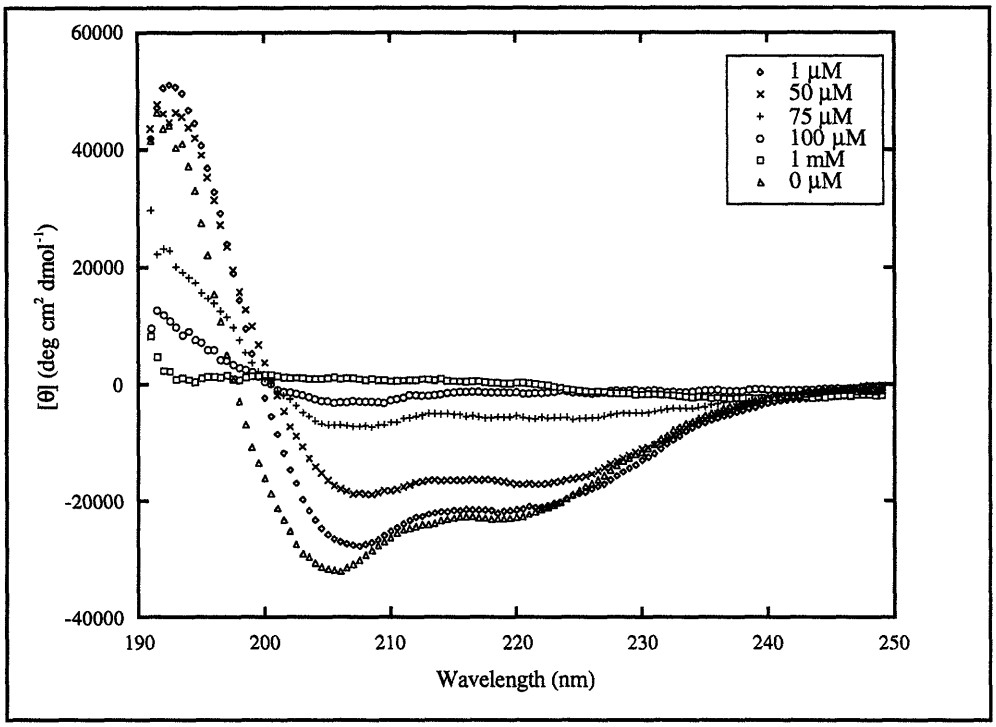

Table 2.5 Percent α-helix of 10 μM β1-40 vs. $ZnCl_2$.

[$ZnCl_2$]	0 μM	1 μM	50 μM	75 μM	100 μM	1 mM
222 nm	87	81	51	10	0	0
208 nm	63	62	51	22	11	8

A titration with $CuCl_2$ also showed large decreases of 87% and 52% in α-helical content at the 208 nm and 222 nm absorbances, respectively, from 0 to 500 μM $CuCl_2$ (Figure 2.9).

Figure 2.9 10 μM β1-40 vs. $CuCl_2$.

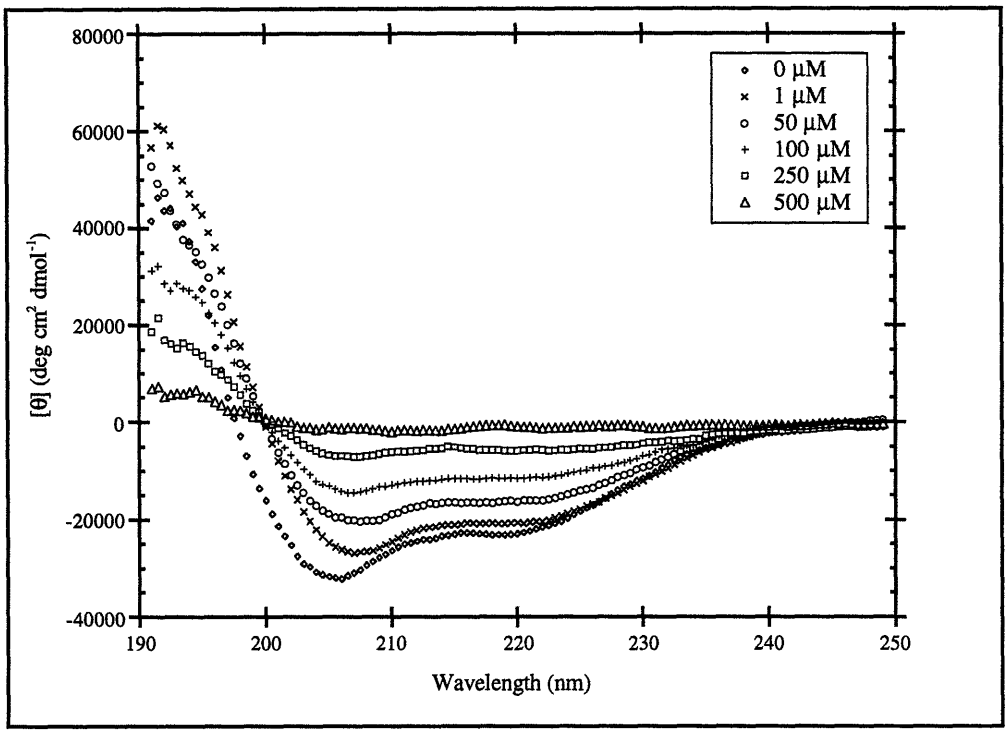

Table 2.6 Percent α-helix of 10 μM β1-40 vs. $CuCl_2$.

	0 μM	1 μM	50 μM	100 μM	250 μM	500 μM
208 nm	87	77	56	35	10	0
222 nm	63	60	49	37	22	11

Circular Dichroism Studies of β1-17

In order to study the effect of the mutations found in the rodent β protein on its conformation, β1-17 was initially studied. The β1-17 sequence contains all three of the amino acid sites that are different in the rodent analog. However, studies revealed that the peptide was too short to possess

any secondary structure other than random coil, even in the presence of TFE (Figure 2.10).

Figure 2.10 50 μM β1-17 vs. TFE.

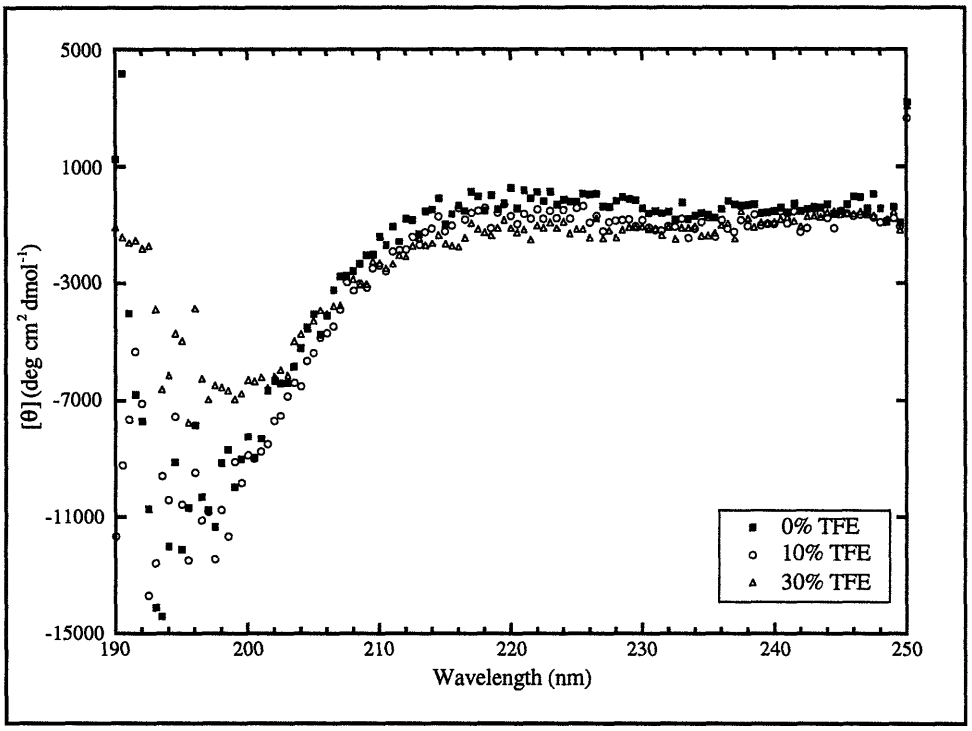

In Figure 2.11, the CD spectra indicate that β1-17 has little or no α-helix or β-sheet, even at a concentration of 300 μM. All subsequent studies were performed using analogs of β1-28.

Figure 2.11 Concentration dependence of β1-17.

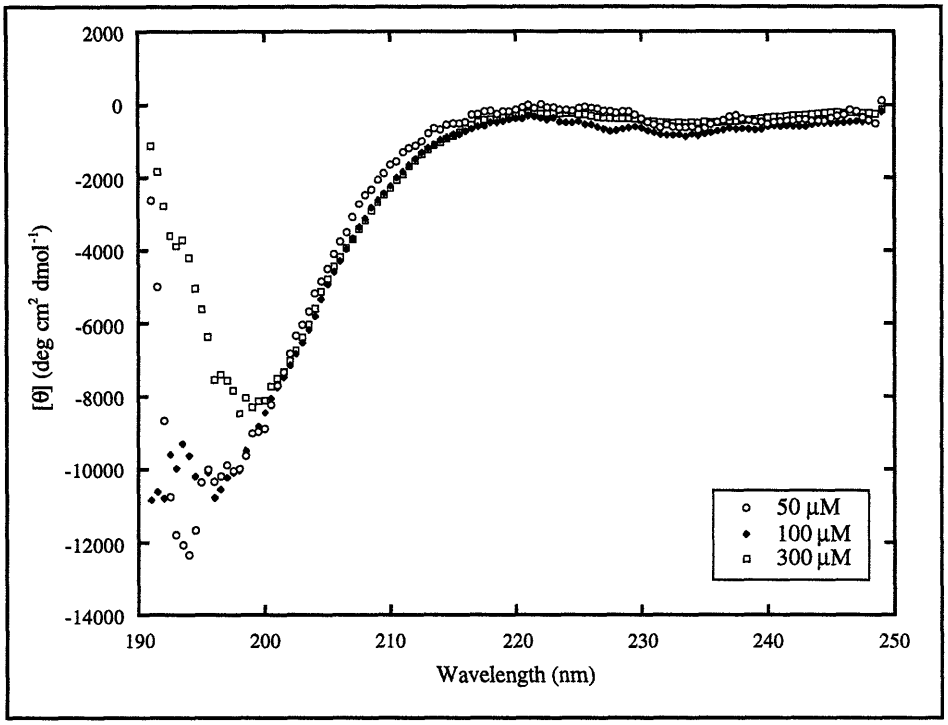

Circular Dichroism Studies of β1-28 Analogs

β1-28 Results

Peptides comprising the first 28 amino acids of the human β1-40 variant as well as the rodent β1-40 variant were synthesized and studied. As was the case with the full-length β protein, incubation of the peptide in buffer can result in significant changes in secondary structure. There was a 37% decrease in α-helical content at the 208 nm absorption when the peptide was incubated overnight (Figure 2.12). Therefore, as with the CD analysis of β1-40, all CD spectra of the β1-28 analogs were taken immediately after the addition of the peptide solution to the buffer.

Figure 2.12 20 μM human β1-28 incubated overnight.

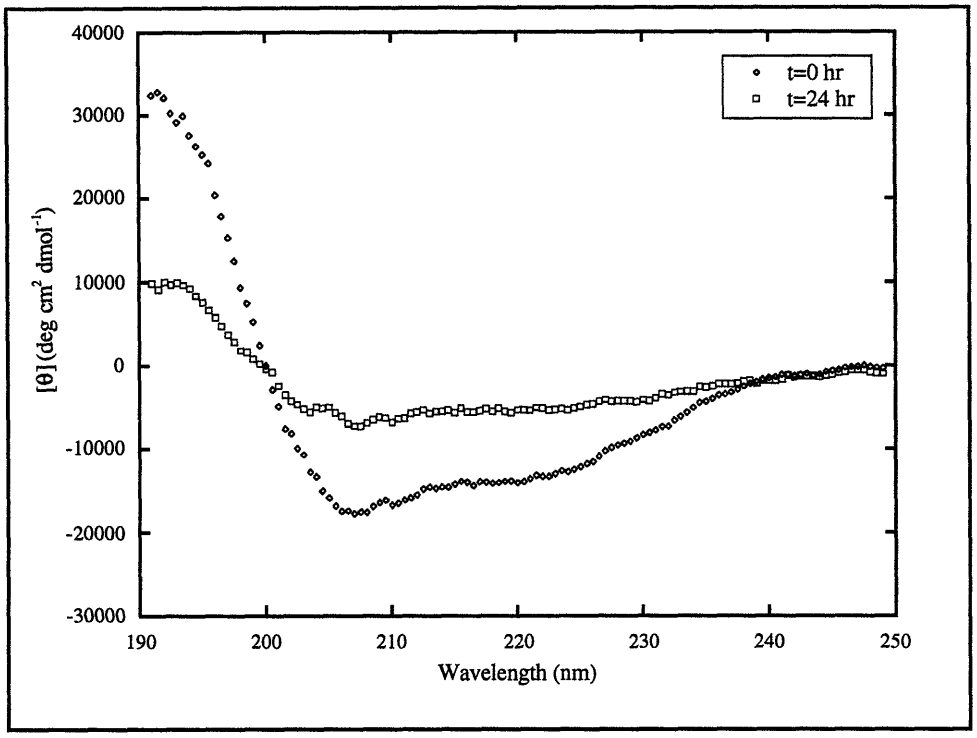

Table 2.7 Percent α-helix of 20 μM β1-28 incubated overnight.

	t=0 hr	t=24 hr
208 nm	47	10
222 nm	42	21

Conformational changes resulting from increasing the amount of HFIP were also examined. Additionally, the effects of metal cations on the secondary structure of the peptides were determined. CD spectra of the peptides were taken in the presence of $ZnCl_2$ and $CuCl_2$. Figure 2.13 shows that there are large conformational changes in human β1-28 upon the addition of a concentrated aqueous stock solution of $ZnCl_2$. A 44% decrease

in α-helix occurs at 208 nm from the addition of 80 μM $ZnCl_2$. Only an additional 3% decrease in α-helix is observed from 80 to 500 μM $ZnCl_2$. A 29% decrease in α-helix is evident at the 222 nm absorption.

Figure 2.13 20 μM β1-28 human vs. $ZnCl_2$.

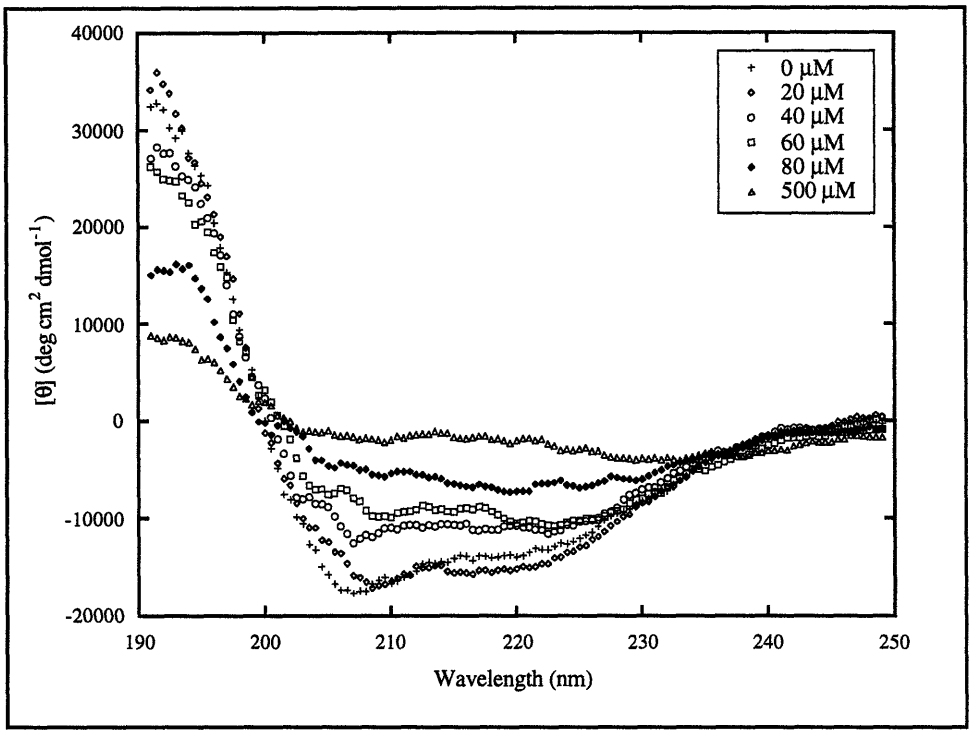

Table 2.8 Percent α-helix of 20 μM β1-28 vs. $ZnCl_2$.

	0 μM	20 μM	40 μM	60 μM	80 μM	500 μM
208 nm	47	43	27	18	3	0
222 nm	42	45	36	35	24	13

The addition of 80 μM $CuCl_2$ caused dramatic changes in the secondary structure of human β1-28 (Figure 2.14). A 51% and 28% decrease in α-helix

content at the 208 nm and 222 nm absorptions, respectively, were observed upon the addition of the $CuCl_2$ (Table 2.9).

Figure 2.14 20 μM β1-28 (16% HFIP) vs. $CuCl_2$.

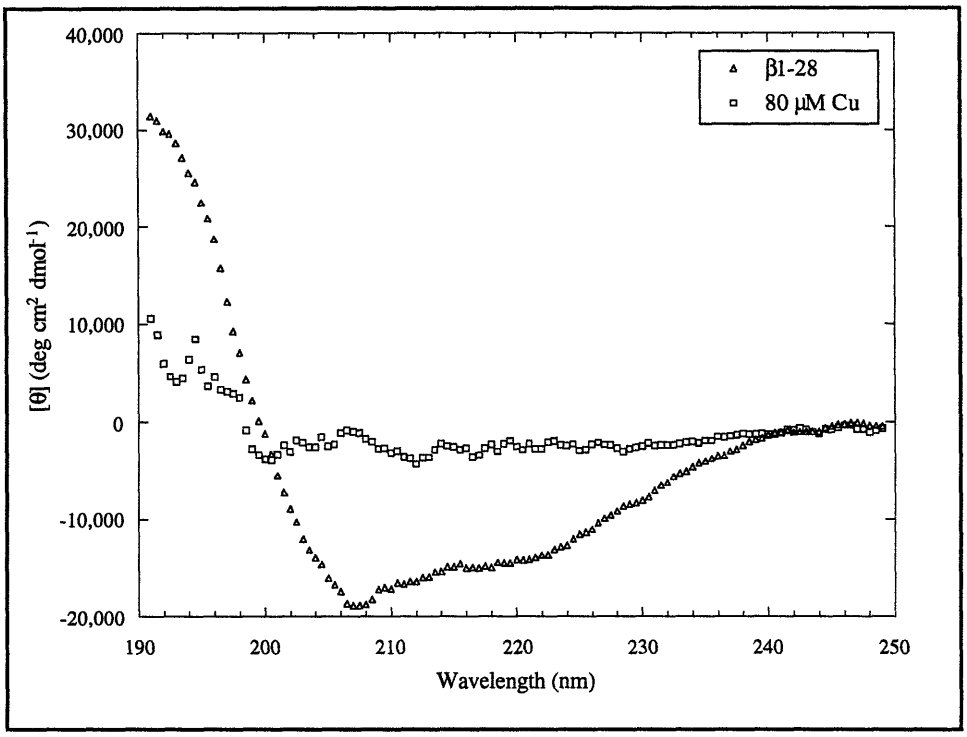

Table 2.9 Percent α-helix of 20 μM β1-28 vs. $CuCl_2$.

	0 μM	80 μM
208 nm	51	0
222 nm	43	15

β1-28 Rat Results

CD studies of β1-28 Rat, which were done in parallel with β1-28 Human, were performed in order to determine the best concentration for the

experiments. Although the 5 μM, 10 μM, and 20 μM concentrations seemed to have a similar conformation (Figure 2.15), experiments were performed at 20 μM peptide.

Figure 2.15 Concentration dependence of β1-28 Rat.

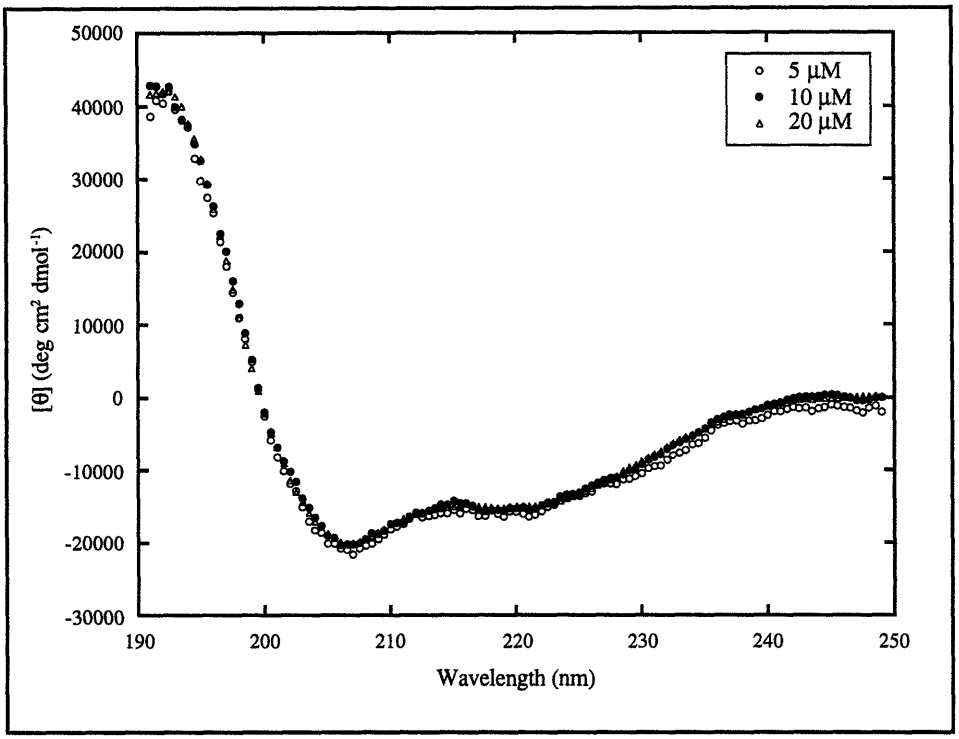

Table 2.10 Percent α-helix of 20 μM β1-28 Rat vs. concentration.

	5 μM	10 μM	20 μM
208 nm	56	53	53
222 nm	48	46	45

While small conformational changes in β1-28 Rat occur upon the addition of $ZnCl_2$ (Figure 2.16), the changes are much smaller than those seen

for β1-28 human. A 15% and 1% decrease in α-helical content are observed at the 208 nm and 222 nm absorbances, respectively, for β1-28 Rat in the presence of 500 μM $ZnCl_2$ (Table 2.11), while a 47% decrease in α-helix is observed at the 208 nm absorbance for β1-28 human.

Figure 2.16 20 μM β1-28 Rat (16% HFIP) vs. $ZnCl_2$.

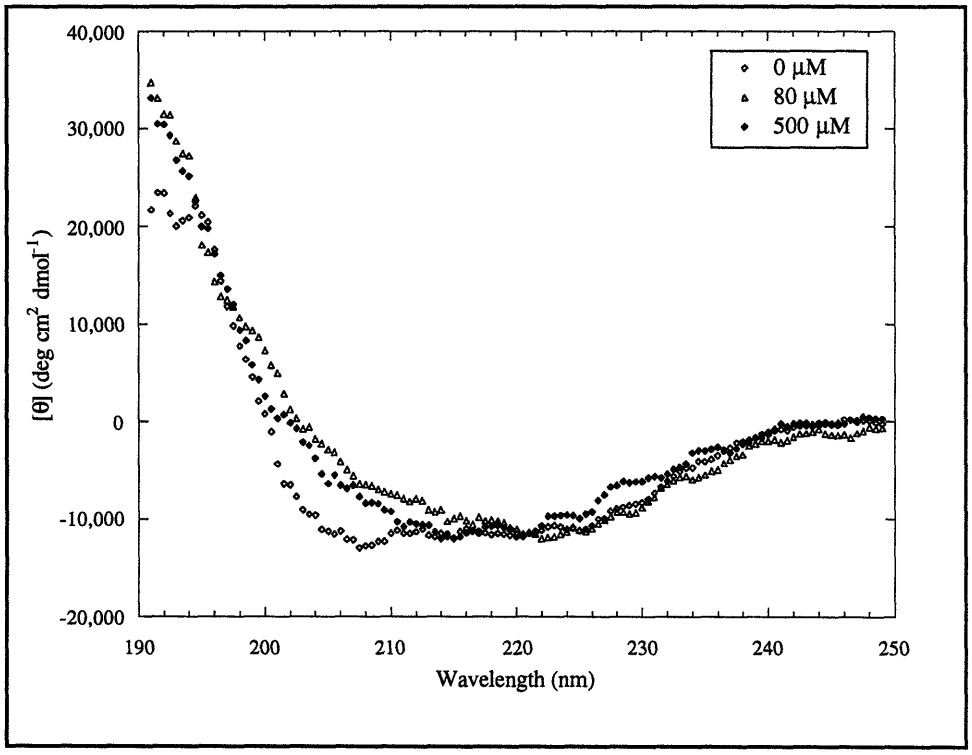

Table 2.11 Percent α-helix of 20 μM β1-28 Rat vs. $ZnCl_2$.

	0 μM	80 μM	500 μM
208 nm	30	9	15
222 nm	36	39	35

The addition of 80 μM $CuCl_2$ results in a 17% and 11% decrease in α-helical content at the 208 nm and 222 nm absorbances (Table 2.12), respectively, but as was the case with the addition of $ZnCl_2$, the changes are much smaller than the 51% decrease in α-helix observed for β1-28 human.

Figure 2.17 20 μM β1-28 Rat (16% HFIP) vs. $CuCl_2$.

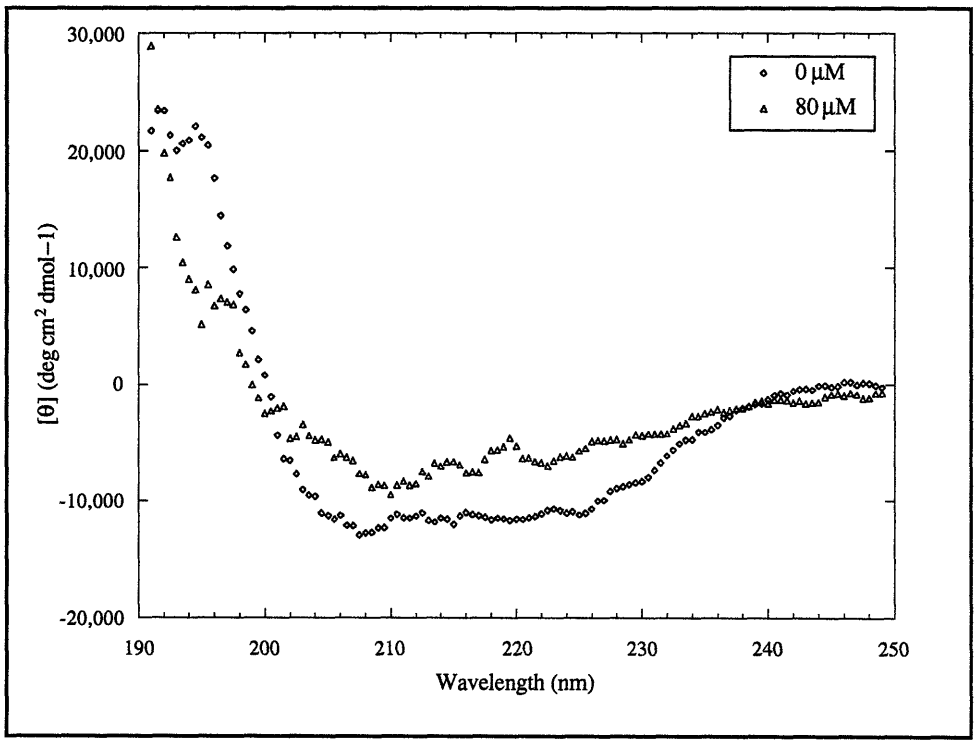

Table 2.12 Percent α-helix of 20 μM β1-28 Rat vs. $CuCl_2$.

	0 μM	80 μM
208 nm	30	13
222 nm	36	25

β1-28 Y10F Results

Large conformational changes are evident in Figure 2.18 which shows β1-28 Y10F in the presence of $ZnCl_2$. A 32% decrease in the percent α-helix is observed at the 208 nm absorbance after the addition of 80 μM $ZnCl_2$ and only an additional 1% decrease occurs from 80 μM to 500 μM $ZnCl_2$. This decrease in α-helix is similar to the 47% decrease in α-helix observed with β1-28 human in the presence of 500 μM $ZnCl_2$.

Figure 2.18 20 μM β1-28 Y10F (16% HFIP) vs. $ZnCl_2$.

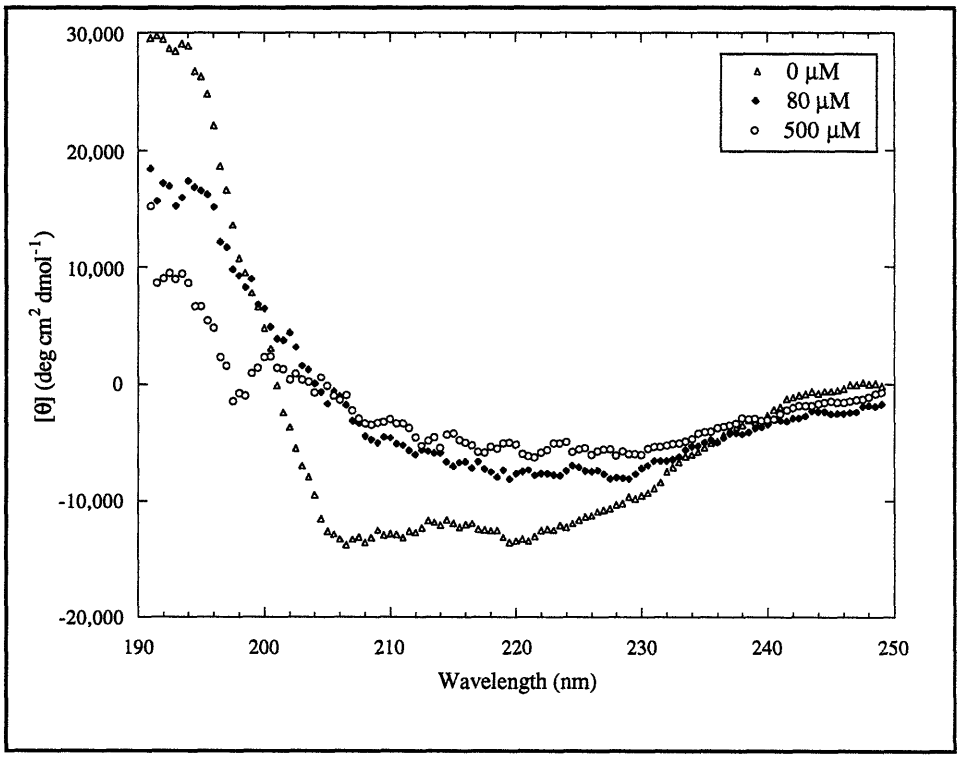

Table 2.13 Percent α-helix of 20 μM β1-28 Y10F vs. $ZnCl_2$.

	0 μM	80 μM	500 μM
208 nm	33	1	0
222 nm	40	27	23

In the presence of 80 μM $CuCl_2$, there was a 33% and 23% decrease in α-helix at the 208 nm and 222 nm absorbances, respectively (Table 2.14). Again, these decreases are consistent with those seen with β1-28 human after the addition of 80 μM $CuCl_2$.

Figure 2.19 20 μM β1-28 Y10F vs. $CuCl_2$.

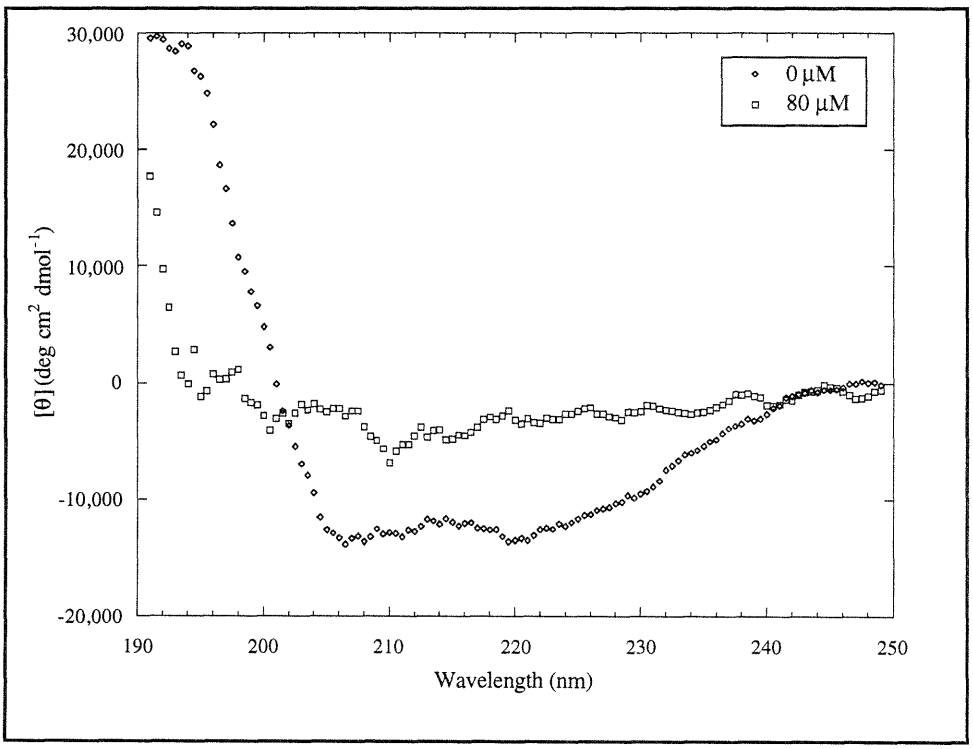

Table 2.14 Percent α-helix of 20 μM β1-28 Y10F vs. $CuCl_2$.

	0 μM	80 μM
208 nm	33	0
222 nm	40	17

β1-28 R5G Results

The β1-28 R5G analog shows very large conformational changes in the presence of $ZnCl_2$ (Figure 2.20). There is a 45% decrease in α-helical content at the 208 nm absorption after the addition of 80 μM $ZnCl_2$ (Table 2.15). This is almost identical to the 44% decrease in the percent α-helix observed upon the addition of 80 μM $ZnCl_2$ to β1-28 human.

Figure 2.20 20 μM β1-28 R5G (16% HFIP) vs. $ZnCl_2$.

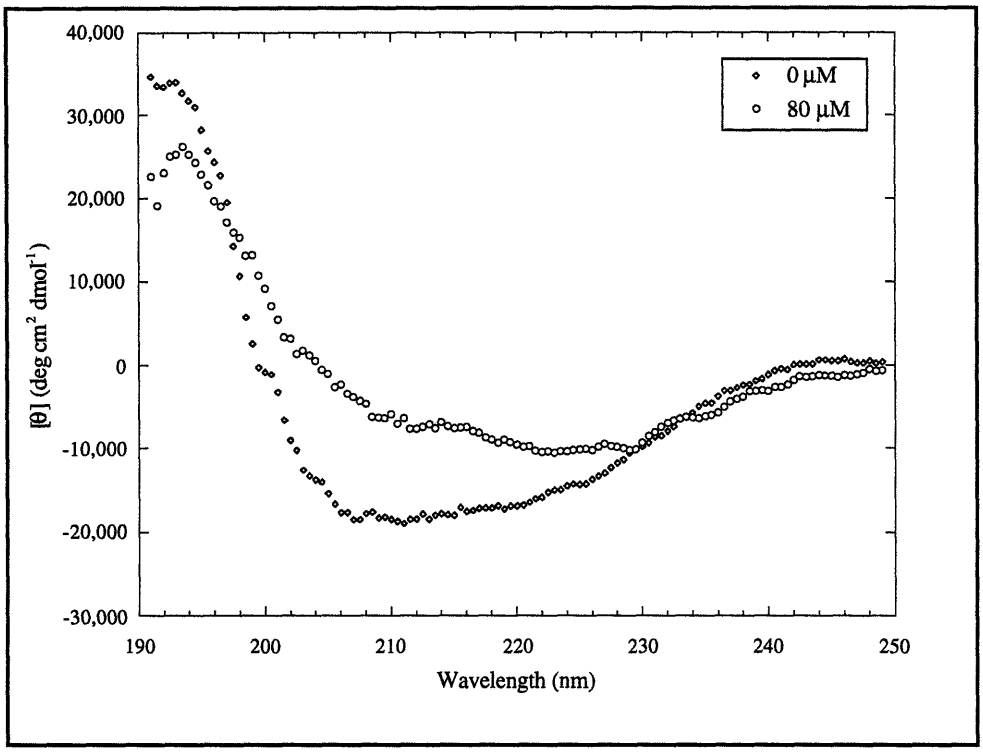

Table 2.15 Percent α-helix of 20 μM β1-28 R5G vs. $ZnCl_2$.

	0 μM	80 μM
208 nm	47	2
222 nm	48	34

β1-28 H13R Results

Figure 2.21 indicates that the β1-28 H13R analog shows the smallest conformational change of the three single mutation peptides upon addition of $ZnCl_2$. No conformational change is observed at the 222 nm absorption even after the addition of 500 μM $ZnCl_2$. The 208 nm absorption, however,

does show a 17% and 27% decrease in α-helix in the presence of 80 μM and 500 μM $ZnCl_2$, respectively (Table 2.16).

Figure 2.21 20 μM β1-28 H13R (16% HFIP) vs. $ZnCl_2$.

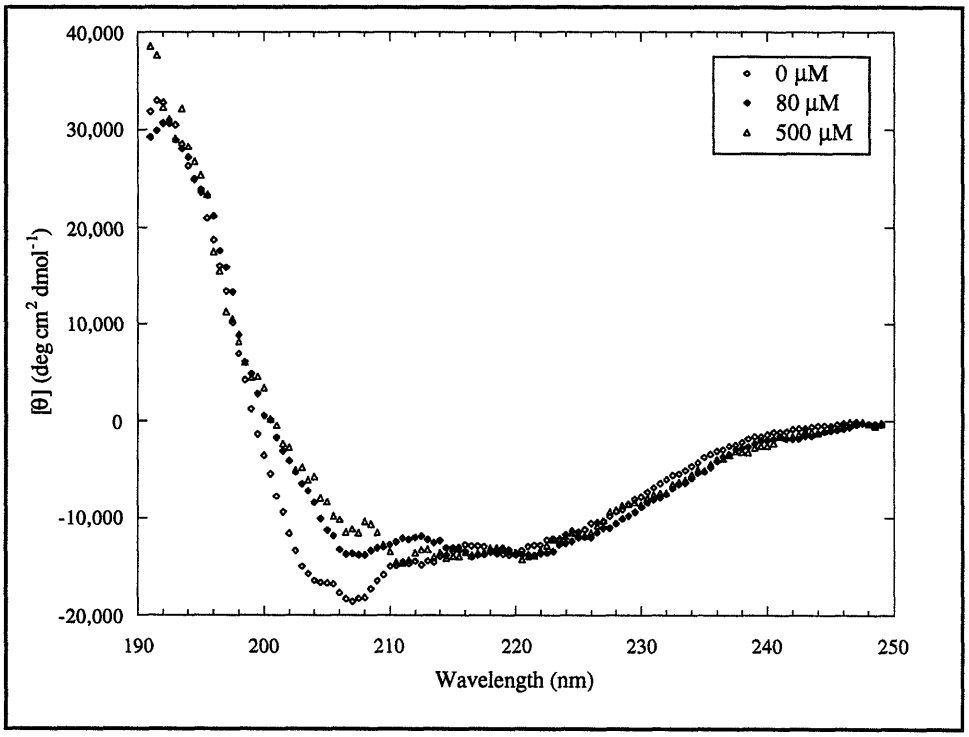

Table 2.16 Percent α-helix of 20 μM β1-28 H13R vs. $ZnCl_2$.

	0 μM	80 μM	500 μM
208 nm	49	32	22
222 nm	41	43	42

β1-28 H13R shows much larger conformational changes in the presence of 80 μM $CuCl_2$ than 500 μM $ZnCl_2$ (Figure 2.22). There is a 36% and 16% decrease in α-helix at the 208 nm and 222 nm, respectively (Table 2.17).

Figure 2.22 20 μM β1-28 H13R (16% HFIP) vs. $CuCl_2$.

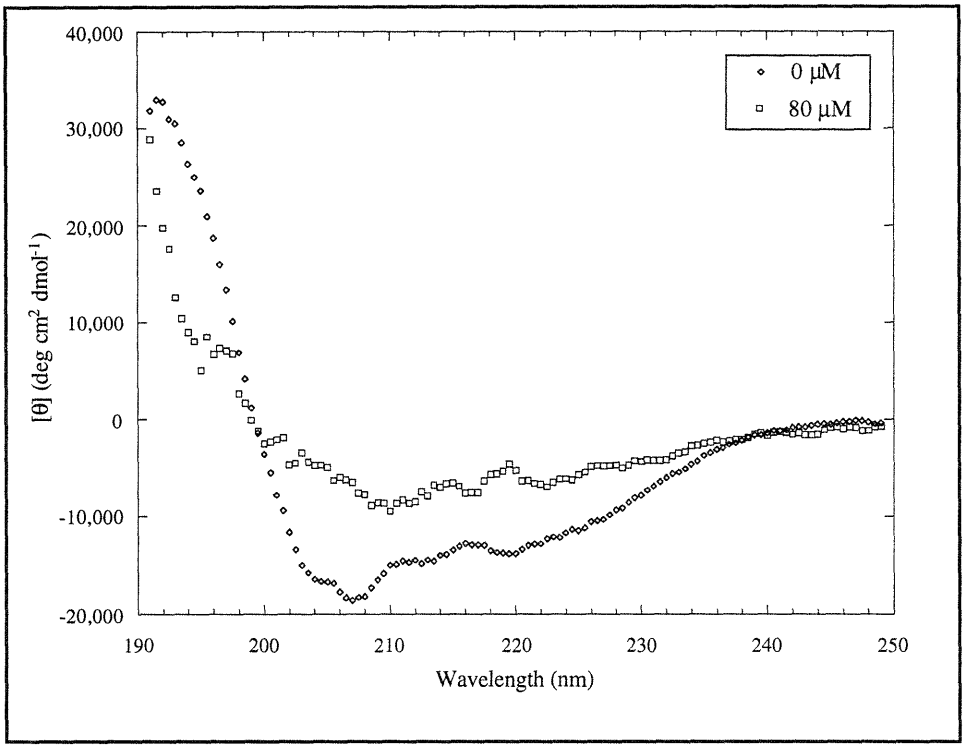

Table 2.17 Percent α-helix of 20 μM β1-28 H13R vs. $CuCl_2$.

	0 μM	80 μM
208 nm	49	13
222 nm	41	25

β1-28 R5G, Y10F Results

The conformational changes observed in the initial studies of β1-28 R5G, Y10F in the presence of $ZnCl_2$ are shown in Figure 2.23, and are much different than those seen with the other truncated peptides. There is a small decrease (11%) in α-helix at 208 nm, however, there is a 24% *increase* in α-

helix at 222 nm (Table 2.18). Additional studies of this peptide are required in order to confirm this unique conformational change in the presence of zinc.

Figure 2.23 20 μM β1-28 R5G, Y10F (16% HFIP) vs. $ZnCl_2$.

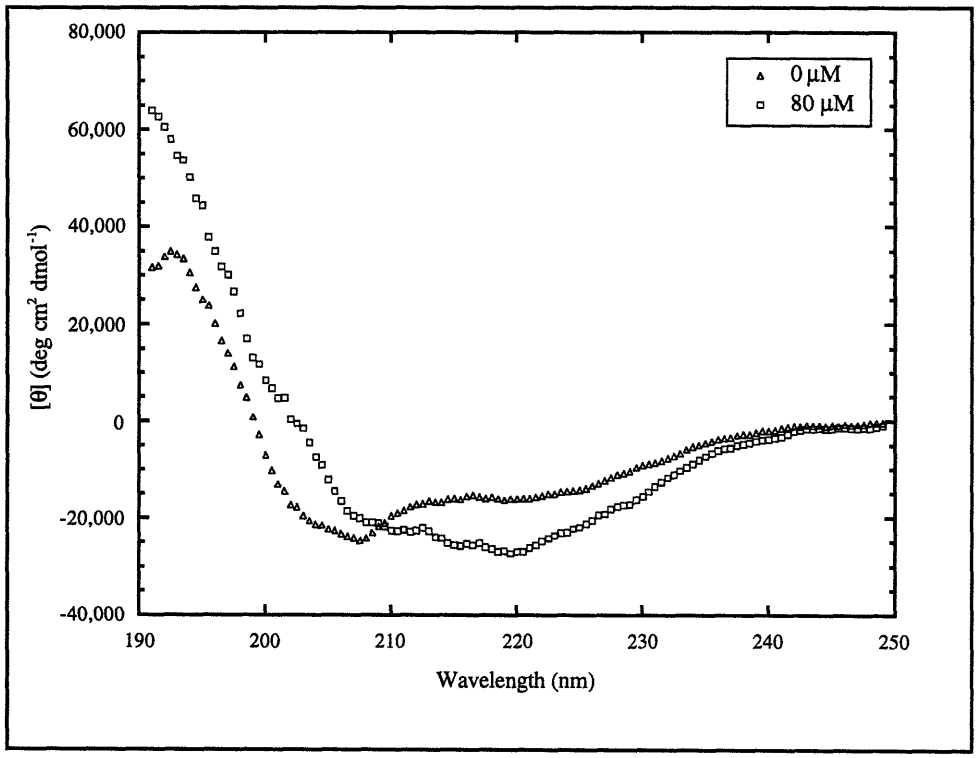

Table 2.18 Percent α-helix content of β1-28 R5G, Y10F vs. $ZnCl_2$.

	0 μM	80 μM
208 nm	69	58
222 nm	47	71

The conformational changes observed in Figure 2.24 that result from the addition of 80 μM $CuCl_2$ to β1-28 R5G, Y10F are similar to the changes

observed in the other peptides. There is a 37% and a 31% decrease in α-helical content at the 208 nm and 222 nm absorbances, respectively (Table 2.19).

Figure 2.24 20 μM β1-28 R5G, Y10F (16% HFIP) vs. $CuCl_2$.

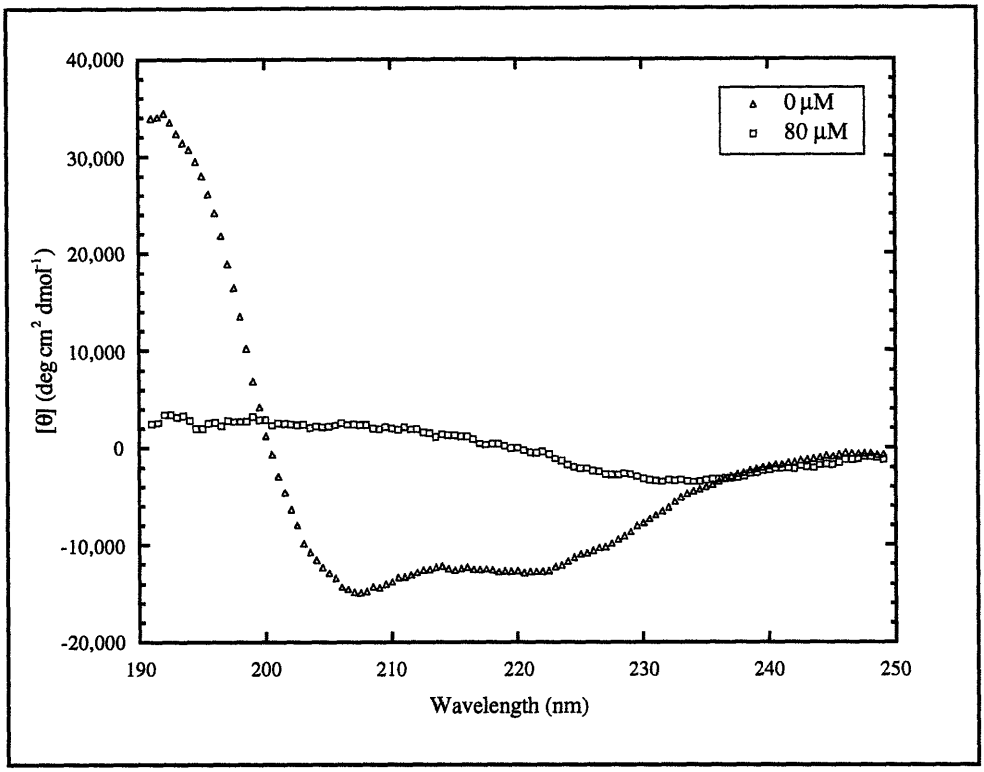

Table 2.19 Percent α-helix of β1-28 R5G, Y10F vs. $CuCl_2$.

	0 μM	80 μM
208 nm	37	0
222 nm	40	9

β1-28 E22Q Results

There was a 37% and an 18% decrease in the percent α-helix of β1-28 E22Q at the 208 nm and 222 nm absorptions, respectively, from 0 to 500 μM

$ZnCl_2$ (Table 2.20). These conformational changes are somewhat smaller that those observed for the wild-type β1-28.

Figure 2.25 20 μM β1-28 E22Q (16% HFIP) vs. $ZnCl_2$.

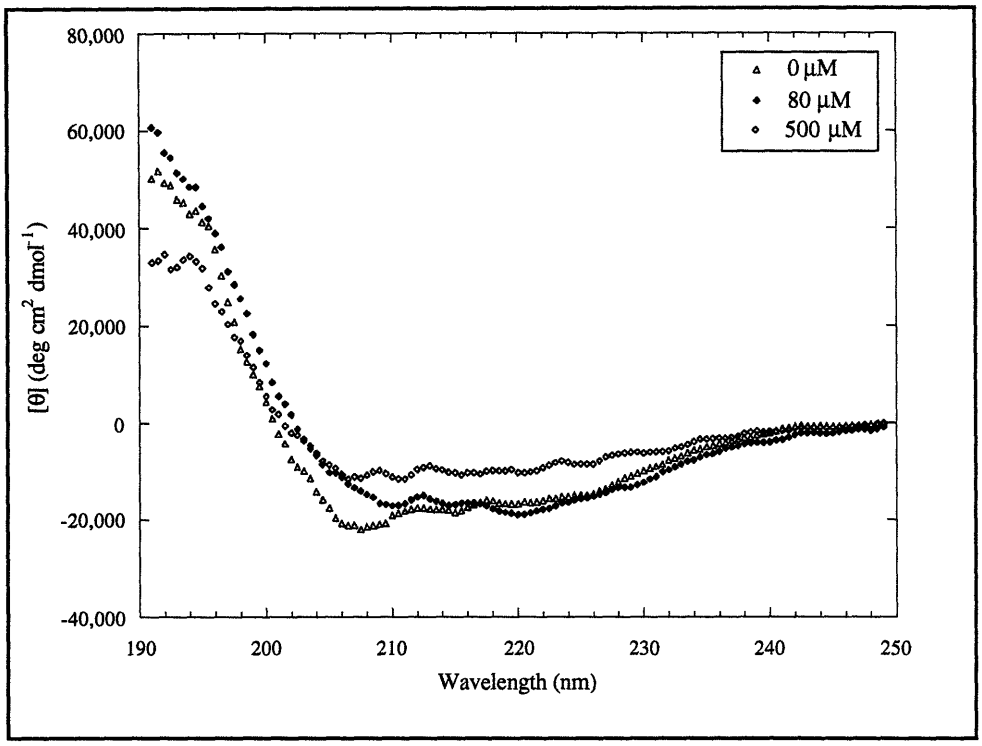

Table 2.20 Percent α-helix of β1-28 E22Q vs. $ZnCl_2$.

	0 μM	80 μM	500 μM
208 nm	60	37	23
222 nm	49	53	31

Figure 2.26 shows the effect of $CuCl_2$ on β1-28 E22Q. There was a 36% and a 19% decrease in α-helix at the 208 nm and 222 nm absorbances, respectively, after the addition of 80 μM $CuCl_2$ (Table 2.21).

Figure 2.26 20 μM β1-28 E22Q (16% HFIP) vs. $CuCl_2$.

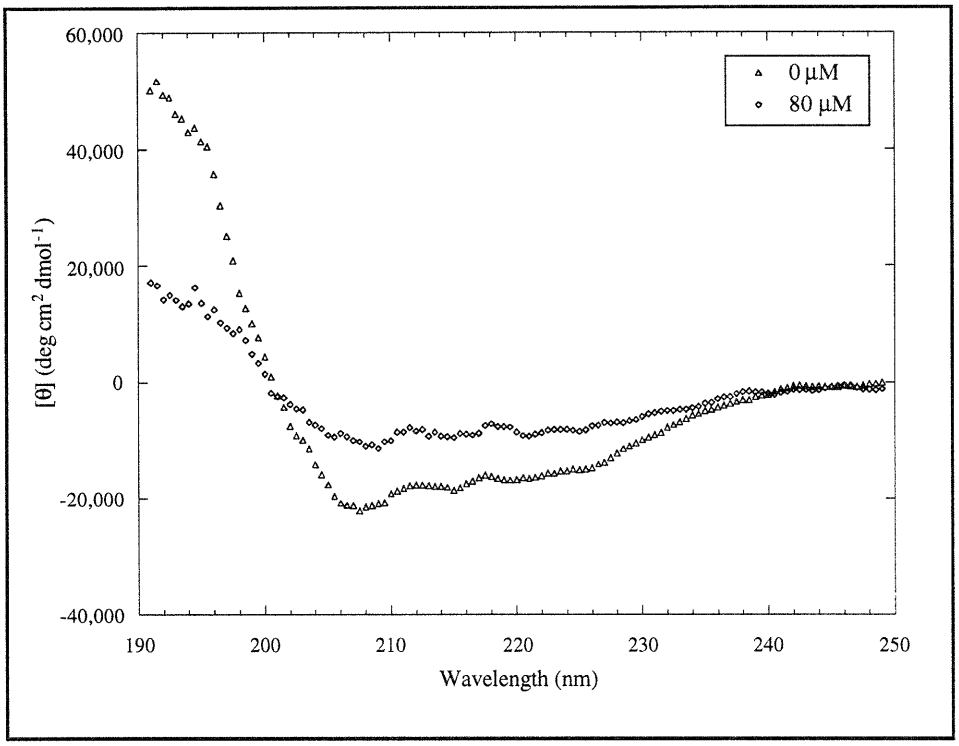

Table 2.21 Percent α-helix of β1-28 E22Q vs. $CuCl_2$.

	0 μM	80 μM
208 nm	60	24
222 nm	49	30

Discussion

CD analysis was initially performed on the full length β protein, β1-40. In order to determine residues critical to zinc-binding in the human and rat β proteins, truncated peptides were synthesized. Studies with β1-17 were

ineffective because the peptide was too small to possess any structure, even in the presence of a helix-inducing, non-polar organic solvent such as HFIP. Several analogs of β1-28 were therefore analyzed in order to determine ligand interactions that were essential for zinc to bind to the peptides. The rat β-amyloid protein differs from the human protein by three amino acid residues (R5G, Y10F, H13R). All three substitutions are located in the N-terminal extracellular 28-residue segment of the β protein. In addition to the human and rat sequences, three peptides were synthesized that each contained one of the three mutations found in the rat β protein. A fourth peptide containing two of the mutations (R5G, Y10F) was also synthesized.

Conclusions made from the experimental results presented above are based on the hypothesis that the larger the conformational change of the peptide in the presence of metal, the stronger the interaction of the peptide with that metal. A conformational change does not demonstrate unequivocally this metal-binding interaction. However, differences between peptides in the amount of conformational change that results from an interaction with metal is a useful tool for examining the effect of amino acid mutations on peptide structure. Provided that these *in vitro* results have *in vivo* significance, the observed differences in metal-binding properties of the β protein variants could be important in the pathogenesis of AD.

The CD spectrum of the β1-28 analogs in buffer alone was consistent with a random-coil conformation.[7] However, the peptides showed increased helicity upon the addition of HFIP, which is known to stabilize regions of peptides or proteins that are intrinsically α-helical in nature rather than *induce* helix formation randomly.[9]

In the presence of 16% HFIP, the β protein analogs differed in the amount of α-helix present even in the absence of metals, which makes

subsequent comparisons between the peptides more difficult. Table 2.22 shows that according to the 208 nm absorbance, β1-28 Rat and β1-28 Y10F initially have less α-helix than β1-28 human, β1-28 R5G, and β1-28 H13R.

Table 2.22 α-helix content of the β1-28 peptides (at 208 nm).

Peptide	% α-helix
β1-28	47
β1-28 Rat	30
β1-28 Y10F	33
β1-28 R5G	47
β1-28 H13R	49

In the presence of 80 μM $ZnCl_2$, a large decrease in α-helicity is observed for the human peptide at 208 nm. The β protein analogs, Y10F and R5G, which each contain only one of the rat peptide mutations also show large decreases in helicity at 208 nm in the presence of $ZnCl_2$. The β1-28 rat and H13R peptides, however, show much smaller decreases in helicity in the presence of zinc. Even after the addition of 500 μM $ZnCl_2$, the peptides show only small decreases in their α-helix content (Table 2.23).

Table 2.23 Decrease in α-helicity of the β1-28 analogs at 208 nm in the presence of either 80 or 500 μM $ZnCl_2$.

Peptide	80 μM Zinc	500 μM Zinc
β1-28	44	47
β1-28 Rat	21	15
β1-28 Y10F	32	33
β1-28 R5G	45	NA
β1-28 H13R	17	0

These results indicate that the histidine at position 13 in the β protein may be important for its interaction with the zinc cations, which may be stabilizing β-structure in the peptide. The replacement of this histidine with an arginine in β1-28 H13R diminishes the effect of the metal on the conformation of the peptide, causing it to behave in a similar manner to the β1-28 rat peptide. Conversely, the R5G and Y10F mutations do not appear to have a dramatic effect on the interaction of the β protein with zinc. Therefore, only one amino acid change (the H13R mutation) of the three changes found in the rat β protein appears to be responsible for the decreased interaction of that protein with metals.

Histidine residues are known to play an important role in other zinc binding proteins such as zinc fingers which regulate transcription. These proteins contain several 30 residue repeats, each of which contains two cysteine and two histidine residues that are ligands to a zinc atom. Other zinc-binding proteins such as carboxypeptidases have two histidine residues and one glutamic acid residue that are ligands to a zinc atom. Therefore, it is

not surprising that the H13R mutation may be essential for the β protein to bind strongly to zinc.

A peptide corresponding to the β protein variant associated with Hereditary Cerebral Hemorrhage with Amyloidosis of the Dutch Type (HCHWA-D) was synthesized. The β protein (β1-39) involved in this disease contains a mutation at residue 22 in which a glutamic acid residue is replaced by a glutamine. An analog of β1-28 with this mutation (β1-28 E22Q) was synthesized in addition to the peptides previously reported.

Large conformational changes are observed after the addition of 80 μM $CuCl_2$. Previous studies involving the interaction of the β protein with copper have presented conflicting data. One study found that copper was not able to displace radioactive zinc form the β protein,[25] while another showed that copper did displace the bound radioactivity.[23] The latter study concluded that the metal-binding site on the β protein may be somewhat non-specific. Results presented herein also indicate that the β protein analogs may have binding sites that are not unique to only one metal.

A smaller conformational change is observed in the β1-28 E22Q peptide than the wild-type variant in the presence of 80 μM $ZnCl_2$, but the two peptides behave more similarly after the addition of 500 μM $ZnCl_2$ (Table 2.24). This suggests that either β1-28 E22Q has a different binding contant than β1-28 human, or that the mutation is not important to the conformation of the protein. Results of another study showed little difference between the wild-type and HCHWA-D β proteins in their ability to bind $^{65}Zn^{2+}$.[23] However, differences in the conformation of the two peptides in the presence of metal that can not be detected by CD, but that are important *in vivo*, may exist and could be critical to the metal-binding properties or proteolytic processing of the protein.

Table 2.24 Decreases in the percent α-helicity of β1-28 E22Q at 208 nm in the presence of either 80 or 500 μM $ZnCl_2$.

Peptide	80 μM $ZnCl_2$	500 μM $ZnCl_2$
β1-28	44	47
β1-28 E22Q	23	37

Experimental

Materials

The Wang resin (Substitution 0.6 mmol/g) and Pam Resin (Substitution 0.4 mmol/g) were purchased from Novabiochem. Boc-amino acids and Fmoc-amino acids were obtained from Advanced ChemTech. BOP reagent was obtained from Richelieu Biotechnologies. DIEA was purchased from Aldrich Chemical and distilled from ninhydrin under reduced pressure. Millex-FG 0.22 μm filters were obtained from Millipore.

Peptide Synthesis (Fmoc)

Fmoc-protected peptides were synthesized manually on the Wang resin using commercially available Fmoc-amino acids. The side chains of histidine and glutamine were protected by trityl groups. The side chains of serine, aspartic acid, glutamic acid, and tyrosine were protected as the *t*-butyl ethers. Lysine was protected by the Boc group and arginine was protected by the PMC group. Amino acids were coupled to the resin with 3 equivalents of

amino acid, 3 equivalents of BOP or PyBOP, and 6 equivalents of DIEA in DMF for 1.5 hr. The Kaiser test [29] was used to monitor coupling efficiency. Unreacted N-termini were acetylated with acetic anhydride and DIEA (10 equivalents each in dichloromethane) for 30 minutes. The Fmoc protecting groups were removed with 50% piperdine/DMF for 25 min. The resin-bound peptides were cleaved and deprotected with the following for 2.5 hr at 25°C: 82.5% TFA, 5% H_20, 5% phenol, 2.5% EDT, and 5% thioanisole. The resin was filtered and washed with 4 mL neat TFA. The filtrate was concentrated and added to cold diethyl ether. The precipitated peptide was pelleted by centrifugation, washed with ether, and dried under vacuum.

Peptide Synthesis (Boc)

Peptides were synthesized manually by Boc chemistry on the Pam resin using commercially available Boc-amino acids. The histidine side chains were protected by benzyloxymethyl groups, the serine and glutamic acid side chains were protected by benzyl groups, the aspartic acid side chains of aspartic acid were protected by either *t*-butyl or cyclohexyl groups, the lysine side chains protected by 2-chlorobenzyloxy carbonyl groups, the tyrosine side chains were protected by 2,6-dichlorobenzyl groups, arginine side chains were protected by mesitylenesulfonyl groups. Amino acids were coupled to the resin with 3 equivalents of amino acid, 3 equivalents of BOP, and 5.3 equivalents of DIEA in DMF for 1.5 hours. The Kaiser test[29] was used to monitor coupling efficiency. Unreacted N-termini were acylated with acetic anhydride and DIEA (10 equivalents of each in dichloromethane) for 30 minutes. The Boc protecting groups were removed with 25% TFA/dichloromethane for 30 minutes.

Deprotection and cleavage of Boc-peptides were achieved by the addition of DMS (13 ml) and *p*-cresol (4.0 ml) to the resin-bound peptide (1.63 g) in a Teflon tube. While under vacuum, anhydrous HF (5 ml) was added into the chamber and the solution was stirred for 2 hours at 0°C. The HF and DMS were then removed by distillation. Additional anhydrous HF (20 ml) was then added to the chamber and the mixture was stirred for 1 hour at 0°C. The HF was then removed and the contents of the chamber were placed under vacuum overnight and then diluted with neat TFA (3 ml). The peptide was precipitated with ice-cold anhydrous ether. The precipitated peptide was collected by centrifugation, washed with additional ether, and dried under vacuum overnight.

Synthesis of β Protein Analogs

Synthesis of β1-28 Human

Synthesized by Santosh Nandan using standard Fmoc chemistry on the Wang resin. *Amino Acid Analysis*: D/N 3.8 (4), E/Q 4.0 (4), S 1.8 (2), G 2.1 (2), H 2.5 (3), R 0.9 (1), A 2.0 (2), Y 0.9 (1), V 2.5 (3), L 1.0 (1), F 2.7 (3), K 2.0 (2). *PDMS*: 3265.9 $(M+H)^+$ and 1633.8 $(M+2H)^+$ (calc. 3262.9).

Synthesis of β1-28 Rat

Synthesized using Boc chemistry on the Pam resin and deprotected as described above. *Amino Acid Analysis*: D/N 3.6 (4), E/Q 3.8 (4), S 1.8 (2), G 3.0 (3), H 1.5 (2), R 0.8 (1), A 2.0 (2), V 3.1 (3), L 1.2 (1), F 3.5 (4), K 2.2 (2). *RPHPLC*: C_4 semi-prep: 80/20 H_2O/CH_3CN (0.1% TFA) 15 mL/min. V_R = 165 mL. C_4

analytical: 60/40 H_2O/CH_3CN (0.1% TFA) 2 mL/min. V_R = 24 mL. *PDMS*: 3165.6 $(M+H)^+$ (calc. 3166).

Synthesis of β1-28 R5G

Synthesized using standard Fmoc chemistry on the Wang resin as described above. Peptide was purified using a C_4 analytical column. *Amino Acid Analysis*: D/N 3.8 (4), E/Q 3.9 (4), S 1.6 (2), G 3.0 (3), H 2.7 (3), A 2.0 (2), Y 0.9 (1), V 2.9 (3), L 1.0 (1), F 3.0 (3), K 2.1 (2). *RHPLC*: C_4 analytical (prep): 80/20 H_2O/CH_3CN (0.1% TFA) 2 mL/min. V_R = 10 mL. *PDMS*: 3160.3 $(M+H)^+$ and 1582.9 $(M+H)^+$ (calc. 3163.8).

Synthesis of β1-28 Y10F

Synthesized using standard Fmoc chemistry on the Wang resin as described above. Peptide was purified using a C_4 analytical column. *Amino Acid Analysis*: D/N 3.8 (4), E/Q 3.9 (4), S 1.6 (2), G 2.0 (2), H 2.6 (3), R 0.9 (1), A 2.0 (2), V 2.8 (3), L 1.0 (1), F 3.7 (4), K 2.0 (2). *RHPLC*: C_4 analytical (prep): 80/20 H_2O/CH_3CN (0.1% TFA) 2 mL/min. V_R = 15 mL. *PDMS*: 3246.6 $(M+H)^+$ and 1624.7 $(M+2H)^+$ (calc. 3246.9).

Synthesis of β1-28 R5G, Y10F

Synthesized using standard Fmoc chemistry on the Wang resin as described above. *Amino Acid Analysis*: D/N 3.9 (4), E/Q 3.9 (4), S 1.8 (2), G 2.9 (3), H 2.6 (3), A 2.0 (2), V 2.7 (3), L 1.0 (1), F 3.6 (4), K 1.6 (2). *RHPLC*: C_4 semi-prep: 75/25 H_2O/CH_3CN (0.1% TFA) 20 mL/min. V_R = 160 mL. C_4 analytical: 80/20 H_2O/CH_3CN (0.1% TFA) 2 mL/min. V_R = 16 mL. *PDMS*: 3151.3 (M+H)+ (calc. 3147).

Synthesis of β1-28 H13R

Synthesized by Santosh Nandan using standard Fmoc chemistry on the Wang resin as described above. *Amino Acid Analysis*: D/N 4.3 (4), E/Q 4.0 (4), S 1.8 (2), G 2.0 (2), H 1.7 (2), R 1.5 (2), A 2.0 (2), Y 0.8 (1), V 2.8 (3), L 1.1 (1), F 3.0 (3), K 2.4 (2).

Synthesis of β1-28 E22Q

Synthesized by Santosh Nandan using standard Fmoc chemistry on the Wang resin as described above. *Amino Acid Analysis*: Amino Acid Analysis: D/N 4.1 (4), E/Q 4.0 (4), S 1.7 (2), G 1.9 (2), H 2.7 (3), R 0.9 (1), A 2.0 (2), Y 0.9 (1), V 2.9 (3), L 1.1 (1), F 3.1 (3), K 2.4 (2).

Purification and Characterization of Peptides

The crude peptides were dissolved in DMSO and purified by reverse-phase HPLC under isocratic conditions on a C_4 semi-preparative column (YMC, 2.0 X 25 cm) with water (0.1% TFA) and acetonitrile (0.1% TFA) as eluents. Peptide fractions were combined, concentrated, and lyophilized to yield a fluffy powder. The purity of the peptides was confirmed by reverse-phase HPLC under isocratic conditions on a C_4 analytical column (Waters, 0.39 X 30 cm). Purified peptides were analyzed by both quantitative amino acid analysis (MIT Biopolymers Lab) and plasma desorption mass spectrometry (PDMS). All peptides showed excellent agreement between the predicted and observed amino acid content and molecular weight.

Circular Dichroism Spectroscopy

CD spectra were obtained with an AVIV spectrapolarimeter in the laboratory of Dr. Daniel Kemp, Department of Chemistry, MIT. Stock solutions of each peptide were prepared in distilled, high grade hexafluoroisopropanol (HFIP) and filtered through 0.22 μm non-aqueous filters (Millex). Concentrations were determined by quantitative amino acid analysis (MIT Biopolymers Laboratory). CD samples were prepared by adding the stock peptide solutions to 1.5 ml Eppendorf tubes containing either buffer only (6.25 mM Tris-Cl, pH 7.4) or buffer plus 80 μM $ZnCl_2$ immediately prior to CD analysis to give a final peptide concentration of 20 μM in 16% HFIP. Samples were incubated at 25°C for 20 min prior to analysis. Each sample was scanned four times in a quartz cell (0.1 cm pathlength) at 0.5 nm intervals over the wavelength range 190 to 250 nm. Solvent and cell backgrounds were subtracted from each sample. Spectra were recorded at 25°C.

Results are expressed in terms of molar ellipticity in units of deg·cm^2/dmol. All CD spectra described above are representative of at least three CD runs. The CD spectra were smoothed by a factor of five using Cricket Graph in order to reduce the noise levels. The percent α-helix was determined using both the 208 nm[7] and the 222 nm[8] absorptions.

References

(1) Selkoe, D.J. *TINS* **1993**, *16*, 403-409.
(2) Hardy, J. *J. NIH Res.* **1993**, *5*, 46-49.
(3) Lorenzo, A.; Yankner, B.A. *Proc. Natl. Acad. Sci. USA* **1994**, *91*, 12243-12247.
(4) Pike, C.J.; Walencewicz, A.J.; Glabe, C.G.; Cotman, C.W. *Brain Res.* **1991**, *563*, 311-314.
(5) Levy, E.; Carman, M.D.; Fernandez-Madrid, I.; Lieberburg, I.; Power, M.D.; Van Duinen, S.G.; Bots, G.; Luyendijk, W.; Frangione, B. *Science* **1990**, *248*, 1124.
(6) Strictland, E.H. *CRC Crit. Rev. Biochem.* **1974**, 113-175.
(7) Greenfield, N.; Fasman, G.D. *Biochemistry* **1969**, *8*, 4108.
(8) Morrisett, J.D.; David, J.S.K.; Pownall, H.J.; Gotto, A.M. *Biochemistry* **1973**, *12*, 1290.
(9) Barrow, C.J.; Yasuda, A.; Kenny, P.T.M.; Zagorski, M.G. *J. Mol. Biol.* **1992**, *225*, 1075.
(10) Chang, C.T.; Wu, C.-S.; Yang, J.T. *Anal. Biochem.* **1978**, *91*, 13-31.
(11) Manaualan, P.; Johnson, W.C.J. *Anal. Biochem* **1987**, *167*, 76-85.
(12) Johnson, W.C.J. *Prot. Struct. Funct. and Gen.* **1990**, *7*, 205-214.
(13) Barrow, C.J.; Zagorski, M.G. *Science* **1991**, 179-182.
(14) Haan, J.; Hardy, J.A.; Roos, R.A. *Trends Neurosci.* **1991**, *14*, 231-234.
(15) Jarrett, J.T.; Berger, E.P.; Lansbury, P.T., Jr. *Biochemistry* **1993**, *32*, 4693-4697.
(16) Fabian, H.; Szendrei, G.I.; Mantsch, H.H.; Otvos, L. *Biochem. Biophys. Res. Commun.* **1993**, *191*, 232-239.
(17) Fraser, P.E.; Nguyen, J.T.; Inouye, H.; Surewicz, W.K.; Selkoe, D.J.; Podlisny, M.B.; Kirschner, D.A. *Biochemistry* **1992**, *31*, 10716-10723.
(18) Hilbich, C.; Kisters-Woike, B.; Reed, J.; Masters, C.L.; Beyreuther, K. *Eur. J. Biochem.* **1991**, *201*, 61.
(19) Johnstone, E.M.; Chaney, M.O.; Norris, F.H.; Pascual, R.; Little, S.P. *Mol. Brain. Res.* **1991**, *10*, 299-305.
(20) Shivers, B.D.; Hilbich, C.; Multhaup, G.; Salbaum, M.; Beyreuther, K.; Seeburg, H.P. *EMBO J.* **1988**, *7*, 1365-1370.
(21) Esler, W.P.; Stimson, E.R.; Jennings, J.M.; Ghilardi, J.R.; Mantyh, P.W.; Maggio, J.E. *J. Neurochem.* **1996**, *66*, 723-732.
(22) Bush, A.I.; Pettingell, W.H.; Paradis, M.D.; Tanzi, R.E. *J. Biol. Chem.* **1994**, *269*, 12152-12158.
(23) Clements, A.; Allsop, D.; Walsh, D.M.; Williams, C.H. *J. Neurochem.* **1996**, *66*, 740-747.
(24) Christianson, D.W. *Adv. Prot. Chem.* **1991**, 42, 281-355.
(25) Bush, A.I.; Pettingell, W.H.; Multhaup, G.; Paradis, M.D.; Vonsattel, J.P.; Gusella, J.F.; Beyreuther, K.; Masters, C.L.; Tanzi, R.E. *Science* **1994**, *265*, 1464-1467.

(26) Jackson, M.J. *in Zinc in Human Biology (Mills C.F., ed), Springer-Verlag, London* **1988**, 1-14.
(27) Frederickson, C.J.; Klitenick, M.A.; Manton, W.I.; Kirkpatrick, J.B. *Brain Res.* **1983**, *273*, 335-339.
(28) Esch, F.S.; Keim, P.S.; Beattie, E.C.; Blacher, R.W.; Culwell, T.; et al. *Science* **1990**, *248*, 1122.
(29) Kaiser, E.; et al. *Anal. Biochem.* **1969**, *54*, 595.

Chapter 3

Apolipoprotein E and its Relationship with Alzheimer's Disease

Despite the key advances that have been made in the field of AD in the past decade, the etiology of the disease has yet to be elucidated. The presence of exogenous proteins has been suggested to play a critical role in the pathogenesis of AD.[1] In this chapter experiments examining the aggregation of the β protein and the effect of apolipoprotein E (apoE) on this process have been performed. The nucleation-dependent polymerization of the β protein has been previously described in detail by Joseph Jarrett in our laboratory.[2] Although controversy exists regarding the role of apoE in AD, experiments from our laboratory demonstrate that apoE is an *in vitro* inhibitor of amyloid formation.

Amyloidosis as a Cause of Disease

Amyloidosis involves the polymerization of proteins that are normally innocuous and soluble into amyloid fibrils as a result of diverse biochemical conditions. The amyloid fibrils accumulate into bundles and then into fibrous plaques, invade the extracellular spaces of organs, and

destroy normal tissue architecture and function.[3] Amyloid deposition is a characteristic of over twenty diseases (Table 3.1). The amyloid deposition may affect only one organ or may occur in multiple organs, as is the case with systemic amyloidosis.

Table 3.1 Precursors of human amyloidogenic proteins and the proposed cause of amyloid formation (P, proteolysis; M, mutation; C, conformational change).[2,3]

Distribution	Precursor (size)	Cause	Amyloid Protein (size)
Systemic	Immunoglobulin (23 kD)	P	Immunoglobulin (5-23 kD)
Systemic	Apolipoprotein-SAA (12 kD)	P	Apolipoprotein-SAA (8 kD)
Systemic	Apolipoprotein-AI (26 kD)	M,P	Apolipoprotein-AI (9-11 kD)
Systemic	Transthyretin (14 kD)	M,P,C	ATTR (5-14 kD)
Systemic	Gelsolin (90-93 kD)	M	Gelsolin (7 kD)
Pancreas	Pro-IAPP (14 kD)	P	IAPP (4 kD)
Thyroid	Calcitonin (9 kD)	P	Calcitonin (6 kD)
Muscular	β-2-microglobulin (12 kD)	C	β-2-microglobulin (12 kD)
Brain	βAPP (110-135 kD)	P,M	β protein (4 kD)
Brain	Cystatin C (13 kD)	M	Cystatin C (12 kD)
Brain	PrP cellular (30-35 kD)	C	Prion (27-35 kD)

Instances of increased fibrillogenesis associated with point mutations in amyloidogenic proteins have been reported. For example, a mutation in cystatin C results in hereditary cerebral hemorrhage with amyloidosis of the Icelandic type (HCHWA-I).[4] Finnish amyloidosis is caused by a mutation in the gesolin peptides.[5]

Although there are some exceptions, most of the amyloid associated diseases share common features. For example, defective proteolytic

processing, high local concentrations, and the existence of structural variants often result in the extracellular accumulation of these proteins in the form of amyloid fibrils. Additionally, most amyloidoses are diseases of aging, with the exception of juvenile rheumatoid arthritis and AD associated with Down's syndrome patients.[3]

Mechanisms for Protein Polymerization

The common factor in all of the amyloidoses seems to be protein-protein interactions stabilized by both the structure of the protein and the microenvironment. The kinetics of amyloid formation by amyloidogenic proteins have been studied in order to elucidate their mechanism of polymerization. Aggregation of these proteins into amyloid plaques could occur according to several different mechanisms, although all mechanisms involving aggregation must initially involve successive bimolecular associations.[6]

The first mechanism is characterized by simple growth in which the addition of each monomer is equally favored regardless of the size of the aggregate. Exponential growth characterizes the second mechanism such that the addition of each monomer to the aggregate is more favorable than the last. The third mechanism is described by nucleation-dependent polymerization. This mechanism is more complicated than the first two mechanisms because there are two phases: the nucleation phase (lag time) and the growth phase. This model assumes that nucleation is entirely rate-limiting.

The nucleation phase is observed as a lag time prior to the aggregation of the protein and is a result of the unfavorable initial equilibria. During the

lag time the gain in enthalpy resulting from the addition of the monomer to the growing oligomer does not outweigh the loss of entropy of the monomer. However, once an oligomer forms that is large enough to allow sufficient contacts between the monomer and the oligomer to make the monomer addition favorable , the addition of monomers becomes rapid and the growth phase begins. This oligomer is defined as the nucleus. The only detectable states in the aggregating solution should be monomers and oligomers that are larger than the nucleus. Any oligomers that are smaller than the nucleus are unstable and constitute no appreciable population. Aggregation of the protein continues until the solubility of the protein, or equilibrium, is reached.

The concentration dependence of the lag time (t_m) is based on Equation 3.1 which predicts that t_m is inversely proportional to the initial monomer concentration (M_o) raised to the number of monomers that make up the nucleus (n). The constant k is unique to each protein polymerization mechanism. Due to the exponential nature of this equation, very small differences in the monomer concentration can result in large changes in the lag time. This concentration dependence can have a significant effect on the *in vivo* formation of amyloid over time.

Equation 3.1 $$1/t_m = k[M_o]^n$$

The mechanism of amyloid formation may be the result of a combination of both thermodynamically- and kinetically-limited processes.[2] In tubulin polymerization, an example of a thermodynamically-limited mechanism, growth is initially slow but can be detected during the lag time. This indicates that tubulin polymerization occurs through a steady-state

Figure 3.1 Nucleation-dependent mechanisms for microtubule formation: A) linear aggregation followed by loop closure, B) sheet assembly followed by tube closure, and C) experimental data and theoretical curves predicted by model B above.

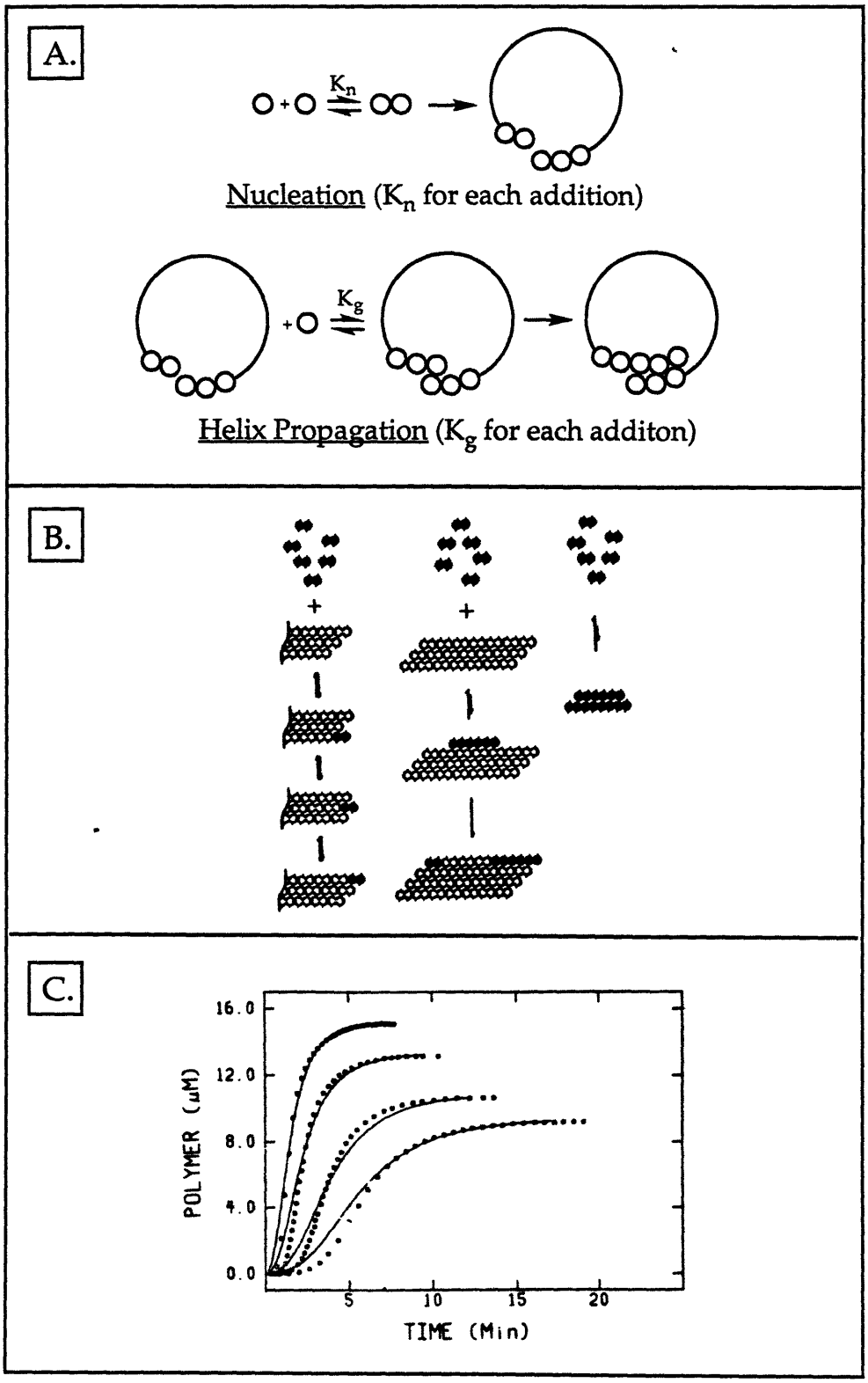

production of nuclei. The mechanism for tubulin nucleation is depicted in Figure 3.1.[2]

An example of a kinetically-limited mechanism is the aggregation of hemoglobin S in sickle cell anemia. The polymerization of hemoglobin S, which is responsible for sickle cell anemia, is one of the best understood protein self-assembly systems.[7] In hemoglobin S, a mutation resulting in the replacement of glutamic acid with valine creates a hydrophobic patch on the molecule which causes it to aggregate into multistranded helical polymers that subsequently aggregate into bundles.

This kinetically-limited polymerization is characterized by the complete absence of growth during the lag time prior to aggregation. This indicates that hemoglobin nucleation does not occur through a steady-state production of nuclei which is observed for tubulin polymerization. The formation of aggregate is slow because the initial rates in the mechanism are very slow. Equilibrium is reached rapidly due to an autocatalytic mechanism that results from heterogeneous nucleation in which prenucleus oligomers are stabilized by pre-existing fibrils, as is depicted in Figure 3.2.[2]

Nucleation-Dependent Polymerization of the β Protein

Previous studies by Joseph Jarrett and Elizabeth Berger have shown that the aggregation of the β protein is a nucleation-dependent process.[8] The kinetic curves that are obtained appear to be described by features from the polymerization of both tubulin and hemoglobin. Nucleus formation is initially rate-limiting, while the growth phase is thermodynamically-limited and reaches steady-state conditions.[2] A long nucleation phase (delay time) occurs prior to the growth phase, however a small accumulation of aggregates

Figure 3.2 Nucleation-dependent mechanisms for the aggregation of hemoglobin S: A) slow homogeneous nucleation followed by rapid heterogeneous nucleation on preexisting fibrils, B) typical experimental data measured by turbidity.

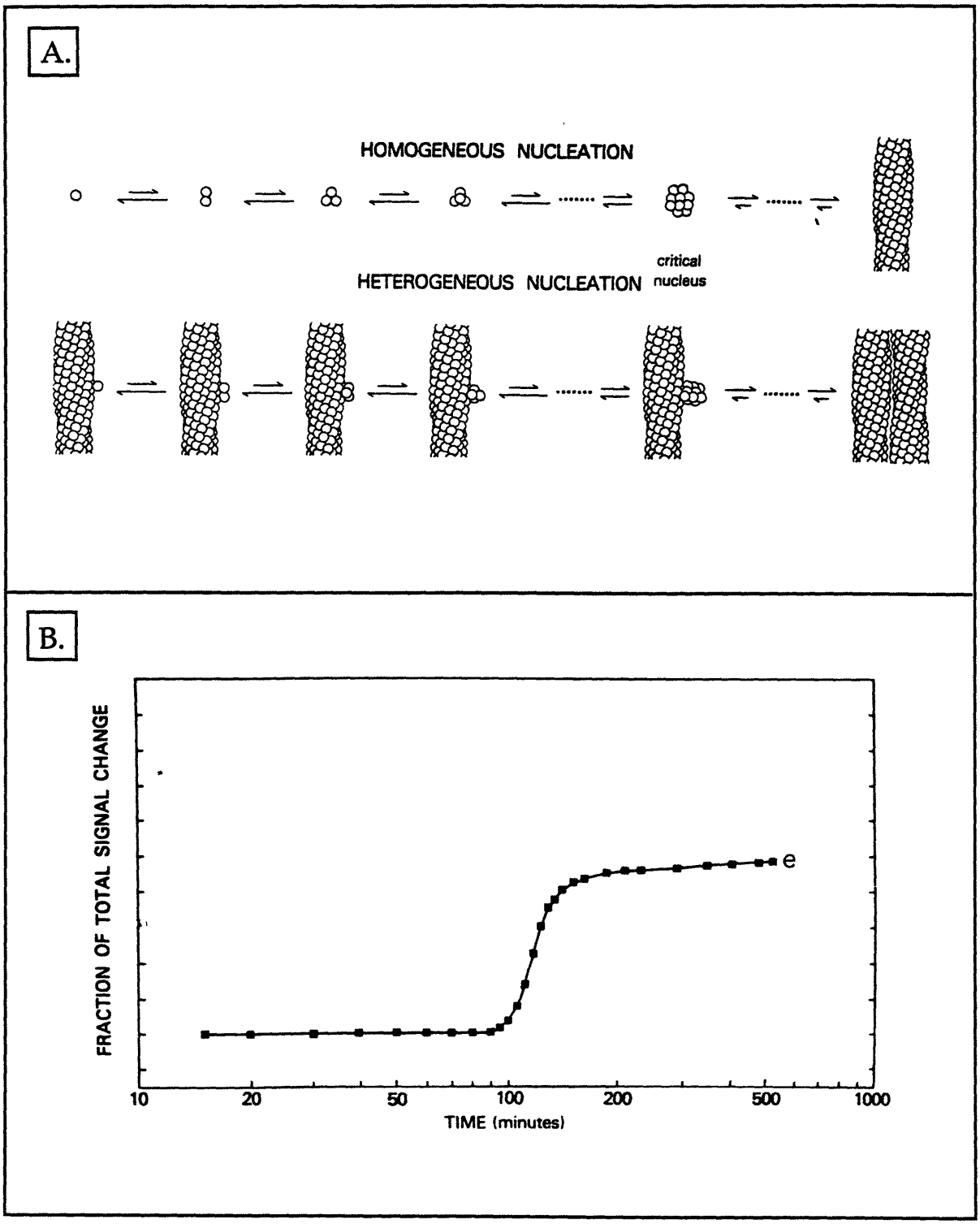

can sometimes be seen during the lag time.

The addition of preformed fibrils (or seeds) to a supersaturated solution of the β protein results in the elimination of the lag time.[2] The seed fibrils act as a nucleus onto which peptide monomers can add. This bypasses the unfavorable formation of the nucleus and results in immediate growth of the amyloid fibrils. Figure 3.3 shows a general mechanism for the formation of amyloid.

Figure 3.3 A general mechanism for nucleation-dependent formation of amyloid fibrils. A lag time occurs due to unfavorable association equilibria (K_n). After the formation of the nucleus, growth is rapid (K_g).

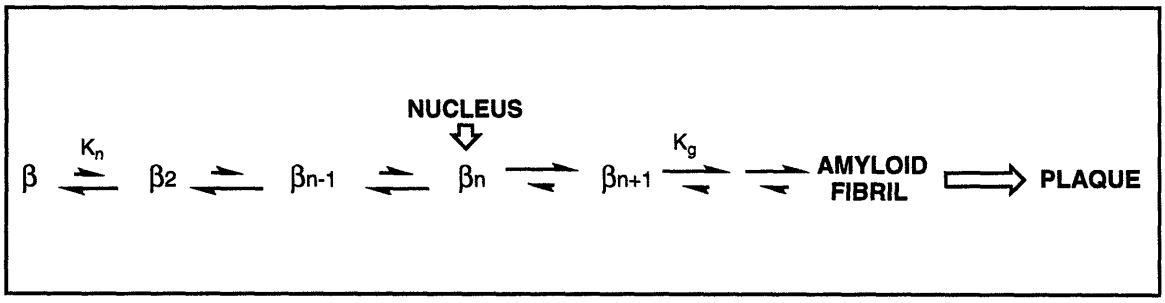

Very large differences in the solubilities of β1-39 and β1-42 have previously been reported.[9] Joseph Jarrett and Elizabeth Berger demonstrated that these three C-terminal residues had a dramatic effect on the aggregation of the β protein.[8] β1-40 and β1-39 have lag times of several days while β1-42 aggregates immediately. Additionally, β1-40 and β1-39 can be seeded by β1-42. This seeding phenomenon suggests a pathogenic role of β1-42 in AD by which small amounts of β1-42 could promote fibril formation by shorter and more soluble variants of the β protein.

Apolipoprotein E

Apolipoprotein E (apoE) is one of the best characterized apolipoproteins in terms of its structural and functional properties of the approximately 14 plasma apolipoproteins described to date. Apolipoproteins can perform one of three major roles in the body.[10] First, apolipoproteins stabilize the pseudomicellar structure of lipoprotein particles due to their ability to bind proteins that participate in the metabolism of lipoproteins as they circulate in plasma. Secondly, apolipoproteins can act as cofactors for various lipid transfer proteins that participate in the metabolism of lipoproteins as they circulate in the plasma. Lastly, two apolipoproteins, apoB100 and apoE, can serve as ligands for cell surface lipoprotein receptors. Receptor-mediated pathways are key components of lipoprotein metabolism and cholesterol homeostasis.[10]

Additional functions and properties have been ascribed to apoE. These include roles in immunoregulation[11], nerve regeneration[12], and lipoprotein lipase[13]. However, the discovery in 1991 that apoE was present in the amyloid plaques found in the brains of AD victims suggested a much more interesting function of apoE than those previously described.[14] In 1993, it was reported by the Roses group at Duke University Medical Center that *APOE4*, a naturally occurring allele of the gene encoding apoE, is a risk factor for late-onset AD.[15]

The polymorphic nature of apoE was established in 1982 using isoelectric focusing and two-dimensional electrophoresis.[16,17] The three major isoforms of apoE (apoE2, apoE3, and apoE4) are the result of three alleles (*APOE2*, *APOE3*, and *APOE4*) at a single gene locus. The expression of two of the three alleles leads to either three homozygous phenotypes, which are apoE2/2, apoE3/3, and apoE4/4, or three heterozygous phenotypes, which

are apoE3/2, apoE3/4, and apoE4/2. The most common allele is *APOE3* and the most common phenotype is apoE3/3. ApoE3 is therefore considered to be the parent form of the protein while apoE2 and apoE4 are variants. ApoE2 is associated with type III hyperlipoproteinemia and is defective in receptor binding.[18] ApoE4 displays normal binding but is associated with elevated plasma and LDL which is consistent with increased coronary heart disease in apoE4/4 homozygotes.[19] ApoE2 and apoE4 each differ from apoE3 by only one amino acid out of 299 (Table 3.2).

Table 3.2 Polymorphic amino acids in the three isoforms of apoE.

	112	158
apoE2	Cys	Cys
apoE3	Cys	Arg
apoE4	Arg	Arg

The gene encoding apoE is located on chromosome 19.[20] ApoE is produced in most organs with significant quantities found in the liver, brain, spleen, lung, and kidney. The second largest concentration (after the liver) of apoE mRNA is found in the brain.[21] ApoE is secreted by a wide variety of cells in the brain, including astrocytes. Following neuronal injury or degeneration, local apoE synthesis by astrocytes is dramatically increased.[22] ApoE is also the major apolipoprotein in the CSF of humans.[23]

Structure of apoE

ApoE was first described in 1973 as an arginine-rich component of triglyceride-rich very low-density lipoproteins (VLDL) with a relative molecular mass (M_r) of 34,000.[24] The sequence of apoE was determined in 1982 by direct protein sequencing of 299 amino acids (Figure 3.4).[25] Human apoE shares a high degree of sequence conservation across several species.[26]

Figure 3.4 The amino acid sequence of human apoE2. The two sites of point mutations (112 and 158) distinguishing the three isoforms are shown in bold.

```
1          10          20          30          40          50          60
KVEQAVETEPEPELRQQTEWQSGQRWELALGRFWDYLRWVQTLSEQVQEELLSSQVTQEL

           70          80          90          100         110         120
RALMDETMKELKAYKSELEEQLTPVAEETRARLSKELQAAQARLGADMEDVCGRLVQYRG

           130         140         150         160         170         180
EVQAMLGQSTEELRVRLASHLRKLRKRLLRDADDLQKCLAVYQAGAREGAQRGLSAIRER

          190         200         210         220         230         240
LGPLVEQGRVRAATVGSLAGQPLQERAQAWGERLRARMEEMGSRTRDRLDEVKEQVAEVR

           250         260         270         280         290
AKLEEQAQQIRLQAEAFQARLKSWFEPLVEDMQRQWAGLVEKVQAAVGTSAAPVPSDNH
```

Based on the Chou-Fasman algorithm for prediction of secondary structure[27], apoE is predicted to be highly helical, segregating into two ordered N- and C-terminal domains connected by a random coil.[25] The α-helix, β-sheet, β-turn, and random structure contributions are predicted to be 62%, 9%, 11%, and 18%, respectively (Figure 3.5).[28]

Figure 3.5 Predicted secondary structure of apoE, showing α-helices, β-sheet, and β-turns (remainder is random coil).[28]

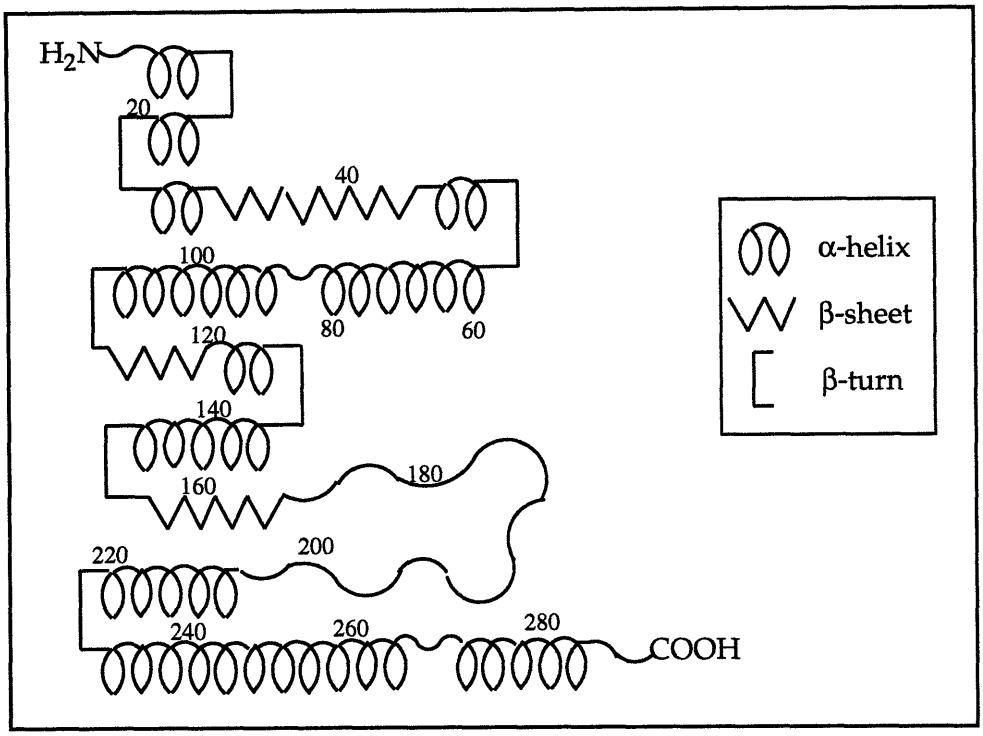

ApoE remains a tetramer over a wide range of concentrations.[29] Additionally, apoE displays two transitions when denatured by guanidine hydrochloride (GuHCl) and protein unfolding is monitored by CD. The first occurs at 0.7 M GuHCl, where most other apolipoproteins are completely unfolded, and the second occurs at 2.4 M GuHCl.[30] These results indicate that apoE contains two independently folded regions, one of which possesses a very high stability that is unique among plasma apolipoproteins.

This observation is supported by evidence demonstrating that upon exposure to limited proteolysis by five proteases, there are two protease-resistant domains.[30] After cleavage with thrombin, a 22 kD N-terminal domain (amino acids 1-191) and a 10 kD C-terminal domain (amino acids 216-299) are generated. The denaturation curves of these two domains indicate

that the 22 kD domain closely approximates the highly stable domain of the full-length apoE while the 10 kD domain approximates the less stable domain.

Size-exclusion chromatography demonstrated that the 22 kD domain is monomeric and the 10 kD domain is tetrameric, most likely with the hydrophobic surfaces of the amphiphilic helices sequestered within the interior of the bundle.[29] This suggests that tetramerization of the full-length protein is mediated by the C-terminal 10 kD domain. Both domains have been shown to by highly helical by CD.

Crystal structures of the 22 kD domains of apoE2, apoE3, and apoE4 have been determined.[31] The structures contain five helices, four of which are arranged in an antiparallel four-helix bundle (Figure 3.6). The hydrophobic side-chains are packed within the interior of the bundle, adding to the stability of the structure, while the hydrophilic side chains are solvent exposed. Due to an inability to make crystals from the 10 kD domain, there is far less structural information for this domain.

While the 10 kD domain of apoE has been defined as the lipid-binding portion of the full-length protein, the 22 kD portion of the molecule has also been shown to bind phospholipids *in vitro*.[32] The hydrophobic side-chains of the 22 kD four-helix bundle are directed toward the interior of the bundle. Lipid association is required for high-affinity binding to the LDL receptor and it is proposed that the hydrophobic faces of the apolipoprotein amphipathic helices interact with the hydrophobic acyl chains of phospholipids.

Figure 3.6 The four-helix bundle motif of the 22 kD domain of apoE3, as determined by its crystal structure.

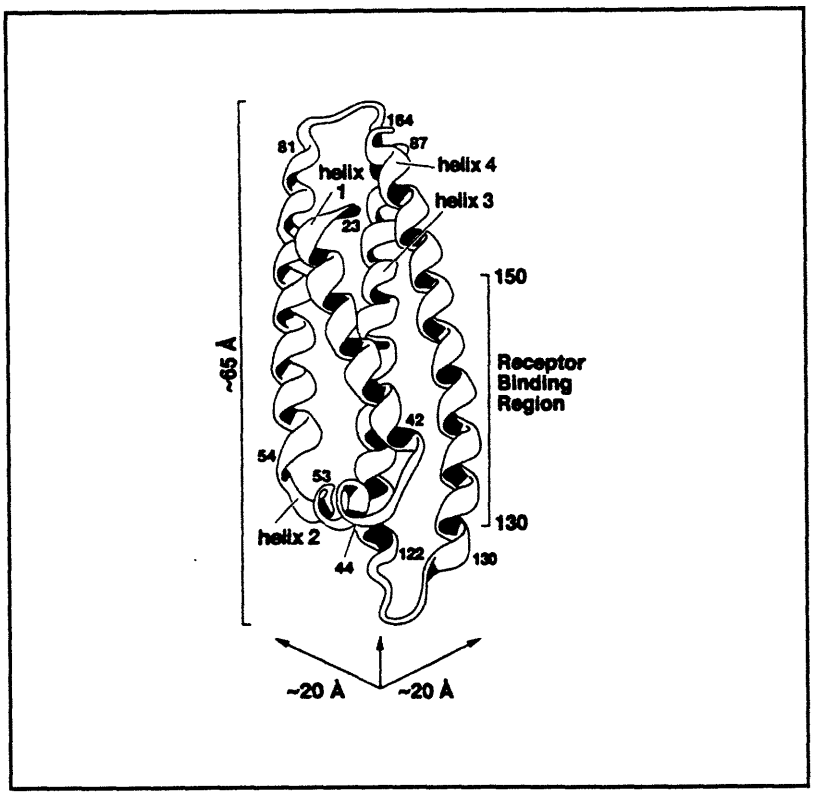

Function of apoE

ApoE plays an important role in plasma lipoprotein metabolism, cholesterol homeostasis, and local lipid transport processes.[28] ApoE is a ligand for the low-density lipoprotein (LDL) receptor, and apoE enriched lipoprotein particles also bind to the LDL-receptor-related protein (LRP).[22] ApoE that is secreted by active astrocytes in the brain performs two functions. ApoE removes the lipids released by degenerating neurons and it transports lipids to sprouting neurons. ApoE also decreases neurite branching and promotes neurite extension away from the neuronal cell body.[22]

ApoE binds to the LDL receptor and selective chemical modification studies have demonstrated that lysyl and arginyl residues are important for

the interaction.[33] Although intact apoE forms a stable tetramer in solution, this tetramerization does not appear to be required for lipid-binding or binding to the LDL-receptor.[29]

The lipid-binding properties of the 22 kD and 10 kD domains were determined by their ability to form complexes with dimyristoylphosphatidylcholine (DMPC). The results indicated that the relative lipid-binding efficiency of the intact apoE was approximately equal to the 10 kD domain, and that the 22 kD was less efficient.[34]

The 22kD domain is capable of associating with phospholipid to form discoidal complexes, although this fragment associates poorly with native lipoproteins. However, when recombined with phospholipid, it was determined that the 22 kD N-terminal domain (amino acids 1-191) was active and therefore must be the receptor-binding domain of intact apoE.[32] The 10 kD C-terminal domain showed no receptor-binding ability, even in the presence of lipid.

While the 22 kD domain appears to be the receptor-binding domain, most evidence suggests that the 10 kD domain of apoE contains the lipid-binding site. According to CD data, the α-helical content of apoE and the 10 kD fragment increased upon phospholipid binding.[29] C-terminally truncated mutants of apoE were studied in order to define more precisely the regions of this domain responsible for its lipid-binding properties.[35] The results demonstrated that the deletion of residues 267-299 impairs the association of apoE with lipoprotein particles, suggesting further that these residues in the C-terminal domain are essential to lipid binding.

The Connection of Apolipoprotein E with AD

ApoE was first suggested as playing a role in the pathogenesis of AD after it was identified as an amyloid-binding protein and was localized in senile plaques.[36] The genetic localization of apoE on chromosome 19 fit in well with previous studies that reported genetic linkages and associations between markers on chromosome 19 and late-onset AD.[37]

Further genetic studies have strengthened the hypothesis that apoE is an important risk factor in AD. The Roses group at Duke University completed a study of apoE genes in 234 people from 42 families afflicted with late-onset AD. By age 80, almost all the people in the study who had two copies of the *APOE4* allele developed the disease.[15] Their overall risk was more than eight times greater than that of people with no copies of the gene. The establishment of apoE4 as a risk factor for late-onset AD was the first major breakthrough in establishing genetic causes for the most common form of AD. Late-onset AD is currently responsible for 75% of all cases of AD.[38]

A gene dosage effect for the risk of developing AD and the age of onset has been observed. People who have two copies of the *APOE4* allele have a much higher risk of developing AD at an earlier age than do people with no *APOE4* alleles. However, people who only have one copy of the *APOE4* allele are intermediate in both their risk for developing AD and the age of onset of the disease (Figure 3.7).[15]

Figure 3.7 Correlation of apoE genotype with AD risk and age of onset.[15]

Apo E genotype (normal pop.)	Percent affected	Mean age at onset
3/3 (61%)	21%	84
3/4 (22%)	48%	75
4/4 (3%)	91%	68

The genetic link between apoE and AD is controversial. It is possible that apoE has nothing to do with the pathogenesis of AD. There could be an AD causing gene lying close enough to the *APOE* locus that genetic epidemiology confuses the two. If this were true, the APOE gene would actually be a marker for the cause of the disease.[38]

Effect of apoE on Brain Morphology, Memory, and Cognition in AD

In addition to an increase in the risk of developing AD, victims of AD who are homozygous for the *APOE4* allele have an increased density of senile plaques in their brains when compared to patients who are homozygous for the *APOE3* allele or who are *APOE3/4* heterozygotes.[39] This suggests that apoE is somehow involved in the clearance of the β protein because it has been demonstrated that plaques do not appear to accumulate over the course of AD.

Additionally, while both AD associated with apoE4 and Down's Syndrome (DS) lead to increased amyloid deposition, they appear to do so by different mechanisms.[40] The plaques formed in DS are larger than those found with apoE4. In AD associated with apoE4, the plaques are similar in

size to those formed in *APOE3* homozygotes, but the number of plaques is increased.

The larger plaques associated with DS may reflect an increase in β protein production and, therefore, in the availability of β protein monomers for plaque growth, while the increase in the number of plaques in *APOE4* homozygotes could be the result of an increased probability of senile plaque formation. These results suggest that the function of apoE, which includes the binding to and the transportation of hydrophobic molecules such as lipids, could also be part of a clearance mechanism for the β protein or β protein aggregates.[39]

If apoE4 is less efficient than apoE3 at clearing small aggregates, this could lead to an increased chance that an aggregate would reach a critical threshold size, leading to an increased number of senile plaques without affecting the size distribution.

In the time since it was determined that the *APOE4* allele is a risk factor for AD, scientists have investigated whether or not the presence of different apoE alleles in AD affect specific cognitive functions or rates of cognitive decline differently. Thus far, the role of apoE in predicting cognitive decline in AD has not been unequivocally proven, however, results seem to indicate that apoE4 may be responsible for lower cognitive performance.

One study characterized the clinical status and apoE genotype of a group of patients over the course of five years with mild cognitive impairment (MCI) that were not clinically diagnosed with AD, and found that the *APOE4* allele appeared to be a strong predictor of clinical progression to AD.[41] Another study based on a random sample of elderly subjects with no signs of dementia monitored memory over 3.5 years and showed that subjects with *APOE2/2* and *APOE2/3* genotypes demonstrated better learning ability

than subjects with one or two copies of the *APOE4* allele. The learning ability of these people declined much more rapidly over time.[42]

Another study that administered cognitive tests over a five-year period to probable AD patients found that the rate of cognitive decline did not vary significantly across apoE genotypes.[43] However, cognitive testing was performed at a more advanced stage of AD. This indicates that apoE4 may affect the pathogenesis of AD only in the initial pre-symptomatic stages of the disease. After the clinical diagnosis of probable AD, the disease may progress identically, regardless of the apoE genotype.

Proposed Role of apoE in AD

There are presently two hypotheses that could explain the role of apoE in AD. The first involves the neurofibrillary tangles and microtubule-associated protein, tau. The second, and more widely supported, involves the amyloid-cascade hypothesis.

Additionally, the effect of apoE4 on amyloid formation in AD can also be described by two scenarios. The first suggests that apoE4 acts as a "pathological chaperone" and promotes the transformation of β protein monomers into an insoluble aggregate, thus facilitating plaque formation.[44] The second scenario suggests that all forms of apoE actually inhibit the formation of amyloid, but apoE4 is actually a less efficient inhibitor than apoE3 and apoE2.[45]

The latter scenario involves the premise that different protein isoforms expressed from polymorphic alleles may have slightly altered functions with cumulative effects as people age. The relationship between apoE polymorphisms and AD was less important when people did not live more than 70 years and when AD was a less prevalent disease. Presently,

several groups have shown the inhibitory effect of apoE on β protein fibril formation, as well as the ability of apoE to attenuate the neurotoxicity of the β protein.[45-48]

ApoE-Deficient Mice as a Model for AD

Depending on whether apoE4 is an inhibitor or a promoter of amyloid formation, there are two types of genetically modified animal models that can be studied. If apoE4 acts as a "pathological chaperone",[44] then a mouse over-expressing apoE4 might be useful in promoting the formation of amyloid plaques *in vivo.* However, if apoE4 is actually an inhibitor of amyloid formation (albeit less efficient inhibitor than apoE3), then amyloid formation in apoE knockout mice that also overexpress APP should be extremely useful because the ability of the animal to suppress amyloid formation should be greatly reduced.

The density of hippocampal synapses of apoE-deficient mice is reduced and they have a diminished regenerative capacity following hippocampal lesions. Studies have also revealed loss of forebrain cholinergic neurons and a preferential decrease in working memory, which are early and prominent features of AD, suggesting that the mouse model may replicate pathogenic processes in AD.[49]

One problem that is encountered when studying apoE-deficient mice is that serum levels of cholesterol are five to six times normal in the apoE-deficient mice. This abnormal lipoprotein phenotype in apoE knockout mice makes the study of AD in these animals more difficult because the animals sometimes die prematurely of aneurysms.[50]

Results from *In Vitro* Studies of apoE and the β Protein

As mentioned above, the possession of the *APOE4* allele has been implicated as a risk factor for late-onset AD. Some have speculated that apoE4 may accelerate amyloid formation because apoE has been colocalized in the senile plaques found in the brains of AD victims[1] and appears to bind to the β protein in vitro.[36] However, this hypothesis has not been experimentally tested.

The formation of amyloid by the β protein is a nucleation-dependent process and is rate-limited by the formation of the nucleus.[8,51] The circulating variant, β1-40, nucleates slowly relative to the C-terminally extended variants, β1-42 and β1-43.[8] Endogenous proteins such as apoE could either promote amyloid formation by stabilizing prenucleus oligomers or seeding growth. Alternatively, apoE could interfere with the aggregation by either inhibiting nucleus formation or by inhibiting growth of the nucleus. Our laboratory has found that apoE4 is a less effective inhibitor of amyloid formation than apoE3.

ApoE is an Inhibitor of Amyloid Formation

In vitro amyloid formation by β1-40, as measured by turbidity, demonstrated a protracted lag time in the absence of agitation. After approximately ten days at a concentration of 40 μM, the growth of amyloid fibrils occurred. The addition of apoE3 or apoE4 to a supersaturated solution of the β protein in a 1:100 molar ratio of apoE:β1-40 ([apoE] = 40 nM) prolonged the lag time significantly. The lag time was extended to more than 20 days upon the addition of apoE (Figure 3.8). However, the addition of

insulin, bovine serum albumin, and α-crystallin at ten times the concentration (400 nM) of apoE had no effect on the observed lag time.

Figure 3.8 The aggregation of β1-40 (40 μM) in the presence of exogenous proteins (40 nM) in the absence of agitation.

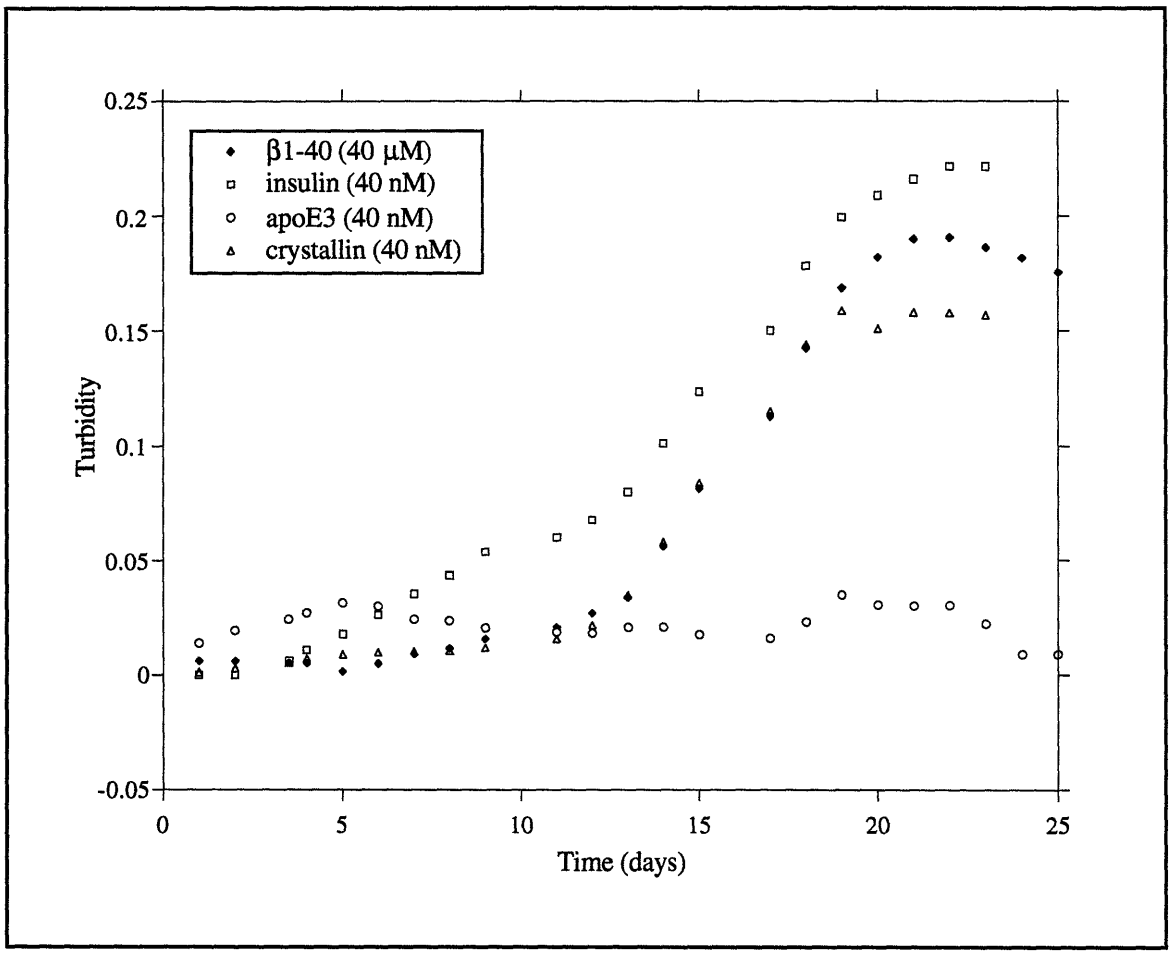

Prenucleus oligomers are rapidly populated for β1-42 at 40 μM causing the peptide to nucleate faster than β1-40.[8] Experiments that tested the ability of apoE to inhibit the aggregation of β1-42 were not successful because amyloid formation occurs much more rapidly and does not exhibit a lag time at 40 μM (Figure 3.9). Our assay did not allow observation of the aggregation

of β1-42 at a concentration closer to its solubility where a lag time would be expected to occur.

Figure 3.9 Aggregation of 40 μM β1-42 in the presence of apoE3 and apoE4 (400 nM).

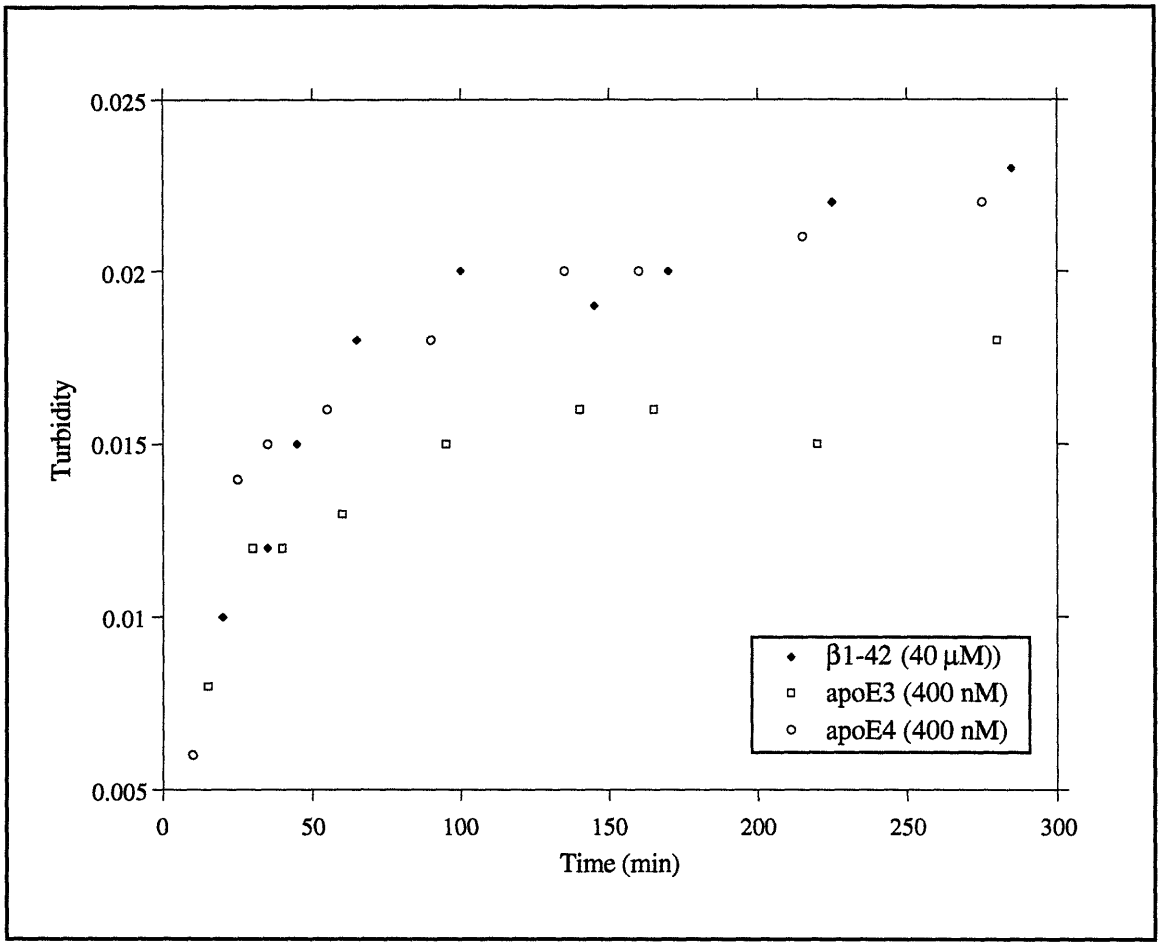

Additional kinetic studies of amyloid formation by β1-40 were done under stirred conditions which increased the nucleation rate significantly, most likely by promoting secondary nucleation events. As in the unstirred assay, an increase in the lag time was observed in the presence of a 1:100 molar ratio of either apoE3 or apoE4 to β1-40 where the apoE concentration

was 800 nM and the β1-40 concentration was 80 μM. The results demonstrated that apoE4 is an equipotent or less potent inhibitor than apoE3 of amyloid formation by the β protein. The lag time for β1-40 was 143 ± 10 minutes; however, when 1% apoE3 was added to a supersaturated solution prior to aggregation the lag time was extended to 258 ± 12 minutes. The lag time in the presence of 1% apoE4 was 210 ± 53 minutes (Table 3.3). A typical representative stirred aggregation experiment showing the effect of apoE on fibril formation is depicted in Figure 3.10.

Table 3.3 Lag times for β1-40 alone and in the presence of 1% apoE3 and apoE4.

	Lag Time (min)
β1-40	143 ± 10
+ apoE4	210 ± 53
+ apoE3	258 ± 12

Because of the extreme sensitivity of nucleation to protein concentration, vibrations, trace impurities, and stirring rate[52], the lag time is extremely difficult to measure more accurately.[51] Consequently, the error in our measurement of nucleation time for apoE4 was approximately equal to the difference between apoE3 and apoE4. An additional complication results from differences in nucleation time between commercial lots of β1-40 (Bachem), possibly due to the presence of undetectable impurities.[53] Therefore, each experiment was done with a single β1-40 lot and only qualitative comparisons were made between experiments done with different lots.

Figure 3.10 Inhibition of the aggregation of 80 μM β1-40 by 1% apoE under stirred conditions.

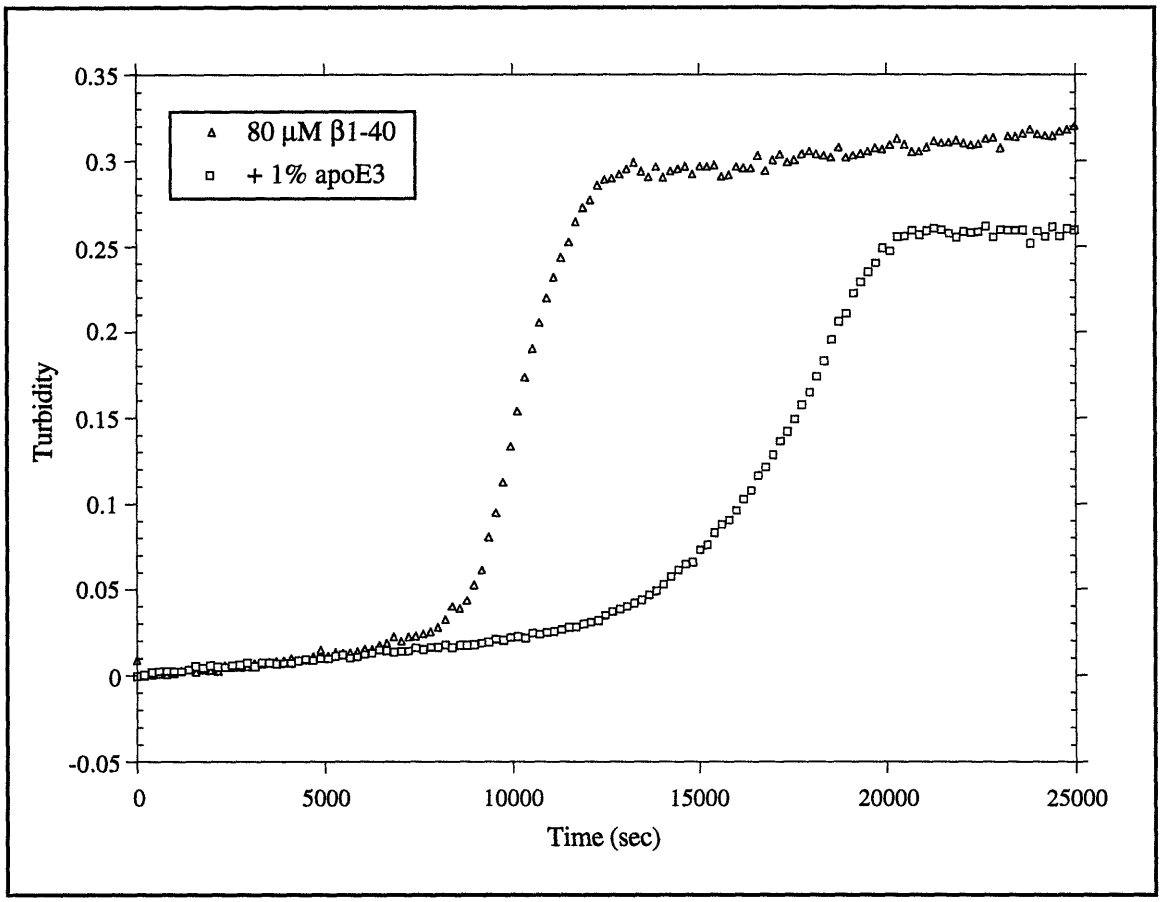

ApoE Does Not Inhibit the Seeding of Amyloid Fibrils

The insignificant effect of apoE on amyloid growth rate and final solubility in the kinetic assays above suggest that apoE does not interfere with the post-nucleation aggregation process. Consistent with that postulate, the presence of 1% apoE3 or apoE4 had no effect on the seeding of amyloid formation by the addition of β1-40 fibrils added to a supersaturated solution (Figure 3.11).

Figure 3.11 The seeding of amyloid formation with 5% preformed amyloid fibrils in the presence of 1% apoE3.

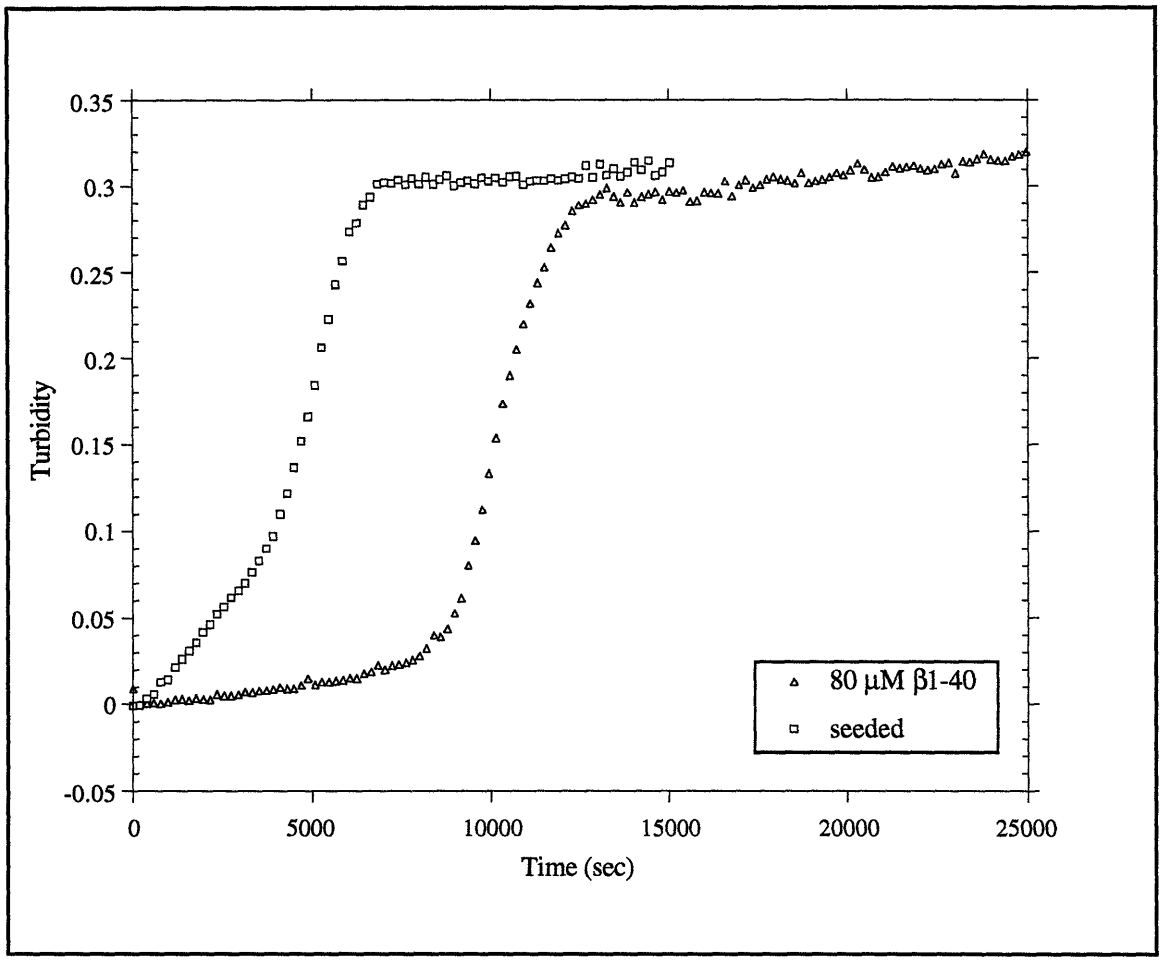

ApoE Does Not Effect the Structure or Solubility of β1-40

Experiments were performed to determine the solubility of β1-40 alone and in the presence of apoE3 and apoE4. Supersaturated solutions of radioiodinated β1-40, with and without 1% apoE3 or apoE4, were allowed to aggregate under stirred conditions for several days. The amount of peptide remaining in solution after three days, or its solubility, was measured by counting the radioactivity. At concentrations sufficient to significantly delay

nucleation, neither apoE3 nor apoE4 had a measurable effect on the solubility of β1-40, which was determined to be 33 ± 4 μM.

No structural differences were observed for amyloid fibrils formed by β1-40 alone or in the presence of apoE3 or apoE4 as demonstrated by FTIR microscopy (Figure 3.12).

Additionally, amyloid fibrils formed in the presence of inhibitory concentrations of apoE3 and apoE4 were indistinguishable from those formed in their absence, with regard to their morphology as seen by electron microscopy (Figure 3.13).

Inhibition of Amyloid Formation by the ApoE3 Dimer

Analysis of apoE3 and apoE4 by SDS gel electrophoresis under non-reducing conditions indicated that apoE3 contained a small amount of dimer (10-30%) under the conditions of the kinetic aggregation assays above (Figure 3.14). This has biological significance as the plasma dimer levels for *APOE3* homozygotes average approximately 27% of their total apoE3.[54] This may help to explain the more efficient amyloid suppression in *APOE3* homozygotes. The wide range in reported dimer levels (12-37%) suggests that factors that alter the apoE3 monomer/dimer ratio may also be important in the pathogenesis of AD. Conversely, apoE4, which does not contain a cysteine at position 112 as apoE3 does, is unable to form a disulfide dimer.

Figure 3.12 Infrared spectra of amyloid fibrils formed by β1-40 alone (A), in the presence of apoE3 (B), and in the presence of apoE4 (C).

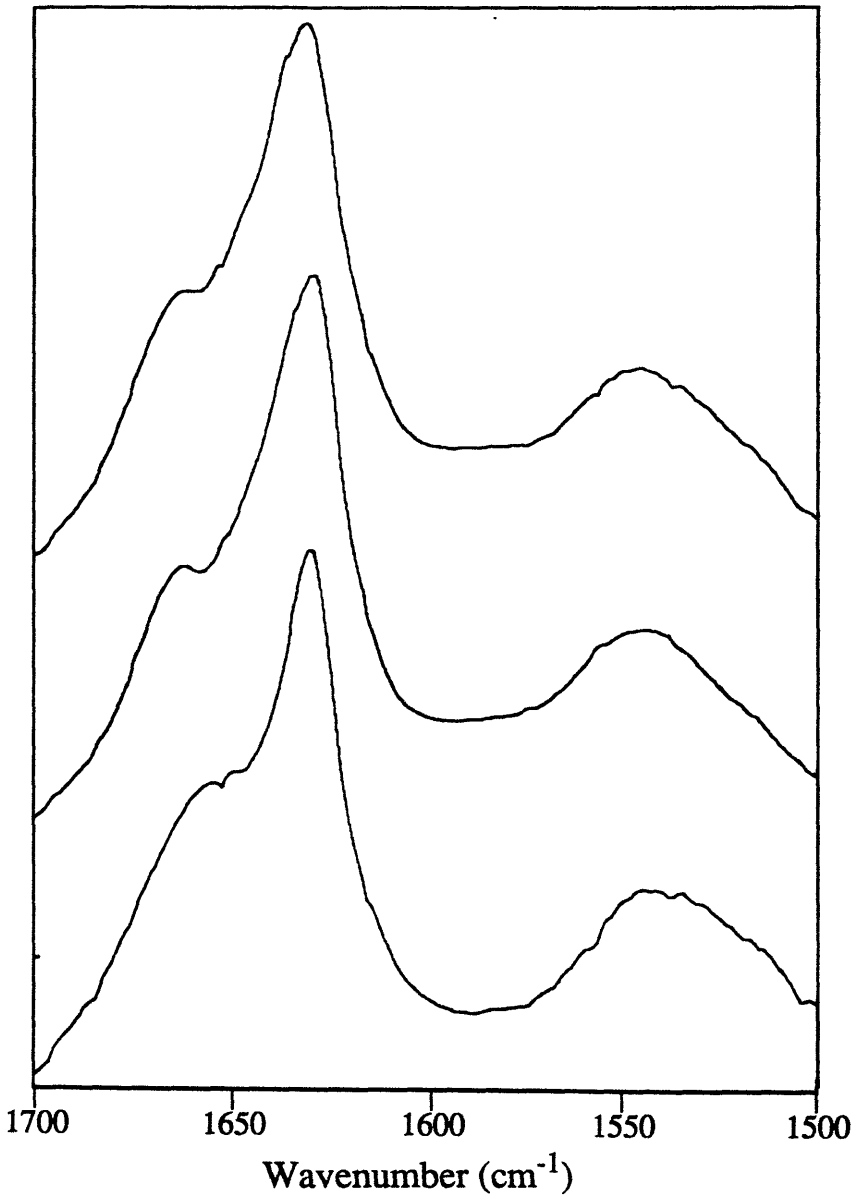

Figure 3.13 Electron micrographs of amyloid fibrils formed by β1-40 alone (A), in the presence of apoE3 (B), and in the presence of apoE4 (C). (Bars = 1000 Å)
(See next page)

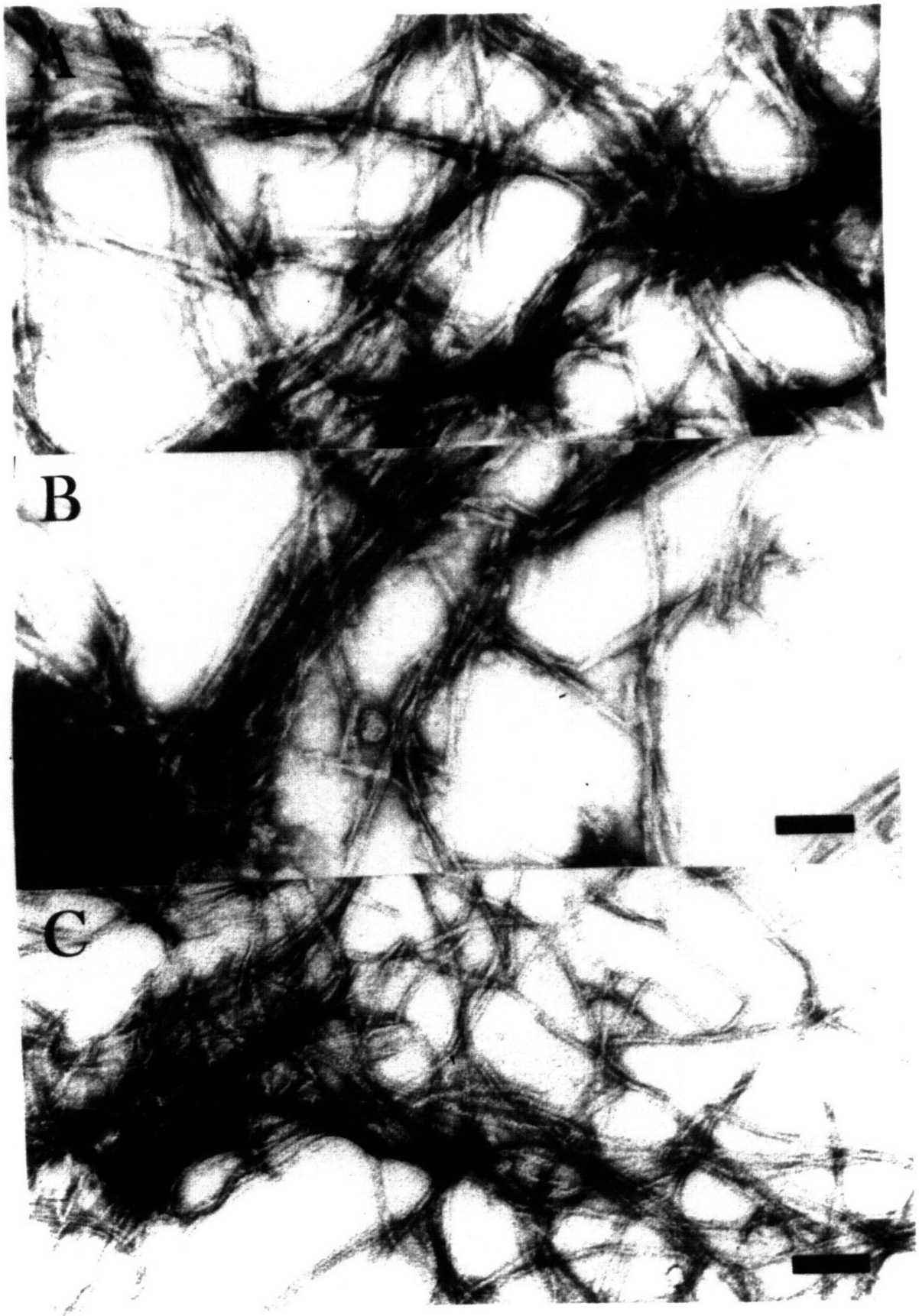
A
B
C

Figure 3.14 SDS-PAGE of the full-length apoE isoforms under non-reducing conditions (lanes 1, 3, 5, and 7) and reducing conditions (lanes 2, 4, 6, and 8) Lanes 1 and 2 are apoE2; lanes 3 and 4 are apoE3; lanes 5 and 6 are the apoE3 dimer; and lanes 7 and 8 are apoE4.

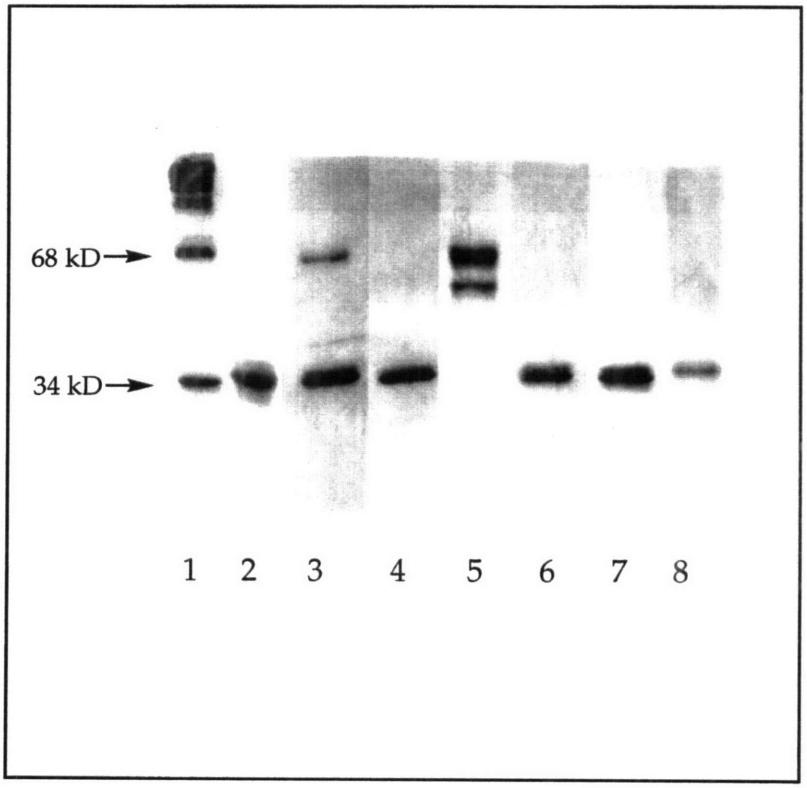

In order to test the possibility that dimerization was responsible for the slight difference in the inhibitory activities of the two variants, the apoE3 covalent dimer was tested and the results are shown in Figure 3.15. The apoE3 dimer at 400 nM, or 0.5% of a molar equivalent based on an 80 μM concentration of β1-40, showed a lag time of 605 ± 50 minutes which was much longer than the 224 ± 100 minutes for apoE4 at twice the concentration. The unusual shape of the inhibited aggregation curves (i.e. slight increase in turbidity before rapid growth begins) suggests that the aggregation mechanism may be altered.

Figure 3.15 Inhibitory effects of 1% apoE4 and 0.5% apoE3 disulfide dimer on the aggregation of 80 μM β1-40.

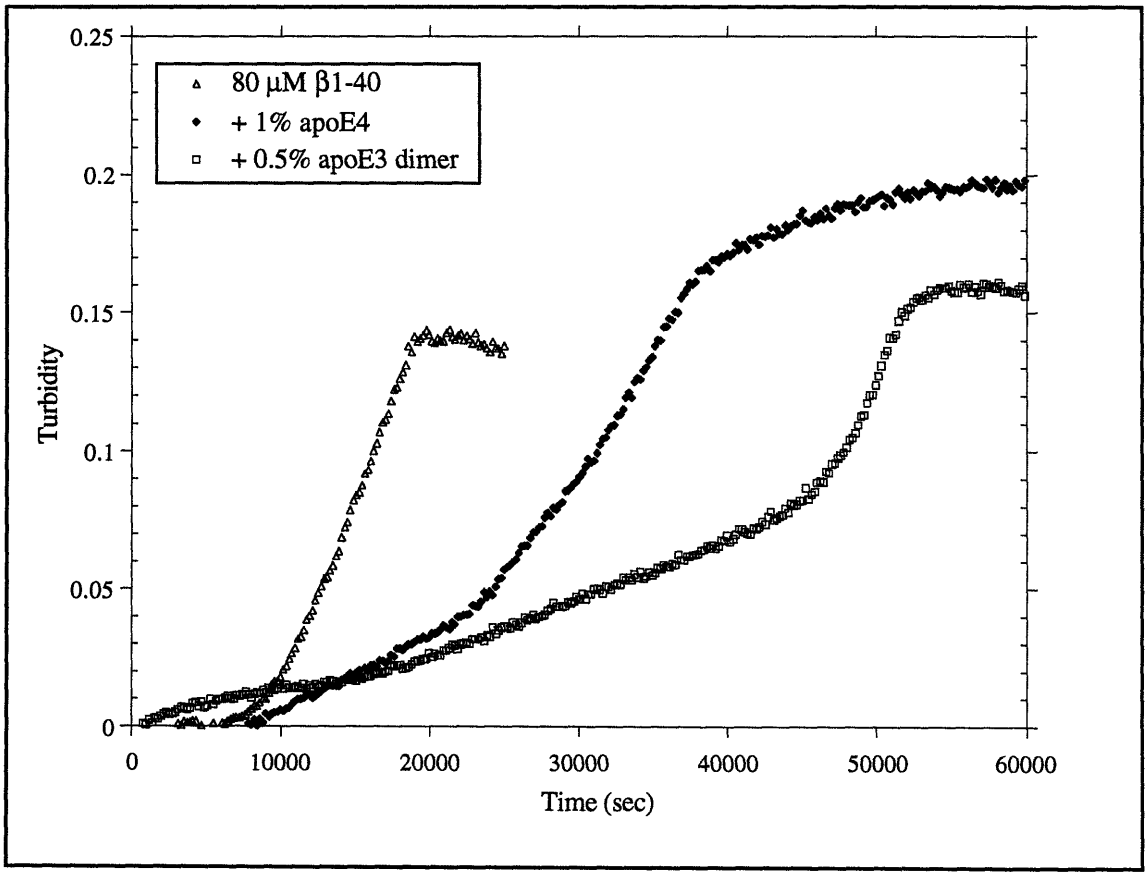

Binding Studies of the β protein with apoE

Previous studies have shown that apoE in cerebrospinal fluid binds with high avidity to immobilized β protein.[36] Additionally, an SDS-stable interaction between the β protein and apoE has been described.[55] In order to test these results, the experiments were repeated in our laboratory following the procedures given in these studies. β1-40 was incubated alone and in the presence of apoE3, apoE4, and the apoE3 dimer. The samples were then run on a denaturing, non-reducing gel (Figure 3.16). After repeating the experiments several times, a band corresponding to a β protein-apoE complex was still not detected.

Discussion

The studies presented herein demonstrate that *in vitro* nucleation of amyloid formation by β1-40 is inhibited by concentrations of apoE3 and apoE4 which are low in the relative (0.1% of a molar equivalent compared to β1-40) and absolute (40 nM) senses. ApoE is known to be produced in the brain and a concentration of 100 nM has been measured in human cerebrospinal fluid.[56] This concentration of apoE is sufficient to delay the nucleation of amyloid in a physiologically significant way. The stoichiometry of inhibition of nucleation by apoE3 and apoE4 suggests that apoE binds to a prenucleus oligomeric intermediate (Figure 3.17) and prevents its elaboration, as opposed to binding to monomeric β1-40. The fact that seeding of amyloid formation is not prevented by apoE3 or apoE4 is consistent with that scenario. Furthermore, 1% inhibitory concentrations of apoE do not appear to effect the

Figure 3.16 SDS-PAGE (non-reducing conditions) of the β protein incubated with apoE3, apoE4, and the apoE3 dimer for 1.25 hours. Lanes 1, 2, 4, 6, and 8 contain β1-40; lanes 2 and 3 contain apoE3; lanes 4 and 5 contain apoE4; lanes 6 and 7 contain apoE3 dimer; and lanes 8 and 9 contain apoE2.

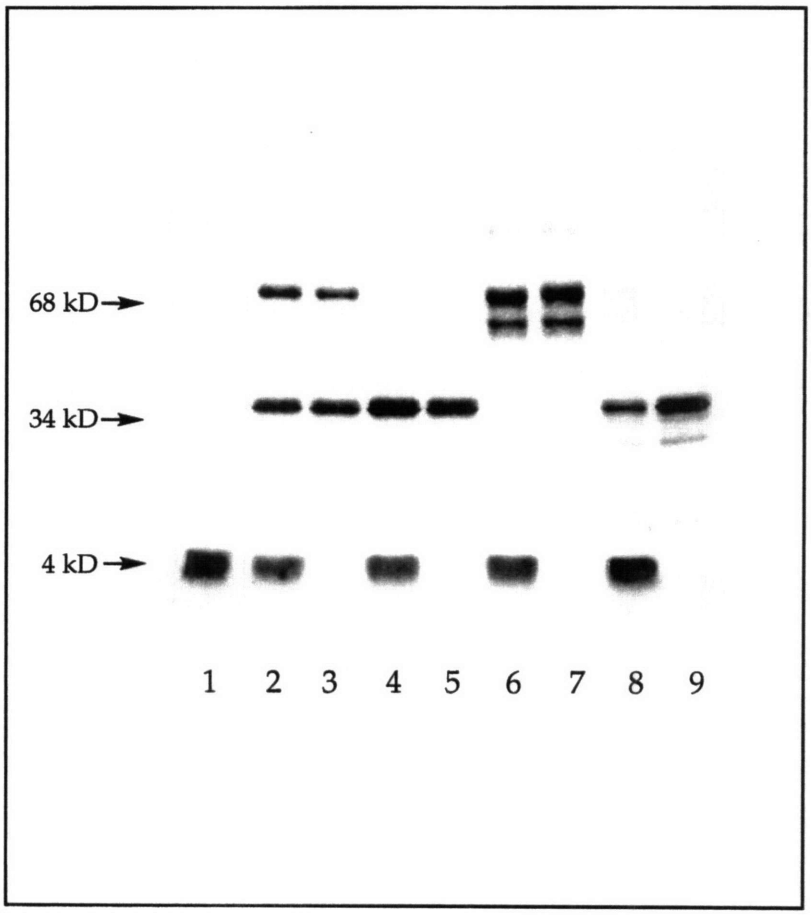

growth, stability, or structure of β1-40 amyloid fibrils. Thus, apoE most likely does not interact strongly with the amyloid nucleus or the subsequent intermediates.

Figure 3.17 A general mechanism for nucleation-dependent amyloid fibril formation, including a working hypothesis for the effect of apoE.

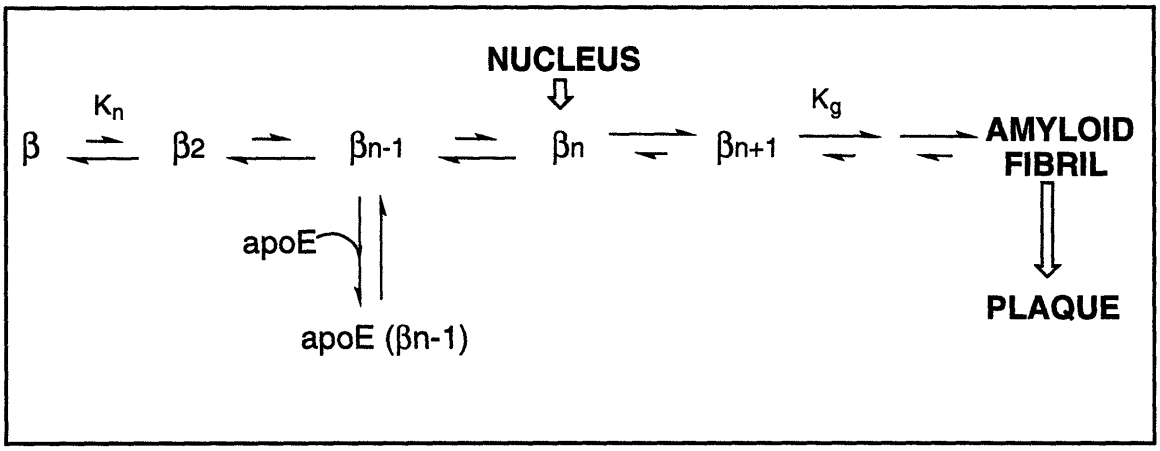

The precision of the assay for amyloid formation utilized herein was insufficient to distinguish the inhibitory activities of apoE3 and apoE4. However, the apoE3 disulfide dimer, which was present at low levels in the apoE3 sample, was a significantly more efficient nucleation inhibitor than apoE4. This effect may derive from the entropic benefit of tethering two β oligomer binding domains.

The correlation of the apoE4 allele with an earlier age of AD onset[15] and an increased amount of amyloid at the time of death[57] has stimulated rampant speculation concerning the underlying molecular mechanism. It has been proposed that apoE4 may promote amyloid formation by stabilizing the aggregating conformation of the β protein[44]. However, the results presented herein prove that both common apoE variants inhibit amyloid formation *in vitro*.

Amyloidogenesis may occur at a low rate in most individuals, due, in part, to the suppression of amyloid nucleation by endogenous apoE. Inefficient suppression of amyloid formation by an apoE4 homozygote could be a contributing factor to the development of AD. The *in vivo* crystallizations of calcium oxalate (from supersaturated urine[58]) and of calcium phosphate (from supersaturated saliva[59]) are also suppressed by endogenous inhibitor proteins. The apoE3 dimer is clearly a more efficient nucleation inhibitor than apoE4, which cannot dimerize. In addition, the plasma apoE4 concentration of an apoE4 homozygote is *ca.* 40% lower than the plasma total apoE3 concentration in an apoE3 homozygote (*ca.* 1.5 mM).[60] The analogous measurement of CSF or brain tissue has not been reported, but if a comparable concentration difference exists in the brain it could partly or fully explain the compromised ability of apoE4 homozygotes to suppress amyloidogenesis. Finally, the correlation between apoE genotype and AD risk may also involve events other than amyloidogenesis.[61]

The findings reported herein have significant practical implications. Transgenic apoE knockout mice in which APP is overexpressed could be excellent models for AD amyloidogenesis, since their natural amyloid suppression system is compromised. It has been observed that low concentrations of apoE attenuate the neurotoxicity of the β protein.[48] This effect may be due to inhibition of amyloid nucleation by apoE, an activity which may have therapeutic benefit. Prenucleus oligomers represent the most efficient target for endogenous amyloid inhibitors since they are sparsely populated during the aggregation process[51] and the inhibitor protein need only be expressed at trace levels. Synthetic, nonpeptide inhibitors could be designed to follow Nature's strategy by "poisoning" the crystallization of amyloid.[53]

Experimental

Materials

The β protein isoform β1-40 was purchased from Bachem. ApoE proteins were obtained from Dr. Karl Weisgraber at the Gladstone Institute (UCSF). ApoE3 and apoE4 were purified as detailed in the literature.[62] The apoE3 dimer was isolated as reported in the literature.[54] The molecular weights of these proteins and their purity were checked by SDS-PAGE under non-reducing conditions. The apoE3 samples also contained a significant amount of dimer (*ca.* 10-30%). The α-crystallin was provided by Dr. J. Horowitz. Insulin was obtained from Sigma and bovine serum albumin was obtained from Pierce. The Lowry protein assay kit was obtained from Pierce. Millex-GV 0.22 μM filters were purchased from Millipore.

Aggregation Assay (Unstirred)

Stock solutions were prepared by dissolving β1-40 (Bachem) in DMSO at 1-1.5 mM. The peptide solution was then sonicated for 30 min and filtered through Millex-FG 0.22 μm filters. The final β1-40 concentration was determined by quantitative amino acid analysis. Sonication and filtration were critical in removing any trace of undissolved seeds that may resist solubilization. In the absence of filtration, immediate nucleation was occasionally observed, presumably due to the undetected presence of undissolved seeds in the DMSO solution. Aliquots of β1-40 stock (40 nmol in *ca.* 40 μL DMSO) were added to aqueous buffer (1000 μL total volume, 100 mM NaCl, 10 mM NaH_2PO_4, pH 7.4). Aggregation was measured by turbidity at 400 nm *vs.* a buffer blank. The peptide solutions were briefly vortexed before each

absorbance measurement in order to evenly suspend the fibrils. For aggregation experiments with apoE, β1-40 stock (40 nmol in DMSO) was added to buffer containing 0.1% of a molar equivalent of apoE3 or apoE4 Absorbance (400 nm) was measured *vs.* a blank containing buffer and apoE.

Aggregation Assay (Stirred)

Stock solutions were prepared as previously described for unstirred assays. Aliquots of β1-40 stock (80 nmol in DMSO) were added to aqueous buffer (1 mL total volume), or to buffer containing 1% of a molar equivalent of apoE. The solutions were stirred continuously (1550 rpm) and turbidity was measured at 400 nm. Lag times were calculated by curve-fitting the steepest growth portion of each aggregation curve and extrapolating to zero absorption. These values were averaged to determine the lag times and standard deviations reported in the text.

Seeding Experiments

A peptide solution of 80 μM β1-40 was stirred for three days to produce amyloid fibrils. The fibrils were sonicated for 20 minutes and a portion of the fibril suspension (50 μL, 4 nmol) was added to 950 μL of an 80 μM β1-40 solution in buffer containing 1% molar equivalents of apoE (800 nM). Aggregation was monitored by turbidity at 400 nm (*vs.* seed alone).

Radioassay

As a complement to the turbidity assay of insoluble amyloid, the amount of peptide remaining in solution during the aggregation process was measured by radioassay. Radioiodinated β1-40 (*ca.* 250 Ci/mmol, provided by

Dr. Harry LeVine of Parke-Davis) was added to a β1-40 stock solution which was prepared as indicated above (1-1.5 mM in DMSO, final specific activity = *ca.* 3.5 mCi/ mmol). Aliquots of peptide stock solution (40 nmol β1-40, 30-40 μL of DMSO stock) were added to buffer (*ca.* 460 μL) and buffer containing 1% of a molar equivalent of apoE3 or apoE4 (0.4 nmol). The samples were stirred and aliquots (30 μL) were removed at various time points and filtered through 0.22 μm filters. The amount of soluble peptide present in the filtrate was measured by scintillation counting.

Solubility Determination

Supersaturated radioiodinated peptide solutions with and without apoE proteins were prepared as above and stirred for three days. A measured aliquot was removed, filtered, and the radioactivity was counted.

Fourier-Transform Infrared Spectroscopy

Amyloid fibrils were prepared as indicated above and analyzed using a NIC PLAN IR microscope (32 fold objective) with a Nicolet 510P FTIR spectrophotometer.

Electron Microscopy

Fibrils for electron microscopy were taken from kinetic aggregation experiments (see above). Aliquots of suspended fibrils were placed onto carbon-coated copper grids and were allowed to sit for 1-5 minutes. These were washed with H_2O, and then were negative stained with 2% uranyl acetate. Electron micrographs (EMs) were taken on a JEOL 1200 CX electron microscope operating at 80kV with a 60,000-fold magnification.

SDS-Polyacrylamide Gel Electrophoresis

Polyacrylamide gels were poured according to the method of Laemmli.[63] All gels were visualized by Commassie Blue R-250. All gels were run in a Novex mini-cell system.

Binding Studies of β1-40 with ApoE

ApoE (1 μg) was incubated for either 15 minutes or 1 hour and 15 minutes at 37°C with β1-40 (60 μg) in phosphate-buffered saline, pH 7.4, in a total volume of 20 μl. Incubation was terminated by the addition of 20 μl of 2X Laemmli buffer (4% SDS with no β-mercaptoethanol) and boiled for five minutes. Proteins were electrophoresed on a 4-20% polyacrylamide gel and stained with Commassie Blue R-250.

Chapter 3 References

(1) Ashall, F.; Goate, A.M. *TIBS* **1994**, *19*, 42-46.
(2) Jarrett, J.T., Amyloid Fibril Formation in Alzheimer's Disease, *Ph.D. Thesis, Massachusetts Institute of Technology,* **1993.**
(3) Sipe, J.D. *Annu. Rev. Biochem.* **1992**, *61*, 947-975.
(4) Ghiso, J.; Jensson, O.; Frangione, B. *Proc. Natl. Acad. Sci. USA* **1986**, *83*, 2974-2978.
(5) Maury, C.P.J.; Nurmiaho-Lassila, E.L. *Biochem. Biophys. Res. Commun.* **1992**, *183*, 227-231.
(6) De Young, L.R.; Fink, A.L.; Dill, K.A. *Acc. Chem. Res.* **1993**, *26*, 614.
(7) Eaton, W.A.; Hofrichter, J. *Adv. Prot. Chem.* **1990**, *40*, 63.
(8) Jarrett, J.T.; Berger, E.P.; Lansbury, P.T., Jr. *Biochemistry* **1993**, *32*, 4693-97.
(9) Barrow, C.; Zagorski, M. *Science* **1991**, *253*, 179.
(10) Weisgraber, K.H. *Adv. Prot. Struct.* **1994**, *45*, 249-302.
(11) Hui, D.Y.; Harmony, J.; Innerarity, T.L.; Mahley, R.W. *J. Biol. Chem.* **1980**, *255*, 11775-11781.
(12) Ignatius, M.J.; Shooter, E.M.; Pitas, R.E.; Mahley, R.W. *Science* **1987**, *236*, 959-962.
(13) Clark, A.B.; Quarfordt, S.H. *J. Biol. Chem.* **1985**, *260*, 4778-4783.
(14) Namba, Y.; Tomonaga, M.; Kawasaki, H.; Otomo, E.; Ikeda, K. *Brain Res.* **1991**, 541, 163-166.
(15) Corder, E.H.; Saunders, A.M.; Strittmatter, W.J.; Schmechel, D.E.; Gaskell, P.C.; Small, G.W.; Roses, A.D.; Haines, J.L.; Pericak-Vance, M.A. *Science* **1993**, *261*, 921-923.
(16) Utermann, G.; Langenbeck, U.; Beisiegel, U.; Weber, W. *Am. J. Hum. Genet.* **1980**, *32*, 339.
(17) Utermann, G.; Steinmetz, A.; Weber, W. *Hum. Genet.* **1982**, *60*, 344.
(18) Mahely, R.W.; Innerarity, T.L. *Biochm. Biophys. Acta.* **1983**, *737*, 197.
(19) Davignon, J.; Gregg, R.E.; Sing, C.F. *Arteriosclerosis* **1988**, *8*, 1-21.
(20) Olaisen, B.; Teisberg, P.; Gedde-Dahl, T. *Hum. Genet.* **1982**, *62*, 233.
(21) Elhourbagy, N.A.; Liao, W.S.; Mahley, R.W.; Taylor, J.M. *Proc. Natl. Acad. Sci. USA* **1985**, *82*, 203.
(22) Utermann, G. *Curr. Biol.* **1994**, *4*, 362-365.
(23) Roheim, P.S.; Carey, M.; Forte, T.; Vega, G.L. *Proc. Natl. Acad. Sci. USA* **1979**, *76*, 4646.
(24) Shore, V.G.; Shore, B. *Biochemistry* **1973**, *12*, 502-507.
(25) Rall, S.C., Jr.; Weisgraber, K.H.; Mahley, R.W. *J. Biol. Chem.* **1982**, *257*, 4171-4178.
(26) Weisgraber, K.H.; Troxler, R.F.; Rall, S.C., Jr.; Mahley, R.W. *Biochem. Biophys. Res. Commun.* **1980**, *95*, 374-380.
(27) Chou, P.Y.; Fasman, G.D. *Biochemistry* **1974**, *13*, 222-245.
(28) Mahley, R.W. *Science* **1988**, *240*, 622-630.
(29) Aggerbeck, L.P.; Wetterau, J.R.; Weisgraber, K.H.; Wu, C.-S.C.; Lingren, F.T. *J. Biol. Chem.* **1988**, *263*, 6249-6258.

(30) Wetterau, J.R.; Aggerbeck, L.P.; Rall, S.C., Jr.; Weisgraber, K.H. *J. Biol. Chem.* **1988**, *263*, 6240-6248.
(31) Wilson, C.; Wardell, M.R.; Weisgraber, K.H.; Mahley, R.W.; Agard, D.A. *Science* **1991**, *252*, 1817-1822.
(32) Innerarity, T.L.; Friedlander, E.J.; Rall, S.C.; Weisgraber, K.H.; Mahley, R.W. *J. Biol. Chem.* **1983**, *258*, 12341-47.
(33) Mahley, R.W.; Innerarity, T.L.; Pitas, R.E.; Weisgraber, K.H.; Brown, J.H.; Gross, E. *J. Biol. Chem.* **1977**, *252*, 7279-7287.
(34) De Pauw, M.; Vanloo, B.; Weisgraber, K.H.; Rosseneu, M. *Biochemistry* **1995**, *34*, 10953-10960.
(35) Westerlund, J.A.; Weisgraber, K.H. *J. Biol. Chem.* **1993**, *268*, 15745-15750.
(36) Strittmatter, W.J.; Saunders, A.M.; Schmechel, D.; Pericak-Vance, M.; Enghild, J.; Salvesen, G.S.; Roses, A.D. *Proc. Natl. Acad. Sci. USA* **1993**, *90*, 1977-1981.
(37) Pericak-Vance, M.A.; Bebout, J.L.; Gaskell, P.C. et al. *Am. J. Hum. Genet.* **1991**, *48*, 1034.
(38) Travis, J. *Science* **1993**, *261*, 828-829.
(39) Rebeck, G.W.; Reiter, J.S.; Strickland, D.K.; Hyman, B.T. *Neuron* **1993**, *11*, 575-580.
(40) Hyman, B.T.; West, H.L.; Rebeck, G.W.; Buldyrev, S.V.; Mantegna, R.N.; Halvin, S.; Stanley, H.E. *Proc. Natl. Acad. Sci. USA* **1995**, *92*, 3596-3590.
(41) Peterson, R.C.; Smith, G.E.; Ivnik, R.J.; Tangalos, E.G. et al. *JAMA* **1995**, *273*, 1274-1278.
(42) Helkala, E.L.; Koivisto, K.; Hanninen, T.; Vanhanen, M. et al. *Neuro. Lett.* **1995**, *191*, 141-144.
(43) Growdon, J.H.; Locasio, J.J.; Corkin, S.; Gomez-Isla, T.; Hyman, B.T. *Neuron*, in press.
(44) Wisniewski, T.; Frangione, B. *Neuroscience Letters* **1992**, *135*, 235-238.
(45) Evans, K.C.; Berger, E.P.; Cho, C.-G.; Weisgraber, K.H.; Lansbury, P.T., Jr. *Proc. Natl. Acad. Sci. USA* **1995**, *92*, 763.
(46) Chan, W.; Wood, S.J.; Wetzel, R. *Unpublished results*
(47) LaDu, M.J.; Falduto, M.T.; Manelli, A.M.; Reardon, C.A.; Getz, G.G.; Frail, D.E. *J. Biol. Chem.* **1994**, *269*, 23403.
(48) Whitson, J.S.; Mims, M.P.; Strittmatter, W.J.; Yamaki, T.; Morrisett, J.D.; Appel, S.H. *Biochem. Biophys. Res. Com.* **1994**, *199*, 163-170.
(49) Reed, T.; Carmelli, D.; Swan, G.E.; Breitner, J.C.; Welsh, K.A. et al. *Arch. Neurol.* **1994**, 1189-1192.
(50) Breslow, J. *Biotech.* **1994**, *12*, 365-370.
(51) Jarrett, J.T.; Lansbury, P.T., Jr. *Cell* **1993**, *73*, 1055-58.
(52) Kondepudi, D.K.; Bullock, K.L.; Digits, J.A.; Hall, J.K.; Miller, J.M. *J. Am. Chem. Soc.* **1993**, *115*, 10211-10216.
(53) Rudolf, A.D.; Larson, M.A. *Theory of Particulate Processes*; **1988**, Academic Press, San Diego.
(54) Weisgraber, K.H.; Shinto, L.H. *J. Biol. Chem.* **1991**, *266*, 12029-34.

(55) Strittmatter, W.J.; Weisgraber, K.H.; Huang, D.Y.; Dong, L.-M.; Salvsen, G.S.; Pericak-Vance, M.; Schmechel, D.; Saunders, A.M.; Golgaber, D.; Roses, A.D. *Proc. Natl. Acad. Sci. USA* **1993**, *90*, 8098-8102.
(56) Pitas, R.E.; Boyles, J.K.; Lee, S.H.; Hui, D.; Weisgraber, K.H. *J. Biol. Chem.* **1987**, *262*, 14352-360.
(57) Schmechel, D.E.; Saunders, A.M.; Strittmatter, W.J.; Crain, B.J.; Hulette, C.M.; Joo, S.H.; Pericak-Vance, M.A.; Goldgaber, D.; Roses, A.D. *Proc. Natl. Acad. Sci. USA* **1993**, *90*, 9649-9653.
(58) Nakagawa, S.H.; Lau, H.S.H.; Kézdy, F.J.; Kaiser, E.T. *J. Am. Chem. Soc.* **1985**, *107*, 7087-7092.
(59) Oppenheim, F.G.; Yang, Y.-C.; Diamond, R.D.; Hyslop, D.; Offner, G.D.; Troxler, R.F. *J. Biol. Chem.* **1986**, *261*, 177-82.
(60) Gregg, R.E.; Zech, L.A.; Schaefer, E.J.; Stark, D.; Wilson, D.; Brewer, H.B., Jr. *J. Clin. Invest.* **1986**, *78*, 815-821.
(61) Nathan, B.P.; Bellosta, B.; Sanan, D.A.; Weisgraber, K.H.; Mahley, R.W.; Pitas, R.E. *Science* **1994**, *264*, 850-2.
(62) Rall, S.C.; Weisgraber, K.H.; Mahley, R.W. *Methods in Enzymology* **1986**, *128*, 273-87.
(63) Laemmli, U.K. *Nature* **1970**, *227*, 423-470.

Chapter 4

Models of the N-Terminal Domain of Apolipoprotein E

Amyloid formation by the β protein proceeds according to a nucleation-dependent polymerization, as was discussed in Chapter 3.[1] The *APOE4* allele is associated with an earlier age of onset of the nonfamilial, late-onset form of AD, in addition to increased β protein amyloid deposition in the brain.[2] We have found that apoE is an inhibitor of amyloid formation and that apoE4 is actually a less efficient inhibitor than apoE3.[3]

Proteolysis of ApoE Yields Two Intact Domains

A 22 kD N-terminal domain comprising amino acids 1-191, and a 10 kD C-terminal domain comprising amino acids 216-299 are produced after the full-length apoE is subjected to proteolysis by thrombin (Figure 4.1A). The 22 kD domain contains the sites that distinguish the apoE isoforms. Experiments in this chapter were designed to determine more precisely the region of apoE responsible for its inhibitory activity by studying the interaction of the 22 kD and 10 kD domains with the β protein.

Examination of the two domains by gel electrophoresis under non-reducing conditions demonstrated that the 22 kD apoE3 protein, which has one cysteine residue, contained approximately 20% of a disulfide dimer while the 10 kD protein existed only as a monomer (Figure 4.1B). The inhibitory activity of apoE was subsequently shown to be contained in the 22 kD portion of the protein. Several recombinant 22 kD apoE isoforms and mutants were expressed and purified in order to isolate regions of the protein that are critical for inhibition.

Conformational Change of ApoE Resulting from Lipid-Binding

X-ray crystallography of the 22 kD domain of apoE that is produced from proteolysis by thrombin has demonstrated that this domain contains five helices, representing more than 80% of the residues present. Four of these helices are arranged in an antiparallel four-helix bundle.[4] The interior of the bundle is packed with the hydrophobic side chains of the protein and the hydrophilic side chains are located on the exterior of the helices and are solvent-exposed.

Studies have shown that lipid is required for the 22 kD domain to exhibit high-affinity binding to the LDL-receptor.[5] The proposed working hypothesis for the binding of the 22 kD domain to phospholipids suggests that the four-helix bundle undergoes a conformational change when associated with lipid. As a result of this conformational change, the bundle opens without major disruption of the α-helical structure (Figure 4.2).[6] The opened structure would have a broad hydrophilic face and hydrophobic face. The hydrophobic face could then interact with the lipid.

Figure 4.1 (A) Proteolysis of apoE by thrombin yields two intact domains. (B) SDS-PAGE of the 10 kD domain (lanes 1 and 2) and the 22 kD domain (lanes 3 and 4) under non-reducing conditions (lanes 1 and 3) and reducing conditions conditions (lanes 2 and 4).

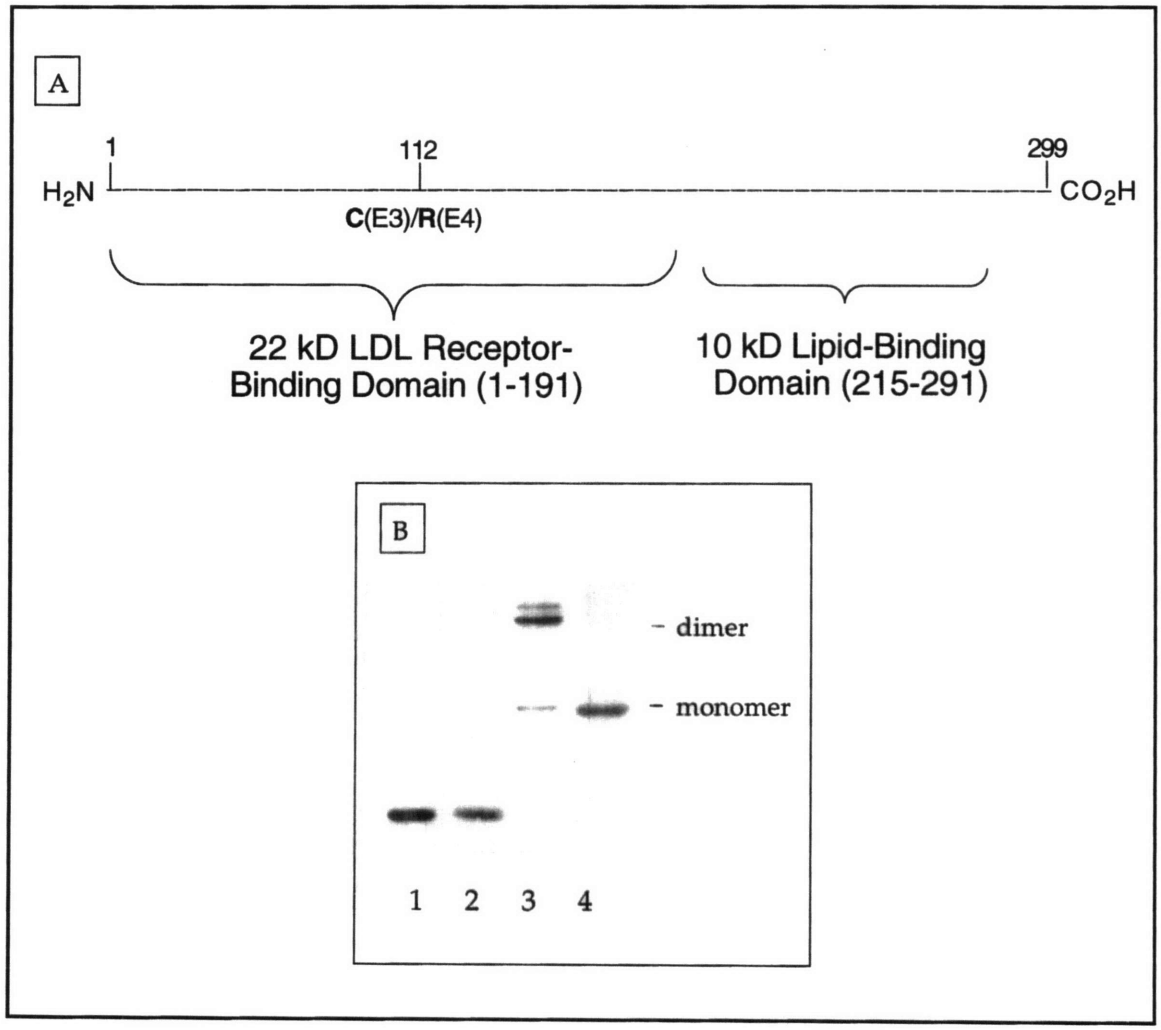

Figure 4.2 Diagram depicting the proposed opening of the 22 kD four-helix bundle upon lipid-binding.

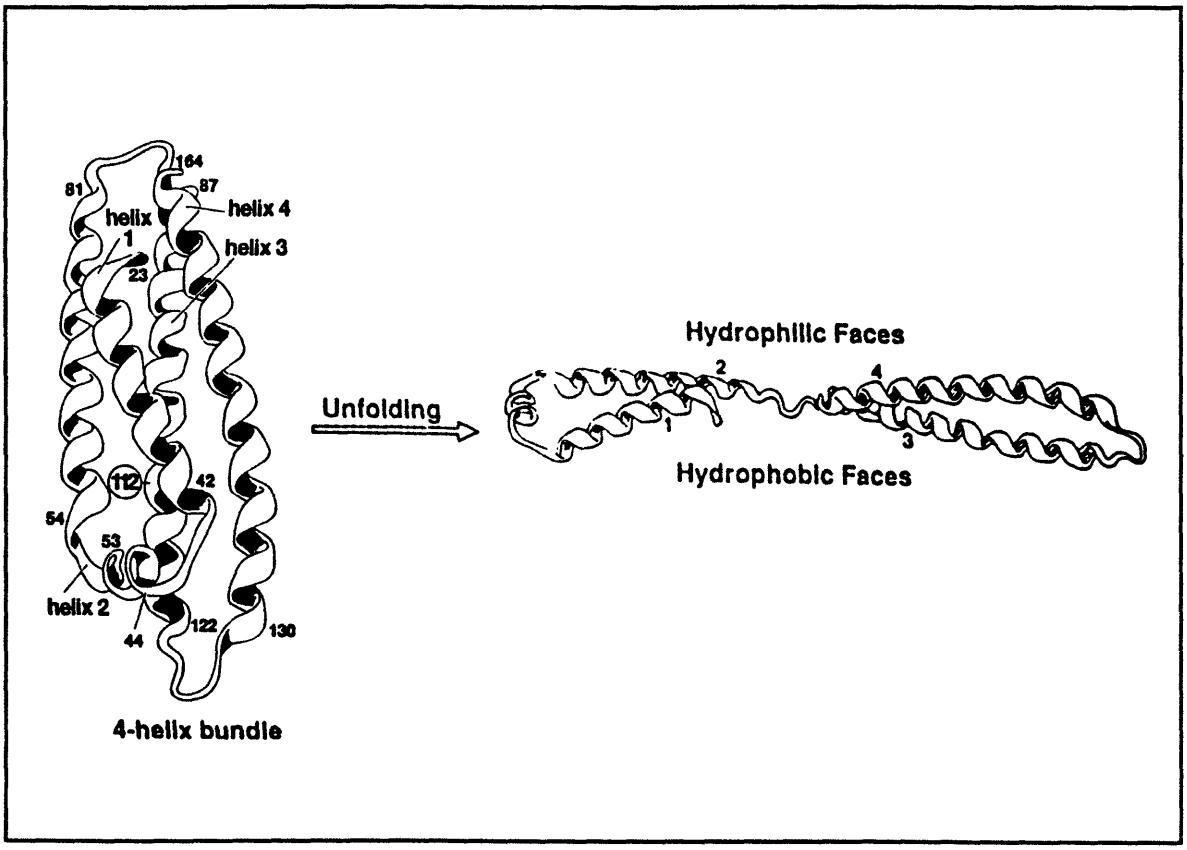

This hypothesis has been reinforced by experimental data. The surface properties of the 22 kD domain at an air-water interface, a system that has been used extensively to model the interaction of apolipoproteins with lipid[7], was examined. The surface pressure-molecular area isotherm was comparable to data for other apolipoproteins and in the range for α-helical homopolypeptides that lie coplanar with the surface.[8] This indicates that the helices of the 22kD fragment also lie coplanar with the surface.

Additional data supporting this hypothesis was produced from experiments with a mutant form of the 22 kD domain of apoE3. A threonine to cysteine mutation at position 57 in apoE was introduced to determine the

effect of an intramolecular disulfide bond between Cys57 and Cys112 on the properties of the domain.[9] The disulfide bond, which bridges two of the helices of the four-helix bundle, added to the stability of the fragment and further protected the domain against denaturation. Additionally, the Cys57 mutant possessed a much lower affinity for lipid than the wild-type 22kD domain. This supports the theory that the four-helix bundle must open in order to bind lipid.

Proposed Inhibitory Mechanism of ApoE 22 kD Domain

One of the many functions performed by apoE involves the binding to and transportation of hydrophobic molecules such as lipids, as is discussed above. This function also suggests that apoE might play a role in binding to other hydrophobic molecules such as the β protein.[10] According to this mechanism, apoE may act as a clearance mechanism for the β protein or β protein aggregates.

The four-helix bundle could open as it is believed to do when binding lipid, however, the hydrophobic face could then bind to the β protein instead of lipid. The apoE-β protein complex could then bind to the LDL receptor where the β protein would subsequently be internalized and degraded.

Additionally, the various isoforms of apoE may have different clearance abilities (inhibitory activities). For example, if apoE4 was able to clear nuclei or small aggregates of the β protein, but was less efficient in this role than apoE3, this could explain why over time *APOE4* homozygotes were more at risk for developing AD. This hypothesis suggests that the rate of amyloid deposition is a reflection of the relative rates of β protein synthesis, aggregation, and clearance.[10]

A Truncated ApoE Variant

The four-helix bundle motif that is present in the 22 kD fragment is unusual when compared to other four-helix proteins. The lengths of the four helices are 19 (helix 1), 28 (helix 2), 36 (helix 3), and 35 (helix 4) amino acids. Three of these helices are much longer than the average helical length of 18 residues found in other proteins sharing this folding motif.[11] Currently it has not been determined if the elongated helical bundles in apoE are a common structural element of other plasma apolipoproteins.

Helix 1 begins at residue 23 and extends to residue 42. Helix 1 is connected to helix 2 by a short connecting helix, encompassing residues 44-53. Helix 2 begins with residue 54 and extends to residue 81. The chain is reversed with a turn defined by residues 82-86. Helix 3 extends from residues 87 to 122. The chain reverses again with a turn comprising residues 123-129 and helix 4 extends from residue 130 to 165. The receptor-binding region has been localized to helix 4 (residues 136-150).

The crystal structure of the 22 kD domain defines only residues 23 to 165. The N-terminal fragment comprising the first 22 amino acids and the C-terminal fragment comprising the final 34 amino acids are both random coil in nature. It was proposed by our laboratory that truncations of the 22 kD domain might further isolate the region responsible for the inhibitory activity of apoE. The most obvious truncations were variants of 22 kD apoE that were missing the N- and C-terminal random-coil fragments.

Additionally, truncations that removed helices from the four-helix bundle would be an interesting method by which to determine whether or not the inhibitory activity of the 22 kD domain was due to this bundle motif.

Expression of the ApoE 22 kD Variants

The previous studies performed with the full length apoE proteins (described in Chapter 3) used proteins that were isolated from human plasma. The isolation of apolipoproteins from plasma is limited by the number of people who have been apoE genotyped and who are willing to donate their blood on a regular basis. Expression of full-length apoE in *E. coli* systems is extremely difficult. Very little protein is produced by the cells, possibly resulting from the high lipid-binding affinity of the 10 kD domain of the protein.[12]

Conveniently, the expression of the 22 kD domain is much easier than the full-length protein. The ability to express the 22 kD domain facilitates the examination of the interaction between apoE and the β protein by providing an easy method to produce truncated proteins and mutants. The apoE2, apoE3, and apoE4 22 kD isoforms were subsequently expressed in *E. coli* cells.

The expression system utilized was the T7 promoter-driven system originally developed by Studier and colleagues.[13] Target genes are cloned into a vector that contains a T7 promoter (e.g. pT7 or pET series) and the resulting construct is transformed into E. coli lysogen BL21(DE3) which contains an inducible T7 RNA polymerase gene. Expression is induced by the addition of isopropyl-β-D-thiogalactopyranoside (IPTG). T7 RNA polymerase is so selective that almost all of the cell's resources are converted to target gene expression and the desired product can comprise more than 50% of the total cell protein after induction. Target genes are initially cloned using hosts that do not contain the T7 RNA polymerase gene so that they are inactive and cannot cause plasmid instability due to the production of proteins that are

potentially toxic to the host cell. The gene encoding for the 22 kD apoE protein was cloned into a vector containing a T7 phage promoter (deonoted as pT22K), which was derived from pBR322. The circular map of pT22K showing unique restriction sites that exist within the apoE gene is shown in Figure 4.3.

Figure 4.3 A schematic diagram illustrating the circular map of pT22K and the unique restriction sites. The solid arrow represents the 22 kD apoE gene. ORI is the origin of replication and Ap is the ampicillin resistance gene.

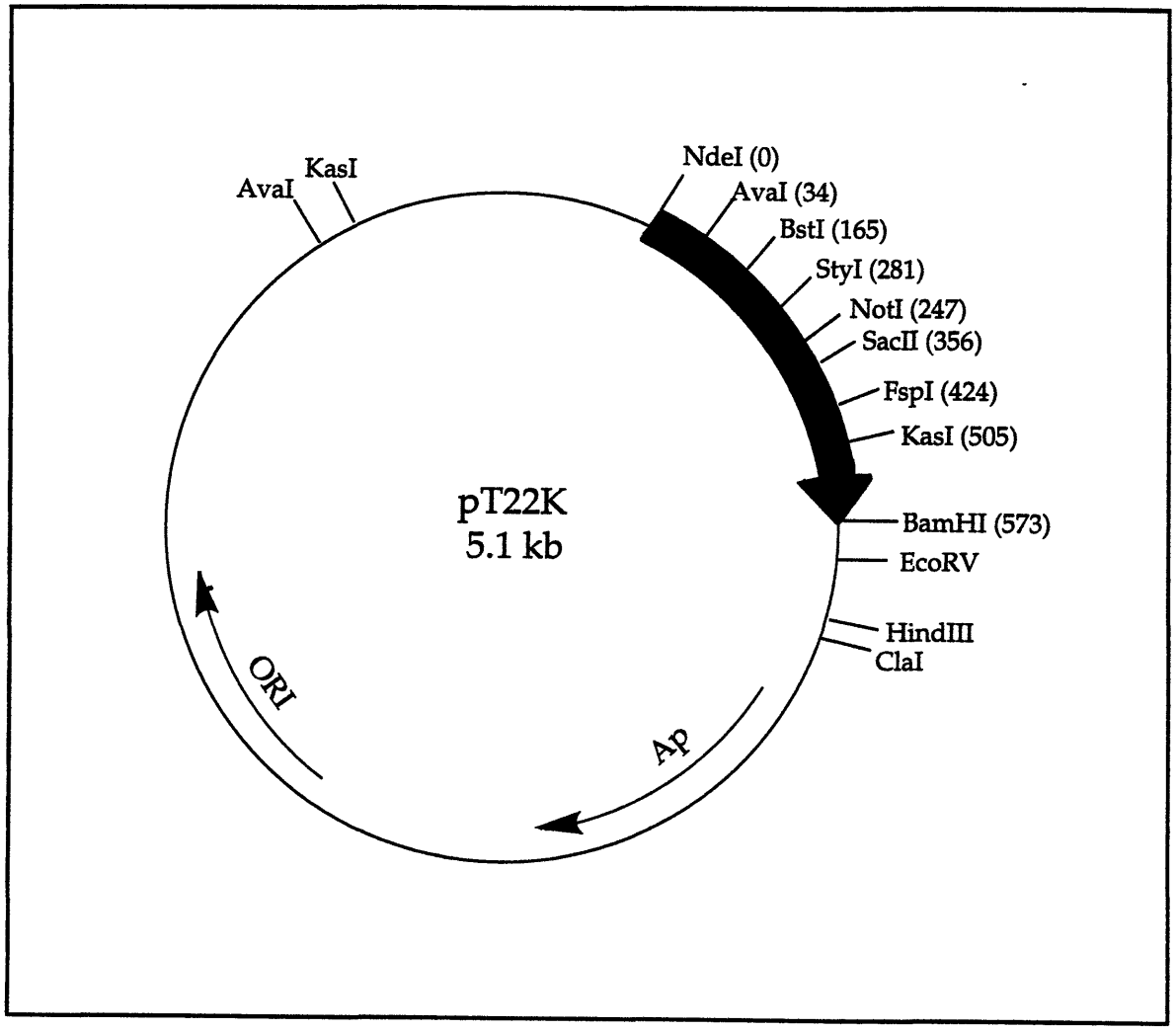

Cell Transformation and Protein Induction

Plasmids containing the cDNA coding sequences of apoE2, apoE3, and apoE4 were transformed into *E. coli* BL21(DE3) cells. After the transformation, the colonies were checked to confirm that they contained the apoE plasmids. The plasmid inserts were cut out of the plasmids using a restriction digest with the enzymes BamHI and NdeI. The digested material was then examined by DNA gel electrophoresis on a 1% agarose gel (Figure 4.4). For each plasmid, two digests were performed: 0 cuts (no enzyme), and 2 cuts (BamHI and NdeI). These experiments confirmed the presence of the desired restriction sites in the plasmid. After the cleavage by the two restriction enzymes, a small 590 base-pair DNA fragment was liberated.

After confirmation by a restriction digest that the cells contained the correct plasmids, the cells were grown on a one liter scale and induced by the addition of IPTG. Induction was monitored over time. Cell samples were removed at various time points during the induction and then examined by SDS-PAGE (Figure 4.5). Protein induction was evident by 1.5 hours and was complete by 3 hours. The 22 kD apoE isoforms were produced in a much greater quantity than any other protein produced by the host cell.

Figure 4.4 DNA gel electrophoresis of the apoE2 (lanes 2, 3, and 4), apoE3 (lanes 5, 6, and 7), and apoE4 (lanes 8, 9, and 10) 22 kD plasmids with no cuts (lanes 2, 5, and 8), one cut (lanes 3, 6, and 9) and two cuts (lanes 4, 7, and 10). Lane 1 is a 123 DNA base-pair ladder standard. The arrow indicates the excised 570 base-pair fragment.

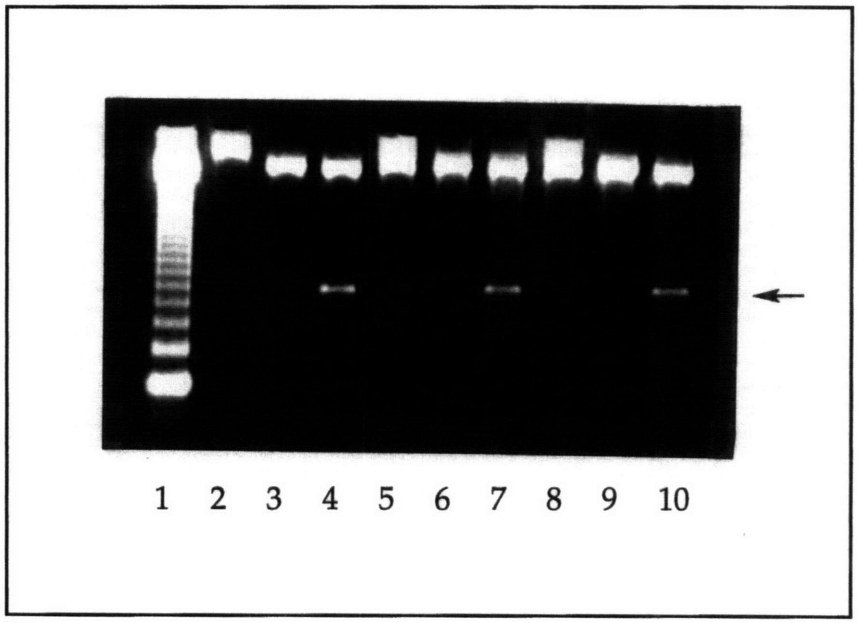

Figure 4.5 SDS-PAGE under reducing conditions of IPTG inductions of the 22 kD apoE isoforms at various time points. (A) apoE2: t=0 hr (lane 2), t=1.5 hr (lane 3), and t=3 hr (lane 4); (B) apoE3: t=0 hr (lane 2) and t=3 hr (lane 3); and (C) apoE4: t=0 hr (lane 2), t=1.5 hr (lane 3), and t=3 hr (lane 4). Lane 1 in each case is a 10 kD protein ladder standard.

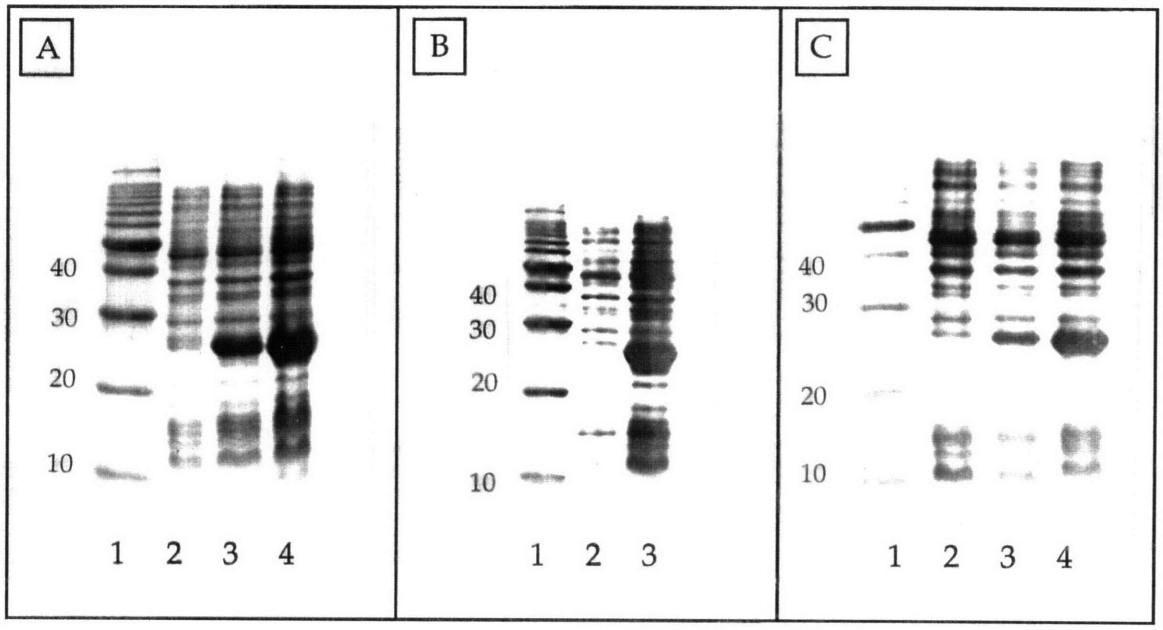

Purification of the 22 kD ApoE Isoforms

The apoE proteins were lysed and genetic material was precipitated from the lysate by streptomycin sulfate. A large quantity of undesired protein was then precipitated from the crude protein solution by ammonium sulfate. SDS-PAGE confirmed that little apoE was lost from these steps. The protein solution was then purified by size-exclusion chromatography. Most of the protein impurities were efficiently separated from the apoE proteins after this step (Figure 4.6). After the apoE peaks were isolated, dialyzed, and lyophilized, they were further purified by ion-exchange chromatography. A pure protein was isolated after the ion-exchange step, as visualized by SDS-PAGE (Figure 4.7).

Inhibition of β Protein Amyloid Formation by the 22 kD Domain

The 22 kD Domain is an Effective Amyloid Inhibitor

The aggregation of the β protein under stirred conditions demonstrates a protracted lag time as measured by turbidity. The addition of a 1% molar equivalent of the N-terminal 22 kD domain of apoE3 (800 nM) to a supersaturated solution of β1-40 (80 μM) resulted in a significant increase in the lag time prior to aggregation (Figure 4.8). However, the C-terminal 10 kD domain at a 1% molar equivalent (800 nM) had no activity under the same conditions.

Figure 4.6 SDS-PAGE under reducing conditions of three peaks (lanes 2, 3, and 4 for each panel) collected after size-exclusion chromatography of apoE2 (A), apoE3 (B), and apoE4 (C). In each panel lane 1 is a 10 kD protein ladder standard and apoE was isolated in peak 2 (lane 3).

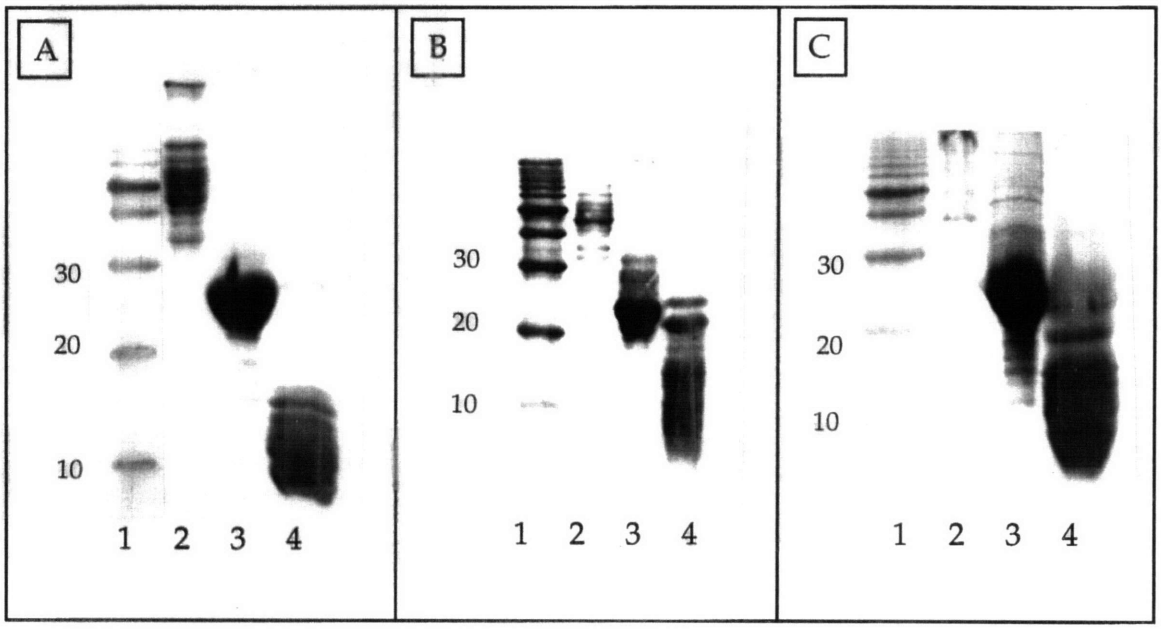

Figure 4.7 SDS-PAGE under reducing conditionsof apoE2 (A), apoE3 (B), and apoE4 (C) isolated by ion-exchange chromatography (lane 2 for each panel). Lane 1 for each panel is a 10 kD protein ladder standard.

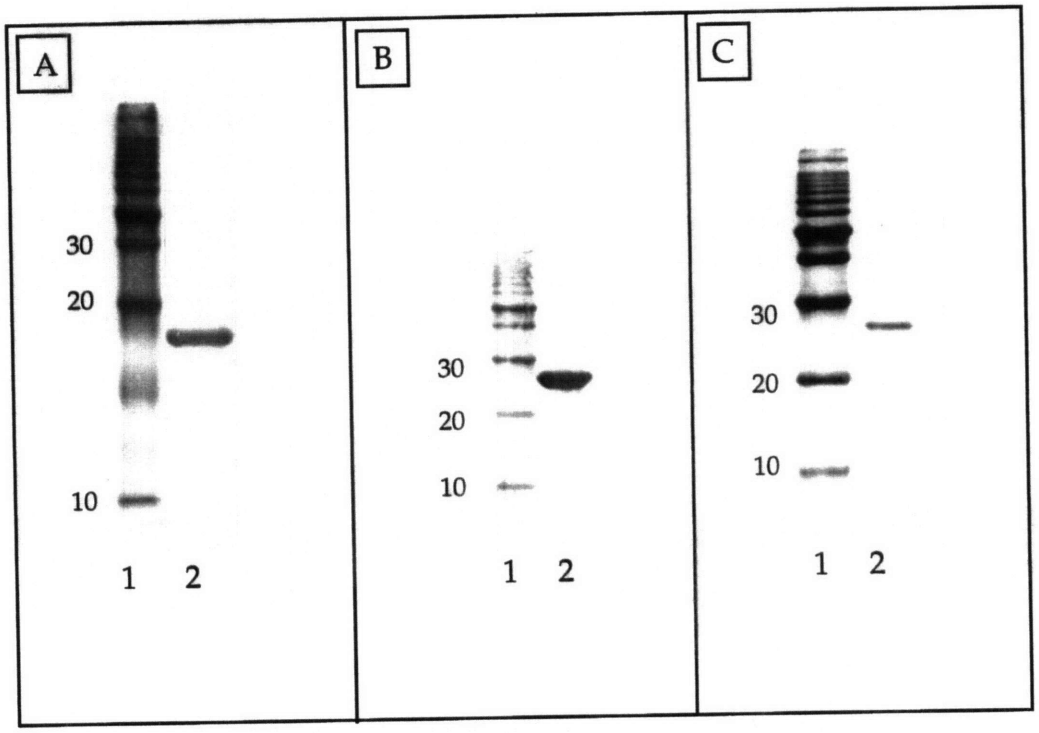

Figure 4.8 Aggregation of β1-40 (80 μM) in the presence of 1% of the apoE proteolytic N- and C-terminal fragments under stirred conditions.

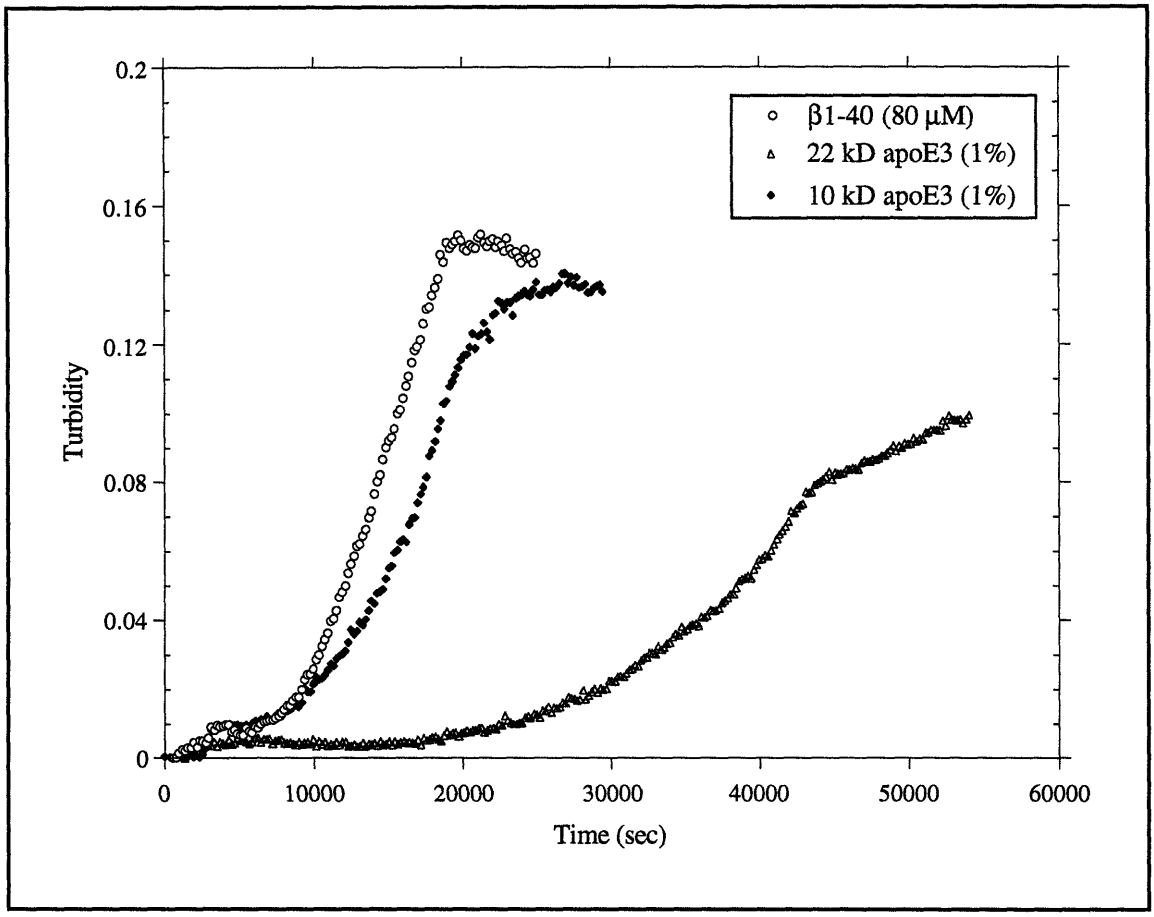

Inhibition of β Protein Aggregation by 2% 22 kD apoE Isoforms

The aggregation of the β protein was examined in the presence of a 2% molar equivalent of the 22 kD apoE2, apoE3, and apoE4 fragments in order to determine differences in inhibitory activity at higher apoE concentrations (Figure 4.9). However, the addition of 2% of the apoE proteins to a supersaturated solution of β1-40 (80 μM) resulted in inhibition of aggregation for more than 24 hours.

Figure 4.9 Aggregation of β1-40 (80 μM) in the presence of 2% 22 kD apoE2, apoE3, and apoE4 under stirred conditions.

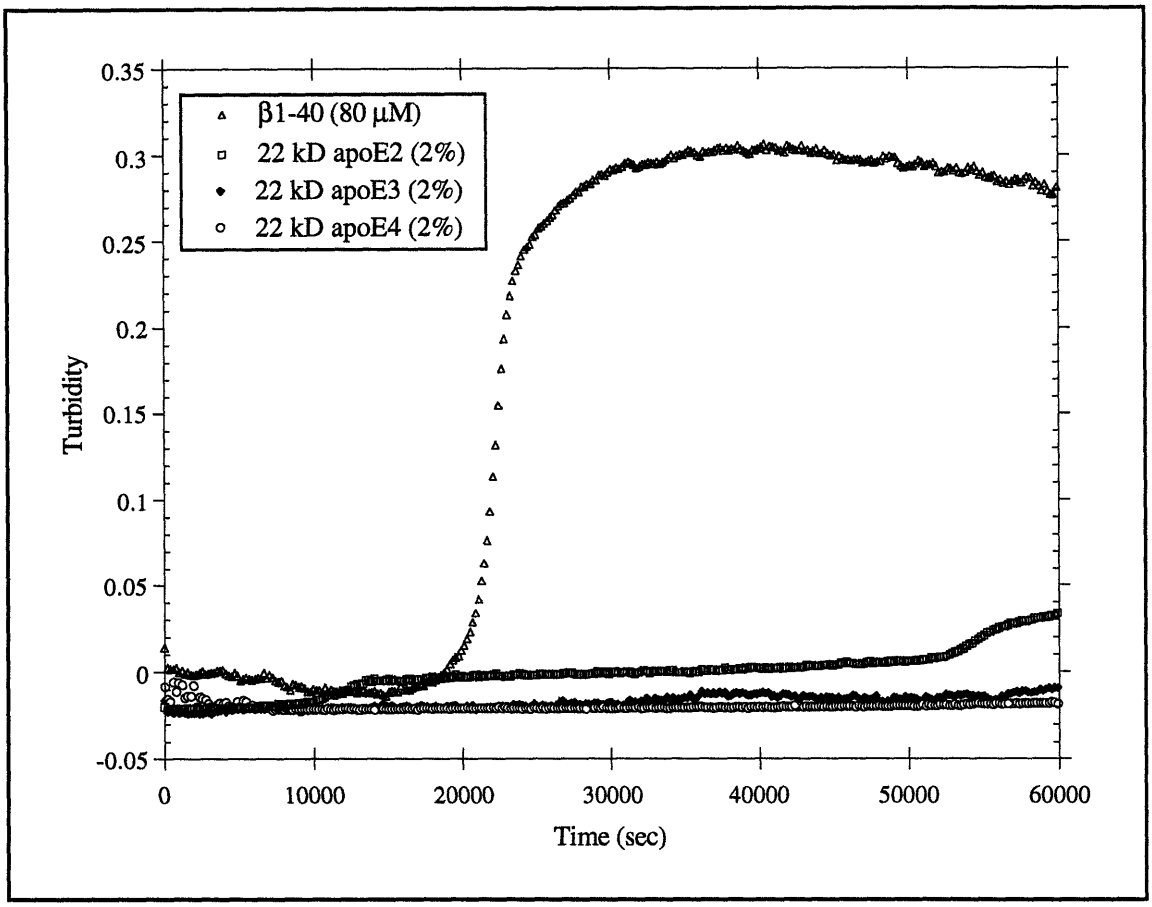

Inhibition of Amyloid Formation is Very Sensitive to ApoE Concentrations

The sensitivity of β protein aggregation to the concentration of the 22 kD apoE isoforms was tested. Stirred kinetic experiments in the presence of varying amounts of the 22 kD apoE3 protein were performed. The results in Figure 4.10 demonstrate that aggregation can be inhibited in the presence of as little as 0.5% of protein in a supersaturated solution of β1-40. Interestingly, the longer that the aggregation of β1-40 is inhibited (i.e. larger percentages of apoE present), the lower the final turbidity.

Figure 4.10 The aggregation of β1-40 under stirred conditions is sensitive to the concentration 22 kD apoE3 present.

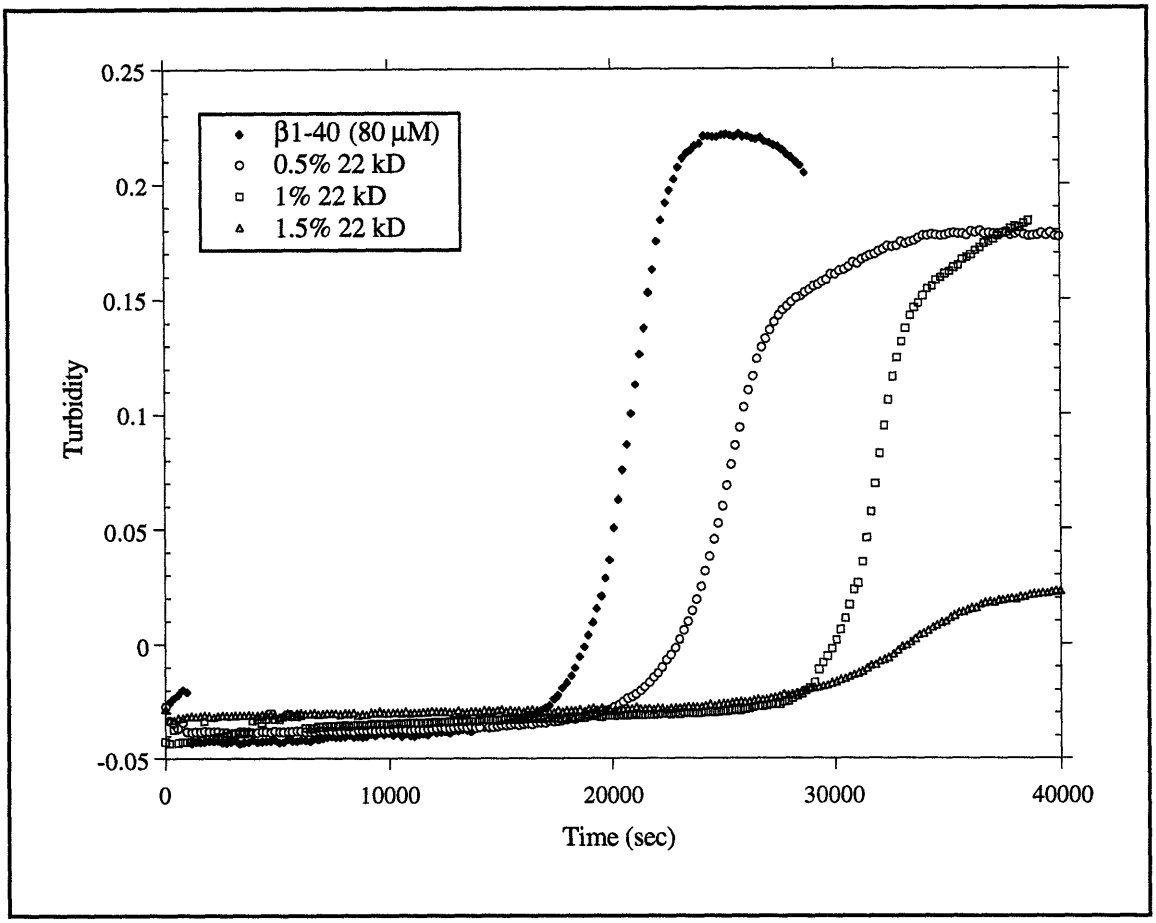

Inhibitory Activities of ApoE3 and ApoE4 are not Distinguishable

The 22 kD isoforms were tested in a stirred aggregation assay with β1-40 in order to distinguish whether or not they possessed different inhibitory activities. When 1% molar equivalent of apoE3 or apoE4 was added to a supersaturated solution of 80 μM β1-40, protracted lag times were observed. However, the lag times resulting from the addition of the two isoforms were identical (Figure 4.11).

Figure 4.11 Aggregation of 80 μM β1-40 in the presence of 1% molar equivalent of 22 kD apoE3 or apoE4.

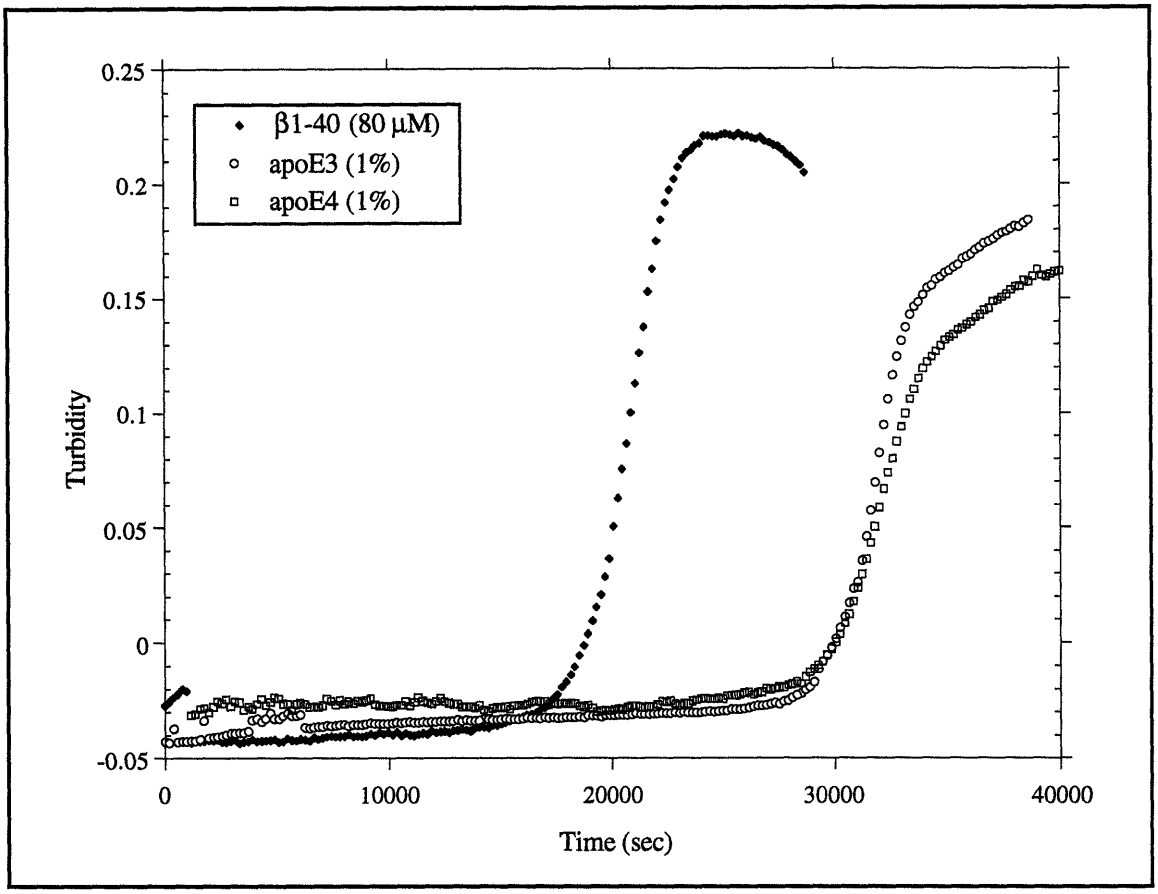

Creation of a 19 kD Truncated ApoE Protein

A 19 kD N-terminally truncated mutant of the 22 kD domain was also expressed in *E. coli*. The truncation was achieved through the use of the Polymerase Chain Reaction (PCR). The first truncated protein to be synthesized was C-terminally truncated and comprised amino acids 1-165. Primers were designed to produce a DNA insert that began at nucleotide 1 and ended at 495 of the 22 kD apoE sequence (Figure 4.12). A flanking primer for the 5' end and an internal primer for the 3' end was used to amplify a DNA insert corresponding to this

Figure 4.12 Translation of cDNA from the 22 kD apoE3 sequence.

```
     1                                                  30
5'   AAG GTT GAA CAG GCT GTT GAA ACT GAA CCG GAA CCC GAG CTG CGC CAG CAG ACC
3'   TTC CAA CTT GTC CGA CAA CTT TGA CTT GGC CTT GGG CTC GAC GCG GTC GTC TGG
AA    K   V   E   Q   A   V   E   T   E   P   E   P   E   L   R   Q   Q   T
      1                                          10

        60                                                  90
GAG TGG CAG AGC GGC CAG CGC TGG GAA CTG GCA CTG GGT CGC TTT TGG GAT TAC CTG
CTC ACC GTC TCG CCG GTC GCG ACC CTT GAC CGT GAC CCA GCG AAA ACC CTA ATG GAC
 E   W   Q   S   G   Q   R   W   E   L   A   L   G   R   F   W   D   Y   L
     20                                              30

            120                                                 150
CGC TGG GTG CAG ACA CTG TCT GAG CAG GTG CAG GAG GAG CTG CTC AGC TCC CAG GTC
GCG ACC CAC GTC TGT GAC AGA CTC GTC CAC GTC CTC CTC GAC GAG TCG AGG GTC CAG
 R   W   V   Q   T   L   S   E   Q   V   Q   E   E   L   L   S   S   Q   V
             40                                              50

                  180                                                 210
ACC CAG GAA CTG AGG GCG CTG ATG GAC GAG ACC ATG AAG GAG TTG AAG GCC TAC AAA
TGG GTC CTT GAC TCC CGC GAC TAC CTG CTC TGG TAC TTC CTC AAC TTC CGG ATG TTT
  T   Q   E   L   R   A   L   M   D   E   T   M   K   E   L   K   A   Y   K
                  60                                              70

                        240                                                 270
TCG GAA CTG GAG GAA CAA CTG ACC CCG GTG GCG GAG GAG ACG CGG GCA CGG CTG TCC
AGC CTT GAC CTC CTT GTT GAC TGG GGC CAC CGC CTC CTC TGC GCC CGT GCC GAC AGG
 S   E   L   E   E   Q   L   T   P   V   A   E   E   T   R   A   R   L   S
                     80                                              90

                              300                                                 330
AAG GAG CTG CAG GCG GCG CAG GCC CGG CTG GGC GCG GAC ATG GAG GAC GTG TGC GGC
TTC CTC GAC GTC CGC CGC GTC CGG GCC GAC CCG CGC CTG TAC CTC CTG CAC ACG CCG
 K   E   L   Q   A   A   Q   A   R   L   G   A   D   M   E   D   V   C   G
                        100                                             110

                                    360                                                 390
CGC CTG GTG CAG TAC CGC GGC GAG GTG CAG GCC ATG CTC GGC CAG AGC ACC GAG GAG
GCG GAC CAC GTC ATG GCG CCG CTC CAC GTC CGG TAC GAG CCG GTC TCG TGG CTC CTC
 R   L   V   Q   Y   R   G   E   V   Q   A   M   L   G   Q   S   T   E   E
                            120                                             130

                                          420                                                 450
CTG CGG GTG CGC CTC GCC TCC CAC CTG CGC AAG CTG CGT AAG CGG CTC CTC CGC GAT
GAC GCC CAC GCG GAG CGG AGG GTG GAC GCG TTC GAC GCA TTC GCC GAG GAG GCG CTA
 L   R   V   R   L   A   S   H   L   R   K   L   R   K   R   L   L   R   D
                                140                                             150

                                                480                                                 510
GCC GAT GAC CTG CAG AAG CGC CTG GCA GTG TAC CAG GCC GGG GCC CGC GAG GGC GCC
CGG CTA CTG GAC GTC TTC GCG GAC CGT CAC ATG GTC CGG CCC CGG GCG CTC CCG CGG
 A   D   D   L   Q   K   R   L   A   V   Y   Q   A   G   A   R   E   G   A
                                    160                                             170

                                                      540
GAG CGC GGC CTC AGC GCC ATC CGC GAG CGC CTG GGG CCC CTG GTG GAA CAG GGC CGC
CTC GCG CCG GAG TCG CGG TAG GCG CTC GCG GAC CCC GGG GAC CAC CTT GTC CCG GCG
 E   R   G   L   S   A   I   R   E   R   L   G   P   L   V   E   Q   G   R
                                        180

      570
GTG CGG
CAC GCC
 V   R
190
```

sequence. This insert was then spliced into a pET plasmid which was subsequently transformed into BL21 cells.

The inserted restriction sites in the plasmid were checked by enzymatic digestion of the DNA with NdeI (5' end) and BamHI (3' end) restriction nucleases. By setting up reactions with either no cuts (no enzyme), one cut (BamHI only), and two cuts (both enzymes) it was possible to confirm the existence of the correct restriction sites. After the plasmid was cut with two enzymes, a small DNA fragment running close to the 492 base pair marker was liberated, indicating the correct restriction sites (Figure 4.13). The calculated number of nucleotides that should be present in the insert is 507 nucleotides. The coding sequence of the purified insert was confirmed by DNA sequencing using an ABI sequencer.

The insert coding for the 19 kD apoE protein was transformed into *E. coli* BL21 cells and protein expression was induced by the addition of IPTG. Figure 4.14 illustrates that protein production is complete after 1.5 hours, as is observed by SDS-PAGE. The protein was purified using both size-exclusion chromatography and ion-exchange chromatography (Figure 4.14).

Inhibition of β Protein Aggregation by a 19 kD Truncated ApoE

The aggregation of β1-40 under stirred conditions was tested in the presence of a 19 kD truncated variant that ends at position 165 of apoE3. The addition of 1% of the 19 kD variant extended the lag time significantly from that of β1-40 alone. Furthermore, the presence of 2% of the 19 kD variant in a supersaturated solution of 80 μM β1-40 resulted in an inhibition of fibril formation past 24 hours, as is shown in Figure 4.15.

Figure 4.13 DNA gel electrophoresis of the restriction digest of plasmids containing the truncated apoE sequence isolated from three colonies (colony 1: lanes 2 and 3, colony 2: lanes 4 and 5, and colony 3: lanes 6 and 7). Lanes 2, 4, and 6 show the uncut plasmids, and lanes 3, 5, and 7 show the plasmids with two cuts and a liberated DNA fragment. Lane 1 is a 123 DNA base-pair ladder standard. The arrow indicates the excised 507 base-pair fragment.

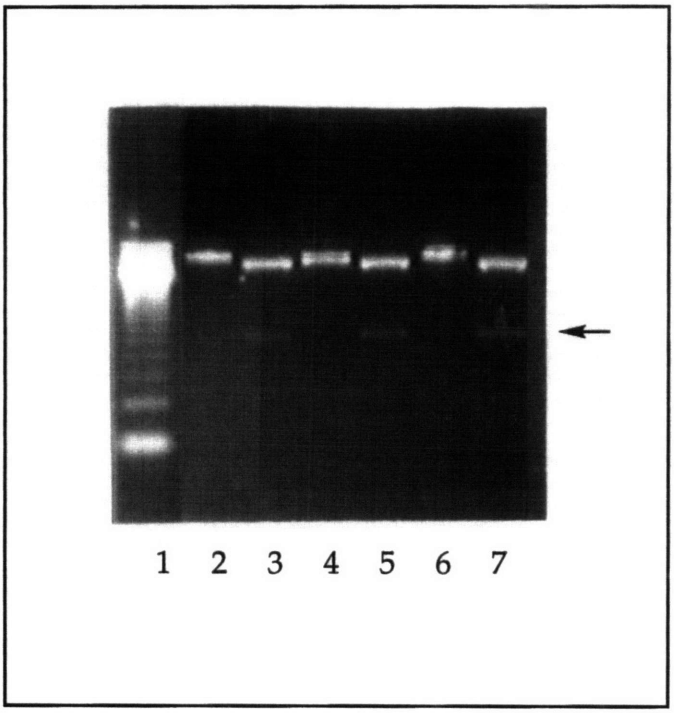

Figure 4.14 SDS-PAGE under reducing conditions of the IPTG induction of the 19 kD protein (A) where lane 2 is t=0 hr and lane 3 is t=3 hr; of the S300 purification (B) where lane 2 is peak 2; and of the pure protein (C) where lane 2 is the protein after ion-exchange chromotagraphy. Lane 1 of each gel is a 10 kD protein ladder standard.

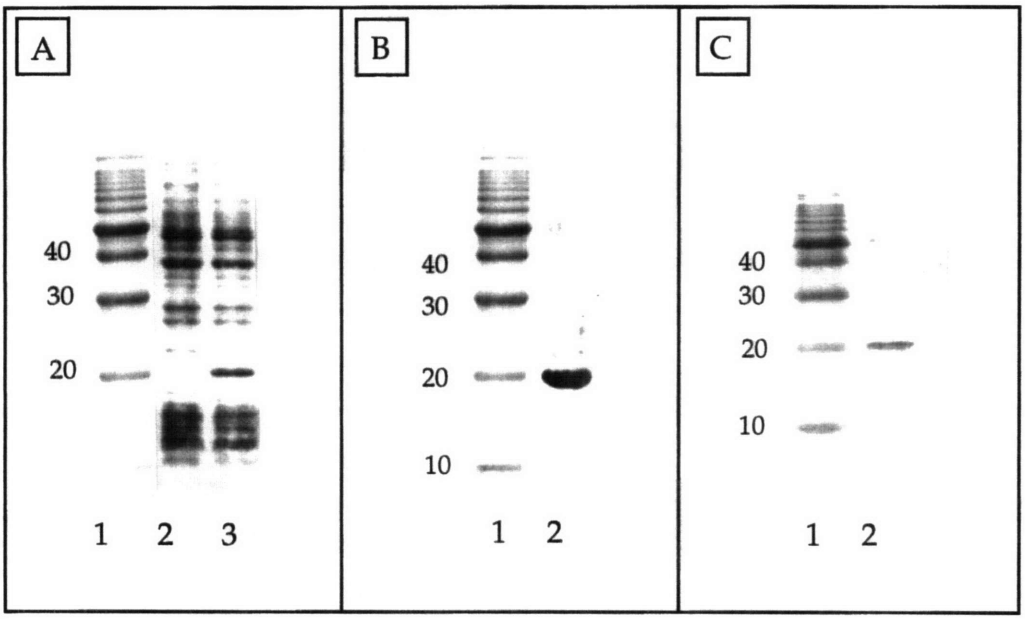

Figure 4.15 Aggregation of 80 μM β1-40 in the presence of the 19 kD truncated variant of apoE3.

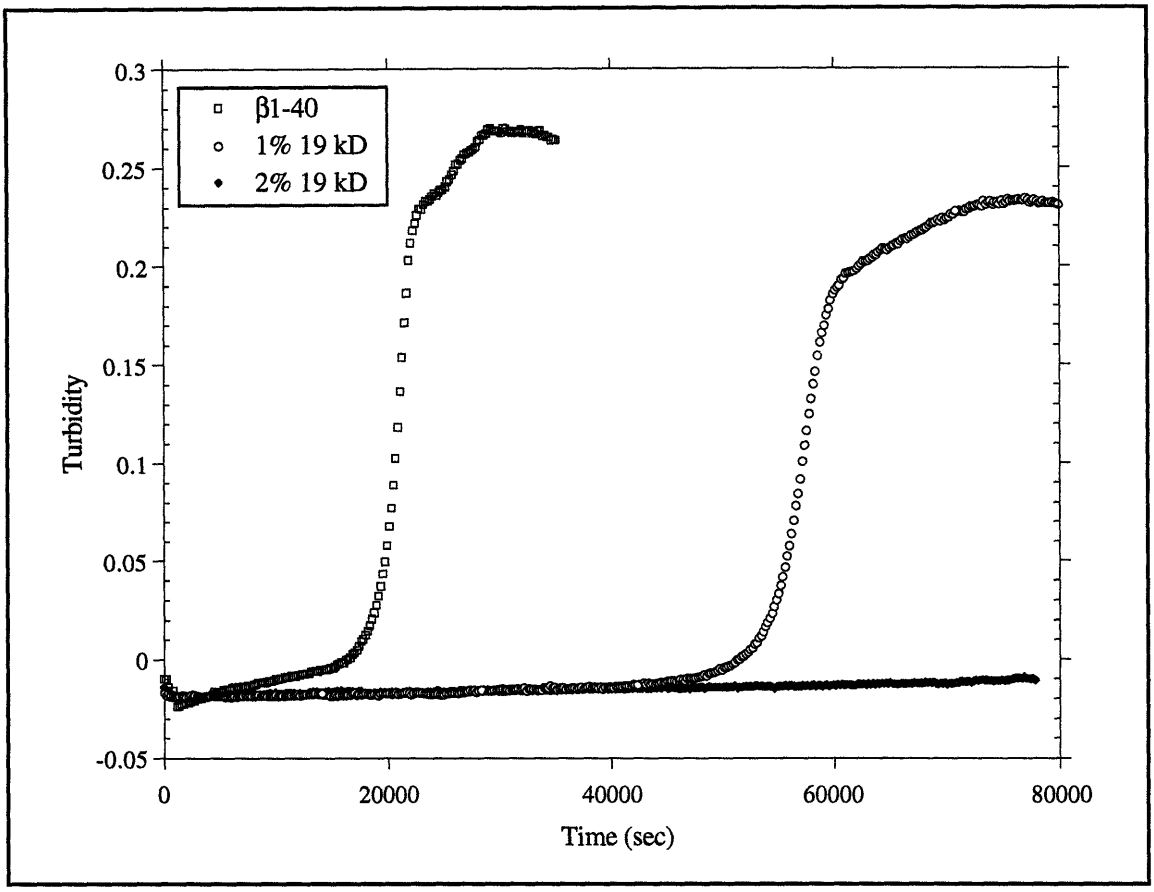

The Cys57 22 kD ApoE3 Appears to Have Diminished Inhibitory Effects

A mutant of the 22 kD apoE3 protein in which a threonine at position 57 is replaced by a cysteine was obtained from Karl Weisgraber at the Gladstone Institute (UCSF). This protein contains two cysteines and is proposed to contain an intramolecular disulfide bond between Cys57 and Cys112 that connects two of the helices in the four-helix bundle, preventing it from opening. This mutant protein has been shown to possess a lower affinity for lipid, as was previously discussed, supporting the theory that the bundle must open in order to bind lipid.[9]

The effect of the Cys57 mutant on the aggregation of β1-40 was examined. In the presence of a 2% molar equivalent of the Cys57 mutant, very little change in the lag time was observed, unlike the other apoE proteins previously described (Figure 4.16). However, aggregation was significantly delayed in the presence of a 4% molar equivalent. This indicates that the Cys57 mutant is a less efficient inhibitor of amyloid formation, possibly due to an intramolecular disulfide bond.

Figure 4.16 Aggregation of β1-40 (80 μM) in the presence of the Cys57 22 kD apoE3 mutant.

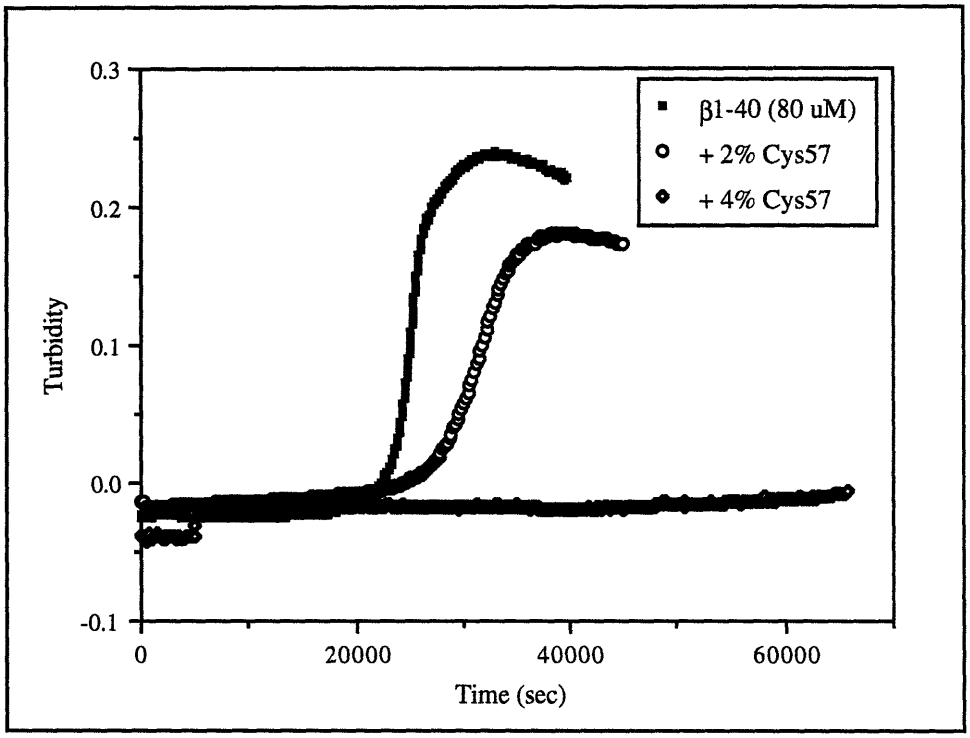

SDS-PAGE of the Cys57 mutant under reducing and non-reducing conditions are identical (Figure 4.17). This does not reveal the actual state of the intramolecular disulfide in either of the conditions since they would

Figure 4.17 SDS-PAGE of the 22 kD Cys57 apoE3 mutant under non-reducing (lane 2) and reducing (lane 3) conditions. Lane 1 is a 10 kD protein ladder standard

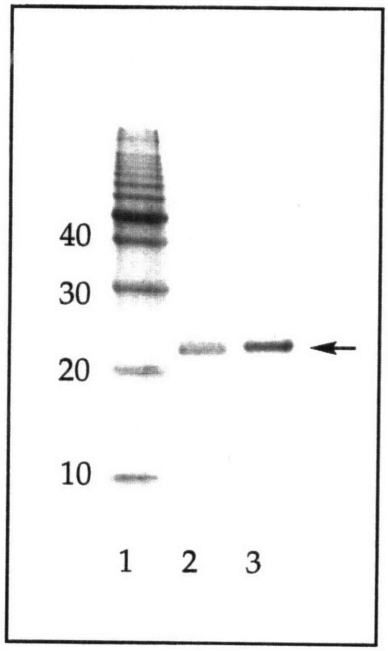

appear identical on a denaturing gel. However, it does indicate that neither cysteine is forming an intermolecular disulfide bond.

Fibril Morphology May be Altered in the Presence of the 22 kD ApoE3

EM results from chapter 3 indicated that there was no difference in morphology between amyloid fibrils produced in the absence and presence of 1% inhibitory concentrations of apoE3 or apoE4. However, other studies have reported that preparations of amyloid fibrils formed in the presence of apoE showed a greater number of fibrils as viewed by EM.[14,15] Several studies that examined the effect of apoE on either the aggregation of the β protein or the morphology of the fibrils are compared in Table 4.1. The significant differences in the experimental conditions and analytical techniques of each study might explain the different results that each group reported.

When samples from the experiment in Figure 4.9 were viewed by Atomic Force Microscopy (AFM), morphological differences were observed. The β1-40 fibrils were shorter than the fibrils formed with apoE and were fewer in number. The discrepancy between the results presented above and those in chapter 3 could be due to differences in procedure or technique. Further studies are required to rule out experimental artifacts.

If the aggregation mixture containing only β1-40 does contain fewer fibrils than the solution with apoE, but reaches a much larger turbidity, then the turbidity assay may not be measuring just fibrillar aggregates. The apoE could be inhibiting one type of aggregation while promoting another. Furthermore, the formation of amyloid fibrils and the consolidation of these fibrils into amyloid plaques may involve different mechanisms. ApoE may inhibit the formation of amyloid fibrils while causing these fibrils, once they

Table 4.1 A comparative analysis of several studies that examine the effect of apoE on β protein aggregation and fibril morphology.

	LANSBURY	WETZEL[19]	POTTER[15]	SANAN[14]	LANSBURY (future)
Conclusion:	apoE inhibits	apoE inhibits	apoE promotes	apoE promotes	N/A
Method of fibril detection:	turbidity assay	gel permeation chromatography and SPR	EM	EM, immunogold	AFM
Measurement:	A400	size-exclusion, Congo red-binding, RU, immunochemical staining	number of fibril crosses	qualitative observation of fibril density	time course of fibril formation in fluid state
Method Detects:	molecules >400 nm in diameter	fibrillar material, protein complexes	fibrillar material that binds to grid	fibrillar material that binds to grid	fibrils growing on the AFM surface
Problems with Method:	amorphous and fibrillar aggregates not distinguished	different fibrillar morphologies not distinguished	selective staining and adhesion, subjective	selective staining and adhesion, subjective	selective adhesion, subjective
β variant Studied:	β1-40	β1-40, β1-42	β1-42	β1-28	β1-40, β1-42
[β variant]:	80 μM	46 μM	80 μM	0.25 μM	80 μM
β Source:	Bachem	Bachem	Hoffman-LeRoche	Bachem	Quality Control Biochemicals
[apoE]:	800 nM	120 nM	400 nM	1.8 nm	400 - 1600 nM
apoE:β:	1:100	~ 1:400	1:200	~ 1:150	1:200 - 1:50
apoE Source:	plasma/ recombinant	recombinant	plasma	plasma	recombinant
pH:	7.4	7.4	7.0	7.3	7.4
stirred/unstirred:	both	unstirred	unstirred	unstirred	both
[salt]:	20 mM NaH_2PO_4, 100 mM NaCl	10 mM NaH_2PO_4, 100 mM NaCl	10 mM Tris-HCl	10 mM NaH_2PO_4, 100 mM NaCl	10 mM NaH_2PO_4, 100 mM NaCl

SPR = Surface Plasmon Resonance, AFM = Atomic Force Microscopy, RU = Response Units

do form, to clump together into plaques that are different from those formed without apoE (Figure 4.18).

Figure 4.18 Proposed effect of apoE on both the nucleation phase of fibril formation and on the formation of plaques by the amyloid fibrils.

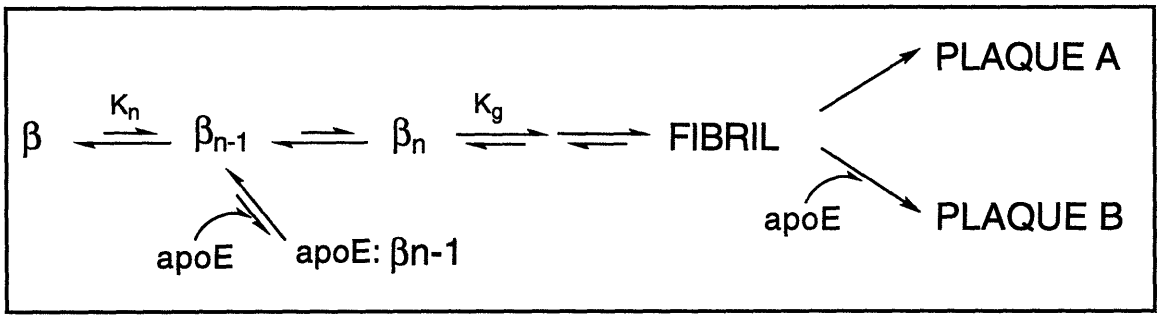

Circular Dichroism of 22 kD ApoE Proteins

CD, which was discussed in detail in chapter 2, is a useful tool for studying the conformation of proteins and peptides. The conformations of several apoE isoforms were studied using this technique. In addition to the three 22 kD polymorphic proteins, apoE2, apoE3, and apoE4, the 19 kD apoE3 truncated variant and a Cys57 apoE mutant were also analyzed. The apoE proteins were analyzed at a concentration of 5 μM in 20 mM phosphate buffered saline at 25°C. Because of their highly helical nature, no organic solvent such as TFE or HFIP was required to induce structure. All data is reported in molar ellipticity. The percent α-helicity was determined from the CD data as it was in chapter 2, using the method of Greenfield and Fasman for the 208 nm absorption[16] and the method of Morrisett for the 222 nm absorption.[17]

The 22 kD ApoE Isoforms Have a Large α-Helical Content

The isoforms were initially studied in buffer alone. The proteins contain a large amount of α-helix at both 208 and 222 nm, and appear to have almost identical conformations. Figure 4.19 shows the CD spectra of the polymorphic 22 kD apoE isoforms, the 19 kD truncated variant, and the Cys57 22 kD apoE3 mutant. The amount of α-helix present in each of the proteins is given in Table 4.2.

Stability Studies of the ApoE Proteins

The 22 kD domain of apoE is unusually stable when compared to other apolipoproteins and exists as a four-helix bundle. If the opening of this four-helix bundle to yield a hydrophobic and hydrophilic face is important for the function of the protein, then differences in the stability of the bundle could be critical in determining the effectiveness of these isoforms in the delivery of hydrophobic molecules. CD was used to probe the stability of the 22 kD apoE isoforms. Differences in the structural stability may be important in modulating the effect of apoE *in vivo*.

Figure 4.19 CD of 5 μM 22 kD apoE proteins and the 19 kD and Cys57 variants in buffer only.

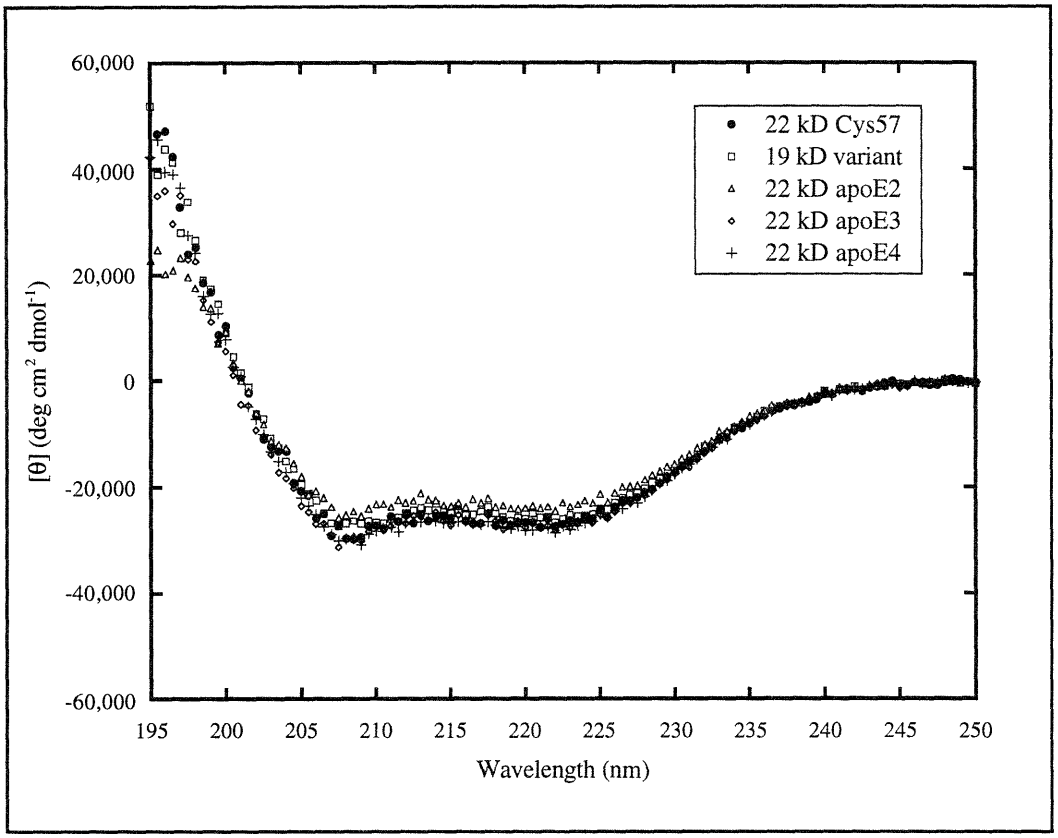

Table 4.2 Percent α-helicity of the apoE isoforms at 208 and 222 nm.

ApoE Isoform	208 nm	222 nm
22 kD Cys57	88	78
22 kD apoE2	78	76
22 kD apoE3	73	71
22 kD apoE4	88	80
19 kD apoE3	89	81

22 kD Cys57 ApoE3

Figure 4.20 shows the CD spectra of the Cys57 mutant in the presence of 1 mM DTT, 1 M GuHCl, and 3 M GuHCl. The two GuHCl concentrations correspond roughly to the two conformational transitions found in the full-length protein (discussed in chapter 3). The spectra of the proteins in the presence of 3 M GuHCl are scattered below 210 nm due to the large absorbance of the GuHCl in this region, therefore, α-helicity was not calculated at 208 nm for the 3 M GuHCl spectra (Table 4.3).

Figure 4.20 CD of 5 μM 22 kD Cys57 apoE3 alone and in the presence of 1 mM DTT, 1 M GuHCl, and 3 M GuHCl.

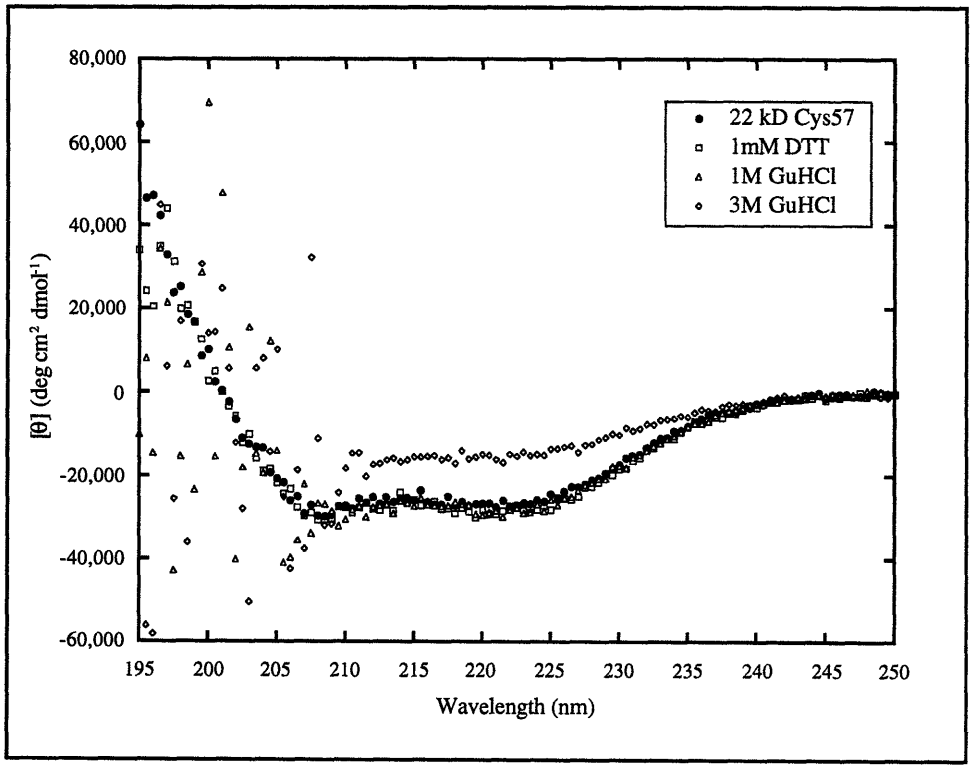

Table 4.3 Percent α-helicity of 5 μM 22 kD Cys57 apoE3.

	208 nm	222 nm
22 kD Cys57	88	78
1 mM DTT	92	78
1 M GuHCl	78	80
3 M GuHCl	NA	45

22 kD ApoE Isoforms

The CD spectra of 22 kD fragments of apoE2, apoE3, and apoE4 alone and in the presence of 1 mM DTT, 1 M GuHCl, and 3 M GuHCl are shown in Figures 4.21, 4.22, and 4.23. The percent α-helicity of each are shown in Tables 4.4, 4.5, and 4.6.

Figure 4.21 CD of 5 μM 22 kD apoE2 alone and in the presence of 1 mM DTT, 1 M GuHCl, and 3 M GuHCl.

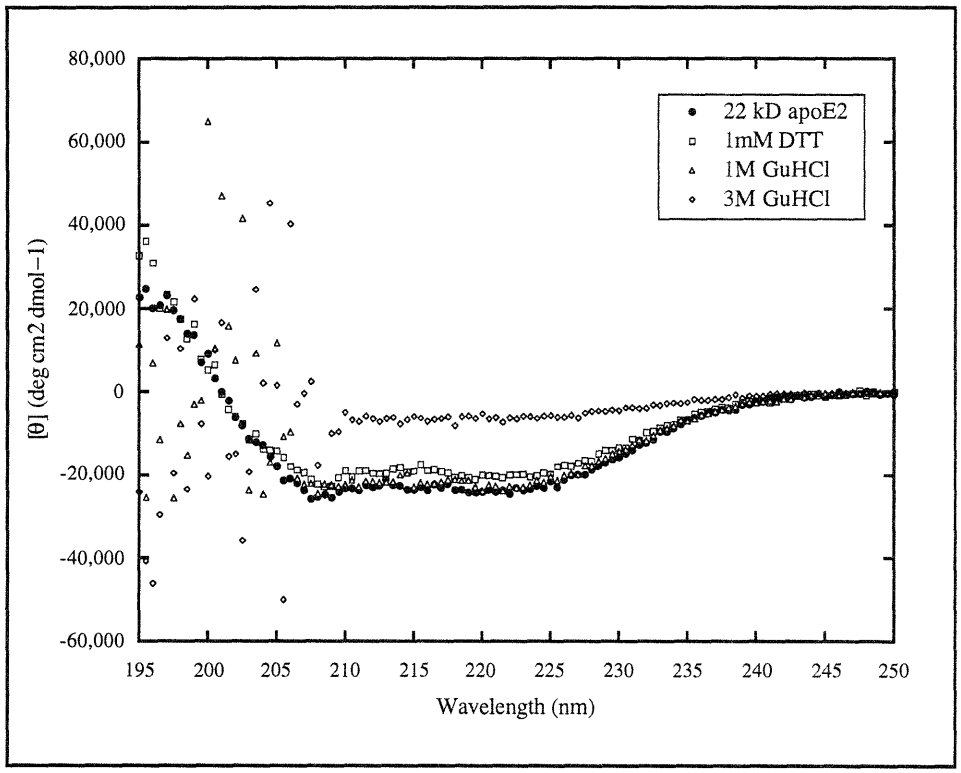

Table 4.4 Percent α-helicity of 5 μM 22 kD apoE2.

	208 nm	222 nm
22 kD apoE2	73	71
1 mM DTT	63	59
1 M GuHCl	70	66
3 M GuHCl	NA	23

Figure 4.22 CD of 5 μM 22 kD apoE3 alone and in the presence of 1 mM DTT, 1 M GuHCl, and 3 M GuHCl.

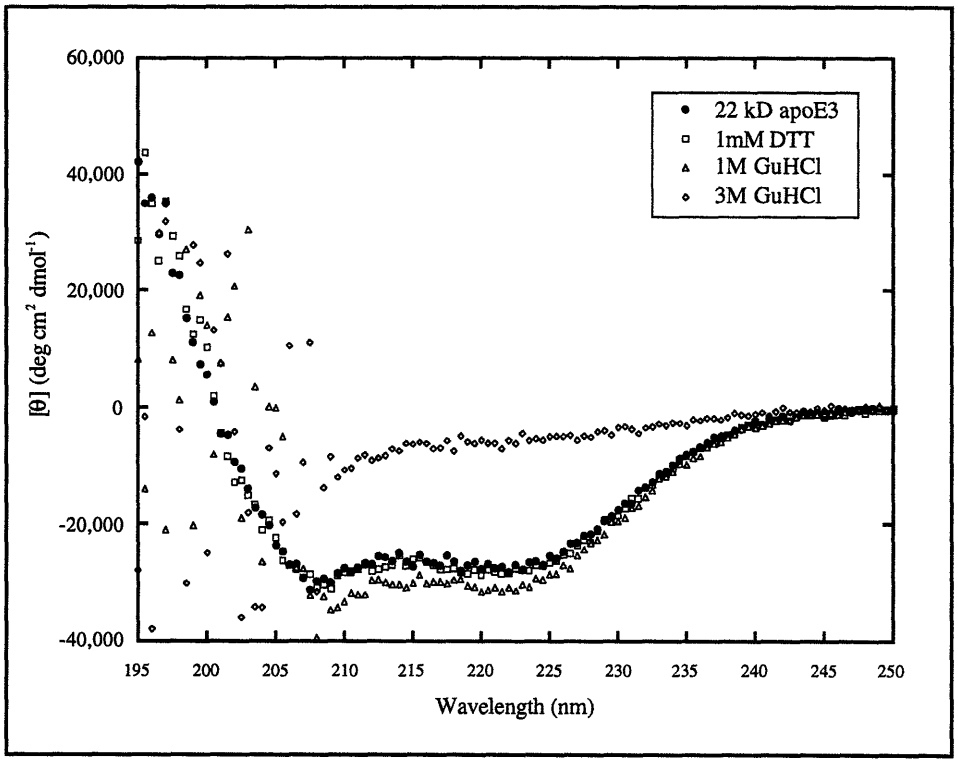

Table 4.5 Percent α-helicity of 5 μM 22 kD apoE3 .

	208 nm	222 nm
22 kD apoE3	88	80
1 mM DTT	92	80
1 M GuHCl	100	87
3 M GuHCl	NA	22

Figure 4.23 CD of 5 μM 22 kD apoE4 alone and in the presence of 1 M GuHCl and 3 M GuHCl.

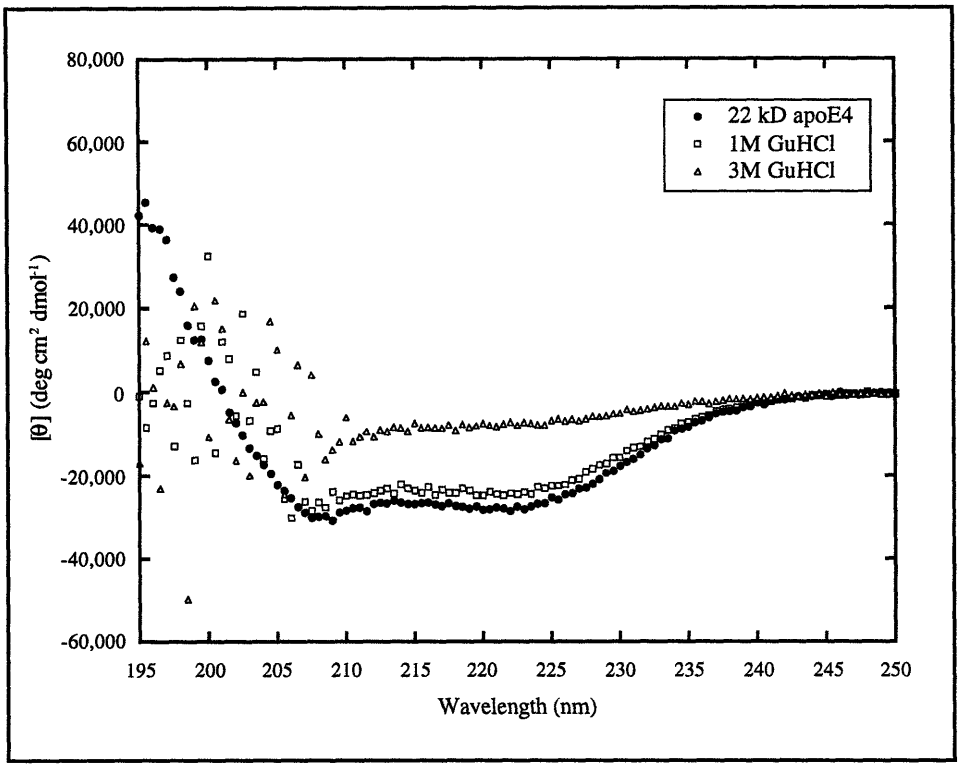

Table 4.6 Percent α-helicity of 5 μM 22 kD apoE4.

	208 nm	222 nm
22 kD apoE4	89	81
1 M GuHCl	77	70
3 M GuHCl	NA	26

19 kD ApoE3 Truncated Variant

The CD spectra for 5 μM 19 kD apoE3 truncated variant are shown in Figure 4.24 and the percent α-helicity is given in Table 4.7.

Figure 4.24 CD of 5 μM 19 kD apoE3 variant alone and in the presence of 1 mM DTT, 1 M GuHCl, and 3 M GuHCl.

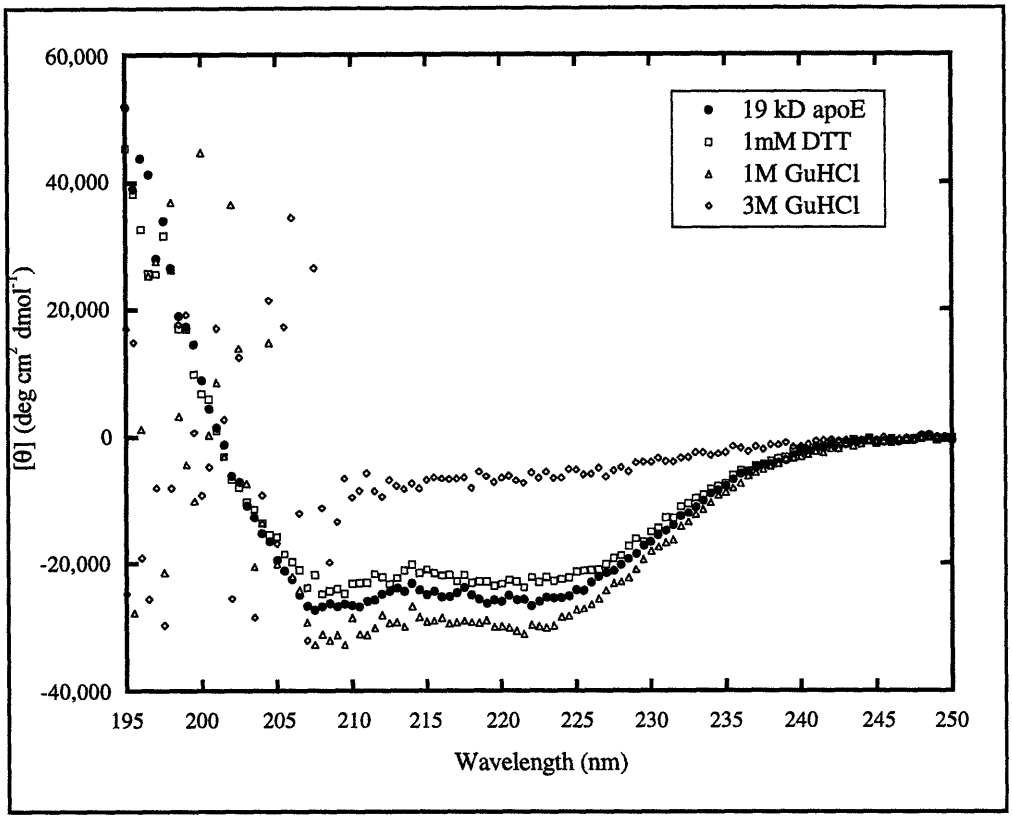

Table 4.7 Percent α-helicity of 5 μM 19 kD apoE3 variant.

	208 nm	222 nm
19 kD mutant	78	76
1 mM DTT	72	65
1 M GuHCl	93	84
1 M GuHCl	NA	22

The Cys57 Mutant Appears to be More Stable

There was not a significant change in the percent α-helicity of any of the apoE isoforms either in the presence of either 1 mM DTT or 1 M GuHCl,

which is in agreement with previously published reports.[18] However, one isoform, the Cys57 mutant, showed a smaller effect from the 3 M GuHCl than any of the other proteins. Figure 4.25 shows the spectra of the five proteins in the presence of 3 M GuHCl between 195 and 250 nm and the percent α-helicity for the 222 nm absorption is given in Table 4.8. The spectra are scattered below 210 nm due to the large absorbance of GuHCl in this region. The Cys57 protein shows a 33% decrease in α-helicity in the presence of 3 M GuHCl while the other proteins show decreases of 48 to 59%.

Figure 4.25 CD spectra of the apoE proteins in the presence of 3 M GuHCl.

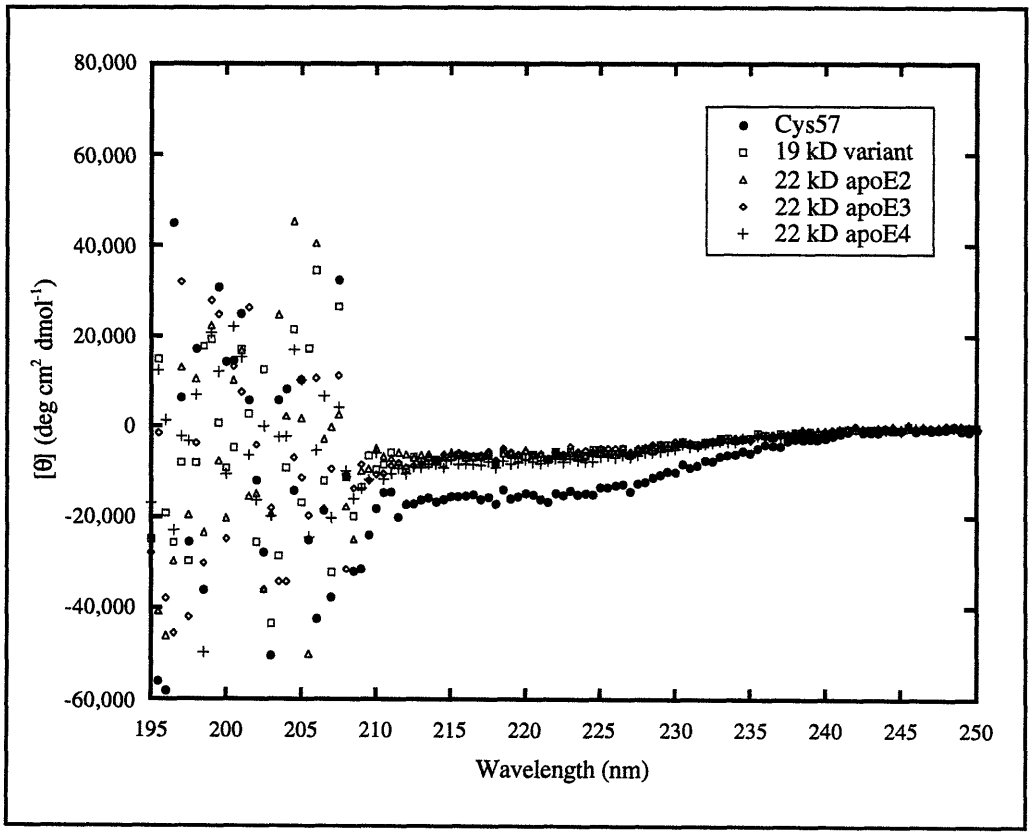

Table 4.8 Decrease in percent α-helicity of the apoE proteins in the presence of 3 M GuHCl.

ApoE Protein	222 nm
22 kD Cys57	33
22 kD apoE2	48
22 kD apoE3	58
22 kD apoE4	59
19 kD variant	48

Discussion

In chapter 3, the ability of apoE to inhibit aggregation of the β protein into amyloid fibrils was described and the role of apoE in the pathogenesis of AD was examined. The studies presented herein narrow the region responsible for the inhibitory activity of the protein down to the 22 kD domain. The three polymorphic isoforms of the 22 kD domain of apoE (apoE2, apoE3, and apoE4) were expressed in *E. coli* and the recombinant proteins were purified and used *in vitro* to test their ability to inhibit β protein aggregation. A 19 kD apoE3 truncated protein was also expressed and purified.

The results show that the 22 kD domain of apoE, like the full-length protein, is an effective inhibitor of amyloid formation at a 0.5% molar equivalent. Interestingly, very small changes in the amount of the 22 kD domain have very large effects on the lag time of the β protein. A supersaturated solution of β1-40 containing 2% of a molar equivalent of either apoE2, apoE3, or apoE4 inhibit aggregation past 24 hours. Additionally,

the final turbidity of aggregated solutions of β1-40 with more than a 1% molar equivalent of apoE is lower than solutions without the apoE. While low levels of apoE do not appear to affect the growth and stability of fibrils, higher concentrations of proteins may have an effect.

The concentration dependence of apoE that was exhibited in the aggregation assay can be explained by the nucleation-dependent model of amyloid formation in which apoE is binding to a large oligomer of β1-40. In this mechanism, very small increases in the amount of apoE present would result in a much larger sequestration of β1-40. This would decrease the effective concentration of β1-40 in solution and could result in a lag time that is longer than 24 hours for experiments with a 2% molar equivalent of apoE.

Results by Ronald Wetzel and coworkers confirm the work presented above. They have also shown that the aggregation of the β protein can be described by a nucleation-dependent mechanism and that apoE is an effective inhibitor of β1-40 aggregation.[19] In addition, they have isolated a high molecular weight complex with an apoE:β protein ratio of 1:95. This complex provides evidence that a small amount of apoE can bind to large β1-40 oligomers.

While both the apoE3 and apoE4 22 kD proteins extended the lag time in the aggregation of β1-40, no difference in inhibitory activity was observed. These results are similar to those produced from the full-length proteins. However, because the apoE protein concentrations are measured by the Lowry test, which can have a significant margin of error, it is very difficult to measure precisely the amount of protein added to the β1-40. This makes comparisons between different isoforms problematic due to the sensitivity of the assay to the apoE concentration.

The 19 kD truncated variant behaved similarly to the 22 kD proteins in that a 1% molar equivalent of the protein produced a significant increase in the lag time. The truncated protein also inhibited the aggregation of the β protein past 24 hours when present at 2%. Therefore, the deleted C-terminal portion of the 22 kD domain that exists as a random coil does not appear to be important to the inhibitory function of the protein.

The proteins were also examined by CD in order to compare their structures and relative stability. At a concentration of 5 μM without the addition of nonpolar helix-inducing solvents the protein contained very large amounts of α-helix (73 to 89%). The proteins were also monitored in the presence of 1 mM DTT, 1 M GuHCl, and 3 M GuHCl. There were no significant changes in conformation in the presence of 1 mM DTT or 1 M GuHCl. These results are in agreement with previous results showing the 22 kD domain to be unusually stable, up to a concentration of 2.4 M GuHCl.

Large changes in α-helicity of all of the variants were observed in the presence of 3 M GuHCl. However, an apoE3 mutant containing a Cys57 mutation showed a smaller decrease in helicity and therefore appeared to be more stable than the other variants. This variant has been shown to have a lower affinity for lipid molecules.

Future Directions

Aggregation conditions that can distinguish between the inhibitory abilities of the apoE variants, if they do exist, should be developed. More truncated forms of the 22 kD domain of apoE should also be produced until the protein no longer possesses inhibitory activity. Variants that are N- and C-terminally truncated and that contain only one, two, or three α-helices

should be tested. Furthermore, a synthetic four-helix bundle in which all four of the helices are identical and joined by linkers could be useful in determining whether or not the four-helix bundle motif alone is sufficient for inhibition. The truncated proteins could also be examined by CD in order to determine their relative stabilities.

Further studies of the effect of apoE concentration on the aggregation and morphology of the amyloid fibrils should be completed. Specifically, the following AFM experiments could be performed to determine if the presence of apoE simply helps the fibrils adhere to the AFM surface, leading to the false conclusion that more fibrils are formed in the presence of apoE:

1) make β1-40 fibrils with no apoE, view by AFM
2) make β1-40 fibrils, then add apoE, view by AFM
3) make β1-40 fibrils with apoE, view by AFM

The effect of lipids on the ability of apoE to inhibit the aggregation of β1-40 should be examined using the turbidity assay. The experiments described were run using apoE that was not bound to lipid, which may not be biologically relevant as apoE is never isolated from plasma in its lipid-free form. Aggregation experiments containing relevant concentrations of lipid should be performed to determine the ability of β protein oligomers to displace the lipid. Additionally, the effect of lipids on the morphology of fibrils formed in the presence of apoE could be examined by AFM.

Most importantly, the development of an assay that could measure the aggregation of the β protein more accurately and reproducibly than the turbidity assay would be extremely useful. One factor that would greatly improve the assays is the creation of a stock solution of β1-40 that would not "age". When the stock solution ages, it produces protein solutions that

aggregate faster than previous runs, possibly due to the creation of small nuclei.

Experimental

Materials

Expression vectors for the apoE2, apoE3, and apoE4 proteins, as well as the purified Cys57 mutant protein were obtained from Dr. Karl Weisgraber at the Gladstone Institute (UCSF). The pET expression plasmid was purchased from Novagen. The Lowery protein assay kit was purchased from Pierce. IPTG was obtained from Boehringer Mannheim. Reagents used for cell growth (Yeast Extract, Tryptone, and Agar) were all purchased from Difco. GuHCl were obtained from Mallincrodt. S-300 size-exclusion beads were purchased from Pharmacia. Ultra Pure Agarose (low melting-point) was purchased from GibcoBRL. The deoxynucleotides were obtained from New England Biolabs. Oligonucleotides were purchased from Midland and enzymes were obtained from New England Biolabs. Aerosol resistant tips were obtained from USA Scientific. DEAE columns were purchased from Waters.

Aggregation Assay (Stirred)

Aggregation was monitored at 400 nm using the turbidity assay. Stock solutions were prepared and experiments were performed as previously described in Chapter 3. Results with the 19 kD apoE3 are based on one experiment.

Preparation of Competent Cells

Overnight cultures (inoculated with a glycerol stock prepared from a single colony of either DH1 or BL21 cells) were grown in 10 ml of L-broth media (10 g tryptone, 10 g NaCl, 5 g yeast extract, dissolved to 1000 ml) containing no ampicillin at 37°C in a shaking incubator. The 10 ml culture was then used to inoculate 1 L of L-broth in 4 L flask and was shaken at 37°C until the OD_{550} was 0.5 to 0.6. The culture was rapidly chilled to 4°C by swirling in an ice/water bath. The cells were harvested in pre-chilled centrifuge bottles and were spun at 5000 rpm for 5 minutes in a Beckman centrifuge (model J2-21) with a rotor cooled to 4°C. During the remainder of the procedure the cells were kept on ice or in a 4°C cold room. The cell pellet was resuspended in 250 ml ice-cold sterile-filtered 100 mM $MgCl_2$, initially suspending the cells in a small volume (50 ml) and then diluting with the remainder of liquid. The cells were spun down as above. The cell pellet was then resuspended in 250 ml of ice-cold sterile-filtered 100 mM $CaCl_2$ as gently as possible as the cells become very fragile in $CaCl_2$. The solution was incubated on ice for 20-45 minutes. The cells were then spun at 3000 rpm for 5 minutes. The cell pellet was then gently resuspended in 50 ml of ice-cold sterile freezing medium (42.5 ml 100 mM $CaCl_2$, 7.5 ml glycerol). The cells were dispensed in 300 µl aliquots into Eppendorf tubes and frozen rapidly in a dry ice/EtOH bath. The aliquots were stored at -80°C.

Purification of Plasmid DNA

Overnight cultures (5-10 ml) of *E. coli*, either DH1 or BL21 strains, were grown as described above, with the exception that ampicillin was added to the L-broth (100 µg/ml). The cells were transformed into Eppendorfs and pelleted

by centrifugation for approximately one minute. The plasmid DNA was then isolated and purified using the QIAGEN Spin Plasmid Kit according to the specified protocol. The DNA was eluted with either water or 10 mM Tris-HCl pH 7.4 (30-50 µl).

Transformation of E. coli

Frozen competent cells were thawed on ice. Competent cells (100 µl/transformation) were aliquoted into pre-chilled sterile Falcon 2059 tubes on ice using sterile technique. For each transformation a positive control (cells transformed with a known amount of purified plasmid to test the competency of the cells) and a negative control (cells with no added DNA to test the purity of the cells) were also performed. The DNA (5-10 ng) was added to the chilled tubes and the cells were swirled gently to mix. For transformations using a ligation mixture in which DNA has been ligated into an expression vector (see below for ligation procedure) an additional control was performed. The empty dephosphorylated plasmid (the cut vector without the DNA PCR insert) was added to the competent cells. The tubes were then incubated on ice for 30-60 minutes. After the incubation, the cells were heat shocked by placing the tubes in a 42°C heat bath for exactly one minute. The cells were cooled on ice for 30 seconds and then placed at room temperature. SOC medium (900 µl) pre-heated to 42°C was added to each tube which was shaken gently on a rotating platform at 37°C for 15-60 minutes. The cells were then spread onto ampicillin plates (no more than 300 µl of transformation mixture per plate), allowed to dry, and incubated upside down at 37°C overnight.

$MgCl_2/MgSO_4$ solution: 12.0 g $MgSO_4 \cdot 7H_2O$
9.5 g $MgCl_2$
Dilute to 100 ml and sterile filter

SOC medium:
4 g tryptone
1 g yeast extract
0.1 g NaCl
4 ml 20% glucose
2 ml $MgCl_2/MgSO_4$ solution
Dilute to 200 ml and autoclaved

Protein Induction

Cultures of BL21(DE3) cells containing the apoE plasmids were grown as described for the production of competent cells above, with the exception that all L-broth medium used contained ampicillin (100 μg/ml). The cultures were grown until they reached an OD_{550} of 0.5 to 0.6. At this point 1 ml of culture was removed for later analysis by SDS-PAGE. IPTG was then added to the culture to give a final concentration of 0.5 mM and the cells were shaken at 37°C for three hours. A sample (1 ml) of culture was removed at 1.5 hours and 3 hours to be analyzed by SDS-PAGE. After protein expression was completed, the cells were harvested at 9000 rpm using a Beckman J2-21 centrifuge. The cell pellets were stored at -20°C. The cell pellets were dissolved in 1x lysis buffer (50 mM Tris pH 7.4, 100 μM DTT, 100 μM PMSF,). The cells were disrupted by passage through a French pressure cell at 16,000 psi, keeping the cells on ice throughout the procedure, and the cell lysate was then spun at 9,000xg for 35 minutes. Streptomycin sulfate (0.2 volumes of a 5% solution) was added to the supernatant which was stirred at 4°C for 30 minutes and then spun at 9,000xg for 20 minutes. Ammonium sulfate was added to the supernatant to yield a 60% solution, the solution was stirred at 4°C for 1 hour, and was then centrifuged at 9,000xg for 20 minutes. The

protein pellet was then dissolved in 1x lysis buffer and solid GuHCl was added to yield 15 ml of a 7 M GuHCl. βME was added to bring the solution to 1% βME. This crude protein solution was subsequently purified by size-exclusion chromatography (see below).

PCR Protocol

The PCR mixture contained in a total of 100 µl: clean, quantitated (A_{260}) plasmid (1 ng to 100 ng), 1 pmol each of primer 1 and primer 2 (see below), a mixture of all four deoxynucleotides (dATP, dGTP, dCTP, and dTTP) at 100 µM each, 10 µl of 10x PCR buffer (100 mM KCl, 200 mM Tris-HCl pH 8.8, 100 mM $(NH_4)_2SO_4$, 20 mM $MgSO_4$, 1% Triton X-100), and 4 µl sterile filtered DMSO, which was added to the PCR reactions in order to lower the effective T_m of the DNA duplexes and is critical for amplifications involving the GC-rich apoE gene. The mixture was overlaid with paraffin oil and heated at 94°C for 3 minutes. The high fidelity *Vent* polymerase (2 U) was used instead of *Taq* polymerase, which has a higher level of spurious mutation, and was added under the oil layer. The tubes were then heated for 30 cycles according to the following program: 94°C (1 minute), 50°C (1 minute), 75°C (2 minutes). Aerosol resistant tips were used for all amplifications in order to prevent contamination of the solutions. All PCR reactions were performed in 0.5 ml Eppendorf tubes. For each PCR reaction, a control reaction was also performed in which no template was added in order to check for contamination in the reagents.

Primer 1 (5' to 3')

AAA GGA AGA GTA TGC ATA TGA AGG TTG AAC AGG

NdeI

Primer 2 (5' to 3')

ATT GGA TCC TTA CCG CAC GCG GCC CTG TTC

BamHI

Synthesis of Truncated ApoE DNA Inserts

In order to make truncated variants of 22 kD apoE3, primers 3 and 4, corresponding to internal sequences of apoE, were designed and purchased from Midland (see below). All PCR was performed as described above, except the truncated primers were used in place of or with the flanking primers described above.

Primer 3 (5' to 3')

AAA GGA AGA GTA TGC ATA TGG GCC AGC GTC GGG A

NdeI

Primer 4 (5' to 3')

ATT GGA TCC TTA GCC CTG GTA CAC TGC CAG

BamHI

Purification of PCR Products

Purification of the products from the PCR reaction was required before digestion. All PCR material was purified using the QIAGEN PCR Purification

Kit according to the specified protocol. The DNA was eluted from the column with H_2O (30 to 50 µl).

Restriction Digest of DNA

For each plasmid, the digest contained the following in a total volume of 10 to 15 µl: NdeI (10 U), BamHI (20 U), and 1 µl of 10x BamHI buffer (1.5 M NaCl, 100 mM Tris-HCl, pH 7.9, 100 mM $MgCl_2$, 10 mM DTT). Each tube was diluted to the final volume (10-15 µl) with H_2O. The samples were incubated in a heated water bath at 37°C for 1 to 1.5 hours. DNA material that was to later to be used in a ligation reaction was gel purified, the DNA band was excised from the gel using a new razor blade, and the DNA was purified using the QIAGEN Gel Purification Kit. DNA was eluted from the columns with H_2O (50-100 µl). For all other digests, the restriction digest was analyzed by gel electrophoresis. The 1% agarose gels contained 1% ethidium bromide, and DNA was visualized by UV light.

Ligation of PCR Insert and Vector

Prior to ligation, the pET vector (0.1 µg) was enzymatically digested as described above. In a total volume of 60 µl, the digested pET vector was then dephosphorylated with shrimp alkaline phosphatase (0.1 U) that contained 6 µl of 10x phosphatase buffer (200 mM Tris-HCl, pH 8.0, 100 mM $MgCl_2$) according to the specified protocol in order to prevent the cut plasmid from reclosing on itself. The mixture was incubated at 37°C for 2.5 hours. The mixture was then heated at 65°C for an additional 15 minutes in order to denature the enzyme. The ligation mixture contained the following in a total volume of 120 µl: 50 µl of the dephosphorylated pET vector mixture, 55 µl of

the gel-purified PCR insert (described above), 12 µl of 10x T4 ligase buffer (500 mM Tris-HCl, pH 7.8, 100 mM $MgCl_2$, 100 mM DTT, 10 mM ATP, and 500 µg/ml BSA), and T4 ligase (400 U). The solution was incubated overnight at 16°C. The ligation mixture was then transformed into either DH1 or BL21 *E. coli* cells (see above).

Purification of 22 kD apoE

Size-Exclusion Chromatography

The crude protein in 7 M GuHCl, which was prepared in the "Protein Induction" section described above, was purified using a size-exclusion column (92 X 4 cm) containing S-300 beads packed in 4 M GuHCl solution (4 M GuHCl, 1 mM EDTA, 0.1 M Tris, pH 7.4, 0.1 % βME). The column was equilibrated with 500 ml fresh 4 M GuHCl solution prior to use. The protein sample (15 ml in 7 M GuHCl (1% βME)) was added slowly to the column by gravity over 15 minutes and fractions were collected (15 minutes per tube) and analyzed at 280 nm. The fractions comprising each peak were combined, transferred into dialysis tubing with a 6-8 MW cut off (Sigma), and dialyzed 5x over 3 days at 4°C in 20 mM ammonium bicarbonate. The protein solutions were lyophilized and the correct protein was identified by SDS-PAGE.

Ion-Exchange Chromatography

The apoE proteins (5 mg) initially purified by size-exclusion chromatography (above) were dissolved in 20 mM Tris-HCl at pH 7.4 (700 µl) to yield a cloudy solution. Urea (600 µl of a 9.8 M solution) was then added, resulting in clear solution. DTT was added (10.2 mg) and the solution was

centrifuged briefly to pellet any remaining insoluble material. The proteins were purified by HPLC using an analytical (7.5 X 75 mm) or semi-preparative (21.5 X 150 mm) DEAE ion-exchange column, according to the gradient described below, with a flow rate of 1 ml/min monitored at 225 nm. The isolated protein was dialyzed in 20 mM ammonium bicarbonate 3x at 4°C, lyophilized, and analyzed by SDS-PAGE.

DEAE Gradient (bufferA/buffer B):

$$100/0 \xrightarrow{25'} 75/25 \xrightarrow{10'} 0/100 \xrightarrow{10'} 100/0$$

Buffer A:	20 mM Tris-HCl Titrate to pH 7.4 and filter
Buffer B:	20 mM Tris-HCl 0.5 M NaCl Titrate to pH 7.4 and filter

Circular Dichroism of Protein Samples

CD spectra were obtained using an AVIV spectrapolarimeter in the laboratory of Dr. Paul Schimmel, Department of Biology, MIT. Stock solutions of proteins were in 0.1 M NH_4HCO_3. Protein concentrations were determined using the Lowery protein determination kit. CD samples were prepared by adding the stock protein solutions to either 20 mM PBS buffer alone or buffer containing 1 mM DTT or buffer containing 1 mM DTT with either 1 or 3 M GuHCl to give a final protein concentration of 5 μM. The samples were incubated at room temperature overnight. Each sample was scanned four times in a quartz cell (0.1 cm pathlength) at 0.5 nm intervals over the wavelength range of 190 to 250 nm at 25°C. Solvent and cell backgrounds were subtracted from each sample. Results are expressed in

terms of molar ellipticity in units of deg·cm^2/dmol. No smoothing technique was used to reduce noise levels.

References

(1) Jarrett, J.T.; Lansbury, P.T., Jr. *Cell* **1993**, *73*, 1055-58.
(2) Corder, E.H.; Saunders, A.M.; Strittmatter, W.J.; Schmechel, D.E.; Gaskell, P.C.; Small, G.W.; Roses, A.D.; Haines, J.L.; Pericak-Vance, M.A. *Science* **1993**, *261*, 921-923.
(3) Evans, K.C.; Berger, E.P.; Cho, C.-G.; Weisgraber, K.H.; Lansbury, P.T., Jr. *Proc. Natl. Acad. Sci. USA* **1995**, *92*, 763.
(4) Wilson, C.; Wardell, M.R.; Weisgraber, K.H.; Mahley, R.W.; Agard, D.A. *Science* **1991**, *252*, 1817-1822.
(5) Mahley, R.W.; Innerarity, T.L.; Pitas, R.E.; Weisgraber, K.H.; Brown, J.H.; Gross, E. *J. Biol. Chem.* **1977**, *252*, 7279-7287.
(6) Weisgraber, K.H. *Adv. Prot. Struct.* **1994**, *45*, 249-302.
(7) Phillips, M.C.; Sparks, C.E. *Ann. N.Y. Acad. Sci.* **1980**, *348*, 122-137.
(8) Weisgraber, K.H.; Lund-Katz, S.; and Phillips, M.C. in *High Density Lipoproteins and Atherosclerosis;* Miller, N. E. Tall, A. R., Ed.; Elsevier: Amsterdam, **1992**; Vol. pp 175-181.
(9) De Pauw, M.; Vanloo, B.; Weisgraber, K.H.; Rosseneu, M. *Biochemistry* **1995**, *34*, 10953-10960.
(10) Rebeck, G.W.; Reiter, J.S.; Strickland, D.K.; Hyman, B.T. *Neuron* **1993**, *11*, 575-580.
(11) Breiter, D.R.; Kanost, M.R.; Benning, M.M.; Wesenberg, G.; Law, J.H.; Wells, M.A.; Rayment, I.; Holden, H.M. *Biochemistry* **1991**, *30*, 603-608.
(12) Horie, Y.; Fazio, S.; Westerlund, J.R.; Weisgraber, K.H.; Rall, S.C. *J. Biol. Chem.* **1992**, *267*, 1962-1968.
(13) Moffatt, B.A.; Studier, F.W. *J. Mol. Biol.* **1986**, *189*, 113-130.
(14) Sanan, D.A.; Weisgraber, K.H.; Russell, S.J.; Mahley, R.W.; Huang, D.; Saunders, A.; Schmechel, D.; Wisniewski, T.; Frangione, B.; Roses, A.D.; Strittmatter, W.J. *J. Clin. Invest.* **1994**, *94*, 860-869.
(15) Ma, J.; Yee, A.; Brewer, H.B.; Das, S.; Potter, H. *Nature* **1994**, *372*, 92-94.
(16) Greenfield, N.; Fasman, G.D. *Biochemistry* **1969**, *8*, 4108.
(17) Morrisett, J.D.; David, J.S.K.; Pownall, H.J.; Gotto, A.M. *Biochemistry***1973**, *12*, 1290.
(18) Wetterau, J.R.; Aggerbeck, L.P.; Rall, S.C., Jr.; Weisgraber, K.H. *J. Biol. Chem.* **1988**, *263*, 6240-6248.
(19) Chan, W.; Wood, S.J.; Wetzel, R. *Unpublished results.*